

NIST NSRDS 100

**Simulation of Electron Spectra for Surface
Analysis (SESSA)
Version 2.2.0
User's Guide**

W.S.M. Werner
W. Smekal
C.J. Powell

This publication is available free of charge from:
<https://doi.org/10.6028/NIST.NSRDS.100-2021>



NIST NSRDS 100

Simulation of Electron Spectra for Surface Analysis (SESSA)

Version 2.2.0

User's Guide

W.S.M. Werner

W. Smekal

*Institute of Applied Physics
Vienna University of Technology, Vienna, Austria*

C.J. Powell

*Materials Measurement Science Division
Material Measurement Laboratory*

This publication is available free of charge from:
<https://doi.org/10.6028/NIST.NSRDS.100-2021>

March 2021



U.S. Department of Commerce
Wynn Coggins, Acting Secretary

National Institute of Standards and Technology
*James K. Olthoff, Performing the Non-Exclusive Functions and Duties of the
Under Secretary of Commerce for Standards and Technology &
Director, National Institute of Standards and Technology*

Disclaimer

The National Institute of Standards and Technology (NIST) uses its best efforts to deliver a high-quality copy of the database and to verify that the data contained therein have been selected on the basis of sound scientific judgement. However, NIST makes no warranties to that effect, and NIST shall not be liable for any damage that may result from errors or omissions in the database.

For a literature citation, the database should be viewed as a book published by NIST. The citation would therefore be:

W.S.M. Werner, W. Smekal and C. J. Powell,
Simulation of Electron Spectra for Surface Analysis (SESSA) - 2.2.0
National Institute of Standards and Technology,
Gaithersburg, MD (2021).

Version 1.0 of this database was released in December 2005.

Version 1.1 was released in December 2006 with an enhancement to the Model Calculation screen that permits the user to display and save the zero-order partial intensities. Previously, a user had to go to another screen to perform these operations.

Version 1.2 was released in March 2010 with the following enhancements: (1) an additional and more intuitive format for specifying the composition of a material; (2) a new capability to perform simulations with polarized photons; (3) the ability to save plots in additional file formats; (4) the addition of a chemical-shift database for selected peaks; (5) improvements in the peak-management software; (6) and the incorporation of a faster random number generator. In addition, an internet SESSA forum was established for user questions and a new SESSA bug-tracking web page was established.

Version 1.3 was released in May 2011 and provided a new database of non-dipole photoionization cross sections, necessary for simulations of X-ray photoelectron intensities with X-ray energies higher than a few keV. In addition, a description was given in Section 9 on how SESSA can be called and controlled from an external application.

Version 2.0 was released in October 2014 with additional capabilities for specifying specimen nano-morphologies (such as islands, lines, spheres and layered spheres on surfaces) and with updated data for electron inelastic mean free paths.

Version 2.1 was released in December 2017 and enables a user to easily create new sample nano-morphologies via the PENGEO geometry package. The present version of SESSA also has additional databases for electron inelastic mean free paths and inner-shell ionization cross sections by electron impact. Software bugs present in Version 2.0 have been corrected that could lead to erroneous results when using the morphology modes Spheres, Layered Spheres and Islands. Finally, a correspondence between the "Help" Menu within SESSA and the manual file is enabled.

Version 2.1.1 contains a fix of a software bug in the calculation of the photoelectron source angular distribution for the non-dipolar case.

Version 2.2, the present version, contains a new database for IMFP values. Surface excitations have been added to the simulations, as well as an effective approximation to account for the energy dependence of the inelastic mean free path.

Certain trade names and other commercial designations are used in this work for the purpose of clarity. In no case does such identification imply endorsement by the National Institute of Stan-

dards and Technology nor does it imply that the products or services so identified are necessarily the best available for the purpose.

Microsoft Windows® 95, Windows® 98, Windows® 2000, Windows® NT, Windows® XP, Windows® 7, Windows® 8, Windows® 10, Windows® Vista are registered trademarks of the Microsoft Corporation. Macintosh and OS X are trademarks of the Apple Corporation. Linux is a trademark of Linus Torvalds.

Table of Contents

1	Introduction	1
2	Getting Started	2
2.1	System Requirements	2
2.2	Installation	2
3	Special Features of SESSA	3
3.1	The graphical user interface (GUI)	3
3.2	The command line interface (CLI)	6
3.3	Representation of Data in SESSA	9
3.4	Output produced by SESSA	12
4	Running SESSA	14
4.1	The PROJECT Menu	14
4.1.1	Synopsis of CLI Commands.	15
4.2	The PLOT Menu	15
4.2.1	Synopsis of CLI Commands.	17
4.3	The PREFERENCES Menu	20
4.3.1	Synopsis of CLI Commands.	20
4.4	The SAMPLE Menu	21
4.4.1	The SAMPLE LAYER Menu	26
4.4.2	Synopsis of CLI Commands.	27
4.4.3	The SAMPLE MORPHOLOGY Menu	29
4.4.4	Synopsis of CLI Commands.	29
4.4.5	The SAMPLE PARAMETERS Menu	30
4.4.6	Synopsis of CLI Commands.	30
4.4.7	The SAMPLE PEAK Menu	35
4.4.8	Synopsis of CLI Commands.	38
4.5	The SOURCE Menu	41
4.5.1	Synopsis of CLI Commands.	43
4.6	The SPECTROMETER Menu	43
4.6.1	Synopsis of CLI Commands.	43
4.7	The GEOMETRY Menu	45
4.7.1	Synopsis of CLI Commands.	45
4.8	The DATABASE Menu	48
4.8.1	Synopsis of CLI Commands.	48
4.9	The MODEL Menu	51
4.9.1	Synopsis of CLI Commands.	53
5	Retrieval strategy and simulation model	56
5.1	Retrieval strategy of the expert system	56

5.2	Algorithm for spectrum simulation	57
5.2.1	The electron spectrum in AES/XPS	57
5.2.2	Multiple inelastic scattering: the partial energy distributions	59
5.2.3	Multiple elastic scattering: the partial intensities.	60
5.2.4	Modeling surface excitations in electron spectra	63
5.2.5	Spectrum modeling beyond the quasi-elastic approximation	66
5.3	Modeling of nanostructured surfaces in SESSA	68
5.4	Current limitations of databases and simulation	69
6	Physical Data in SESSA	71
6.1	Databases used in SESSA	72
7	Tutorials	80
7.1	Peak Intensities	81
7.1.1	Angular distribution of photoelectrons emitted from a homogeneous Au sample: Chandrasekhar's H -function.	81
7.1.2	Angle-resolved XPS for a homogeneous Al sample.	84
7.1.3	Angle-resolved XPS for an oxidized silicon wafer with a carbon contamination layer	86
7.1.4	Angular distribution of photoelectrons emitted from a stratified overlayer-substrate sample	89
7.1.5	Depth distribution function (DDF) in XPS: comparison with experiment	92
7.1.6	Surface morphology: influence of surface roughness.	95
7.2	Spectral Shape	97
7.2.1	Au overlayers on a Pb substrate: spectral shape as a function of overlayer thickness and emission angle	97
7.2.2	Need for empirical data to realistically describe spectral shapes.	99
7.2.3	Transfer of spectral data between different spectrometers	101
7.2.4	Handbook of simulated XPS spectra.	103
7.3	Techniques other than conventional AES/XPS	104
7.3.1	Total Reflection XPS (TRXPS)	104
7.3.2	Ion-induced Auger-electron emission.	108
8	Tutorials for simulating advanced geometries using PENGEO	110
8.1	Simulations with external PENGEO geometry files	110
8.2	Example: Simulation for infinite core-shell cylinders	112
8.2.1	Analytical model	112
8.2.2	SESSA simulation	114
8.2.3	Results	114
8.3	Example: Simulation for dispersed powder of core-shell particles including the angular distribution of photoelectrons	116
8.3.1	Creation of dispersed powder geometries of identical core-shell particles	117
8.3.2	Creation of dispersed powder geometries of core-shell particles with variable structural parameters	119
8.3.3	Visualization of dispersed powder geometries using LaTeX and PGF/TikZ	120
8.3.4	Simulation template for dispersed core-shell nanoparticle geometries	120
8.3.5	Simulation of the angular distribution of photoelectrons from a dispersed powder of core-shell particles	122
8.4	Guidelines for creating PENGEO geometries	125

9 Calling SESSA from an external application	131
9.1 The Program SESSA_LINUX.c	131
9.2 The Program SESSA_WINDOWS.c	133
10 Getting Help and additional information	136
10.1 Getting Help	136
10.2 General Information	136
10.3 Known issues	137
10.3.1 Porting session files between operating systems	137
11 Survey of applications of SESSA in the scientific literature	138
12 Contacts	142
13 Acknowledgments	143
14 Bibliography	144

1 Introduction

The objective of this database is to facilitate quantitative interpretation of Auger–electron and X-ray photoelectron spectra (AES/XPS) for surface analysis and to improve the accuracy of quantitation in routine analysis. For this purpose, the database contains physical data required to perform quantitative interpretation of an electron spectrum for a specimen with a given composition. Retrieval of relevant data is performed by a small expert system that queries the comprehensive databases. A simulation module [1, 2] is also available within SESSA that provides an estimate of peak intensities as well as the energy and angular distribution of the emitted electron flux (see Section 4.9). The information needed by the expert system to accomplish its task closely matches instrument settings made by an experimenter when actually performing a measurement and is complemented by an initial estimate of the sample composition.

SESSA can be used for two main applications. First, data are provided for many parameters needed in quantitative AES and XPS (differential inverse inelastic mean free paths, total inelastic mean free paths, differential elastic-scattering cross sections, total elastic-scattering cross sections, transport cross sections, photoelectric cross sections, photoelectric asymmetry parameters, electron-impact ionization cross sections, photoelectron lineshapes, Auger-electron lineshapes, fluorescence yields and Auger-electron backscattering factors). Second, Auger-electron and photoelectron spectra can be simulated for layered samples and for nanostructures such as islands, lines, spheres, and layered spheres on surfaces. The simulated spectra, for compositions and dimensions specified by the user, can be compared with measured spectra. The compositions and dimensions can then be adjusted to find maximum consistency between simulated and measured spectra.

The design of the software allows the user to enter the required information in a reasonably simple way. The modular structure of the user interface closely matches that of the usual control units on a real instrument. In other words, any user who is familiar with a typical electron spectrometer can perform a retrieval/simulation operation with the SESSA software in a few minutes for a specimen with a given composition.

Section 3 familiarizes the user with some special features of the software. These features include a separate window for graphical representation of a selected physical quantity that is fully controllable by the user (see Section 4.2), a popup menu showing the reference to the literature for each retrieved datum, an on-the-fly database selection popup menu and, last but not least, the fully parallel operation of the graphical user interface (GUI) and the command line interpreter (CLI).

Section 4 presents a detailed and comprehensive description of the functionality of the software, while Section 5 provides a description of the SESSA design and the means by which simulations are performed with SESSA. The sources for the physical data in SESSA as well as the simulation algorithm are described in Section 6, and Section 7 highlights some of the key features of the software with the aid of a few tutorials that are contained in this package in the form of CLI command files. Section 8 provides specific tutorials for use with SESSA 2.1 and gives guidance on the creation and use of PENGEO files for describing different types of nanostructures on surfaces. Section 9 describes how SESSA can be controlled by an external application. Additional help information is given in Sections 7 and 11.

2 Getting Started

2.1 System Requirements

- Operating System

The software has been tested to run on a personal computer with Windows operating systems such as Windows® 95, Windows® 98, Windows® NT, Windows® Vista, Windows® 7, Windows® 8, Windows® 10, Windows® 2000 and Windows® XP. NIST also supplies files for the database to run on Mac OS X and LINUX platforms. These files have been tested to run on these platforms but have not been as extensively tested as the Windows versions. They are considered by NIST to be non-supported software. The authors nevertheless welcome bug-reports, suggestions and comments for this software (as described in Section 11).

- Available Disk space

The databases and software need approximately 100 MB of disk space.

- Random Access Memory

The minimum amount of RAM required to run the program amounts to ~ 5MB. The exact amount of RAM needed depends on the type of the problem under study. When a simulation is performed, the minimum required RAM increases to 10 MB. When simulations are performed for large-scale complex problems (see Section 4.9) memory usage can increase even further.

2.2 Installation

For installation on a personal computer with the Windows operating system, follow the instructions to run *SESSA_setup.exe*. For other platforms, see the installation instructions.

3 Special Features of SESSA

SESSA contains a number of databases with data concerning excitation and transport of signal electrons (Auger electrons and photoelectrons) in solids. These databases are queried by a small expert system that retrieves all information needed for the interpretation of experimental results. The expert system needs a specification of the expected sample structure and of the experimental configuration, and will then retrieve physical data relevant to the specified experiment. If desired, the simulation of a specified experiment can be performed. The sample composition is specified by providing the thickness and composition for each of a number of layers and for the dimensions and compositions of nanostructures.

Two alternative methods are provided for user interaction with SESSA: a graphical user interface (GUI) and a command line interface (CLI). These interfaces operate in parallel: the action taken by SESSA is determined by the commands received by the CLI but does not depend on the way the command was generated. The CLI can process commands produced in three different ways: (1) commands typed on the CLI console; (2) a single command or a series of commands read from a file; and (3) commands generated by the GUI. Some of the general features of the CLI and the GUI are described in this Section to familiarize the user with the operation of the software. A detailed description of the software functionality and user interaction can be found in Section 4. Representation of several data types in the software is discussed in Section 3.3, and the output produced by SESSA is described in Section 3.4.

The notation used in this Chapter uses the following conventions: GUI commands are enclosed in quotation marks ("") while CLI COMMANDS and variables as well as filenames are set in a different font.

3.1 The graphical user interface (GUI)

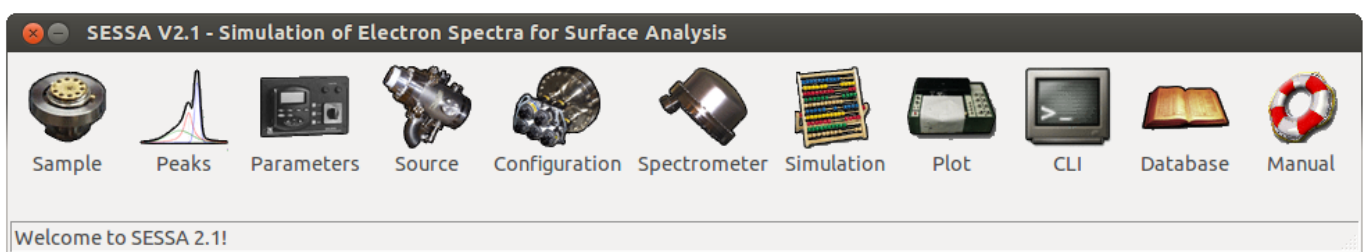


Figure 3.1: The main menu of SESSA.

The main menu of SESSA is shown in Fig. 3.1. The GUI in SESSA is organized by means of a number of submenus that can be reached via the main menu in the usual way. The available submenus and their shortcut commands are shown in Table 3.1. In each menu, data for a number of quantities are available for display and can be manipulated by the user. For a detailed description of the purpose of these menus, see Section 4.

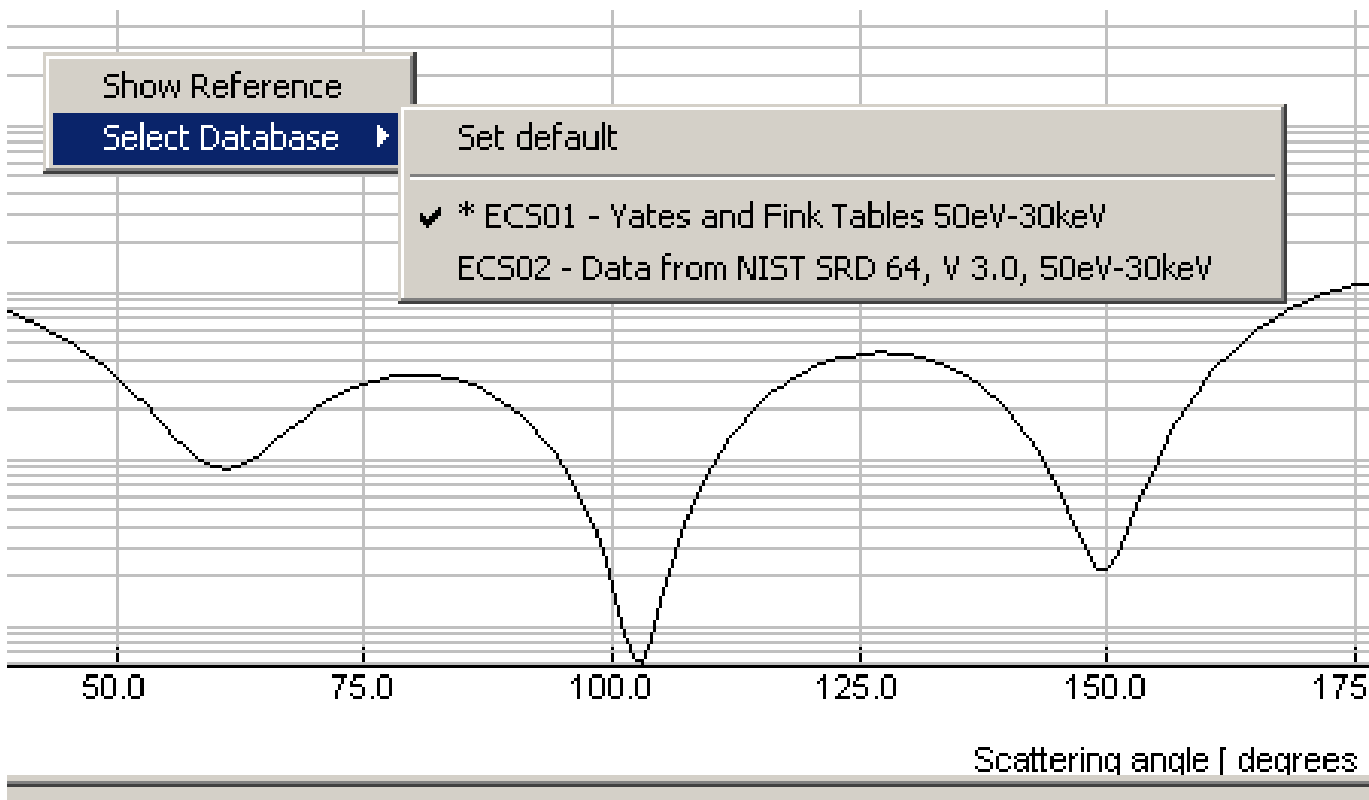


Figure 3.2: Example of a database selection popup menu.

Apart from the usual components of a typical GUI, SESSA also provides a graphical display of certain quantities. For example, press CTRL-3 for a graphical representation of the differential elastic–scattering cross section and the differential inverse inelastic mean free path. These displays cannot be changed in any way by the user. By double clicking on any of these displays, however, an additional plot window is opened that allows full user access to the display variables by means of a right mouse click (see Section 4.2). This plot window can also be opened from within the CLI by an appropriate command.

Two special features of SESSA are the traceability of the data and the on-the-fly selection of databases. By means of a right mouse click on a numerical value retrieved from a database, or on the corresponding graphical display, a menu pops up that offers two choices: either to activate the reference dialog or to activate the on-the-fly database selection menu (see Fig. 3.2). If the

Project		Project (Main) menu
Sample: layers	CTRL-1	Sample Composition
Sample: peak	CTRL-2	Parameters concerning signal electron generation
Sample: parameters	CTRL-3	Parameters concerning signal electron transport
Experiment: source	CTRL-4	Source of exciting radiation
Experiment: geometry	CTRL-5	Geometrical configurations
Experiment: spectrometer	CTRL-6	Spectrometer settings
Model	CTRL-7	Model Calculations
Database	CTRL-8	Selection of default databases for all relevant quantities
CLI Console	CTRL-9	User interaction via the command line interface (CLI)

Table 3.1: (Sub) menus of the GUI and their shortcut commands.

latter is selected, the user can choose between the different databases that are available for the quantity in question. Alternatively, the user can reset the choice of the database to the default database, i.e., the database that has been selected in the database defaults menu (see Section 4.8).

Since not every database in SESSA is extensive, in that it contains a datum for a given quantity for any arbitrary element, energy subshell, etc., it may happen that the requested datum is not returned by the selected database. In such cases, the expert system automatically queries the other databases available for the quantity in question. In this way, at least one of the databases contains a value or a credible estimate for the requested datum. In some cases, this “backup” database will rely on a theoretical or semi-empirical expression to predict the desired quantity. In the database selection popup menu, the database selected by a user is indicated by the sign \checkmark , while an asterisk (“*”) indicates the database that was successfully queried (see Fig. 3.2).

Most quantities in SESSA that are represented by a single value can be changed by the user if desired. The database selection menu provides a quick way to retrieve any value from a database. Quantities that can only be represented by an array of values, such as the differential cross section, cannot generally be directly changed by the user. The reference dialog is part of an im-

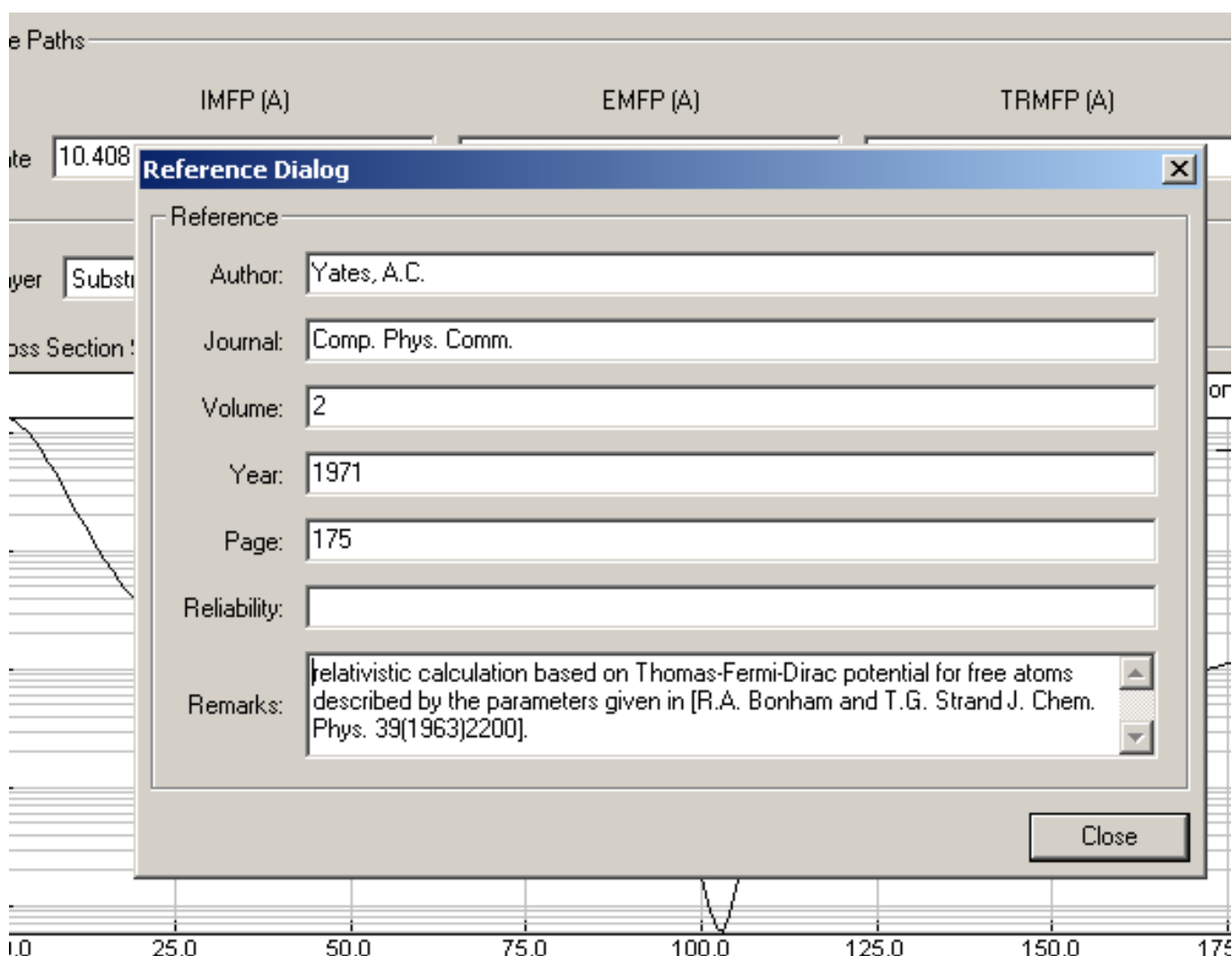


Figure 3.3: The reference dialog window.

lementation feature that provides full traceability of the data retrieved by SESSA: Every datum is accompanied by a reference that can be inspected at any time. In the GUI this is achieved by a right mouse click either on the numerical value of a parameter or on its graphical display window, as shown in Fig. 3.2. An example of the resulting information is given in Fig. 3.3. When fundamental physical data concerning an electron spectrum are given as outputs by the database (see Section 3.4), numbered references for all retrieved data are written to a separate file with the ending "refs.txt", while the remarks in the lower two boxes of the reference dialog window are accordingly numbered and written to a file with the extension "rems.txt".

3.2 The command line interface (CLI)

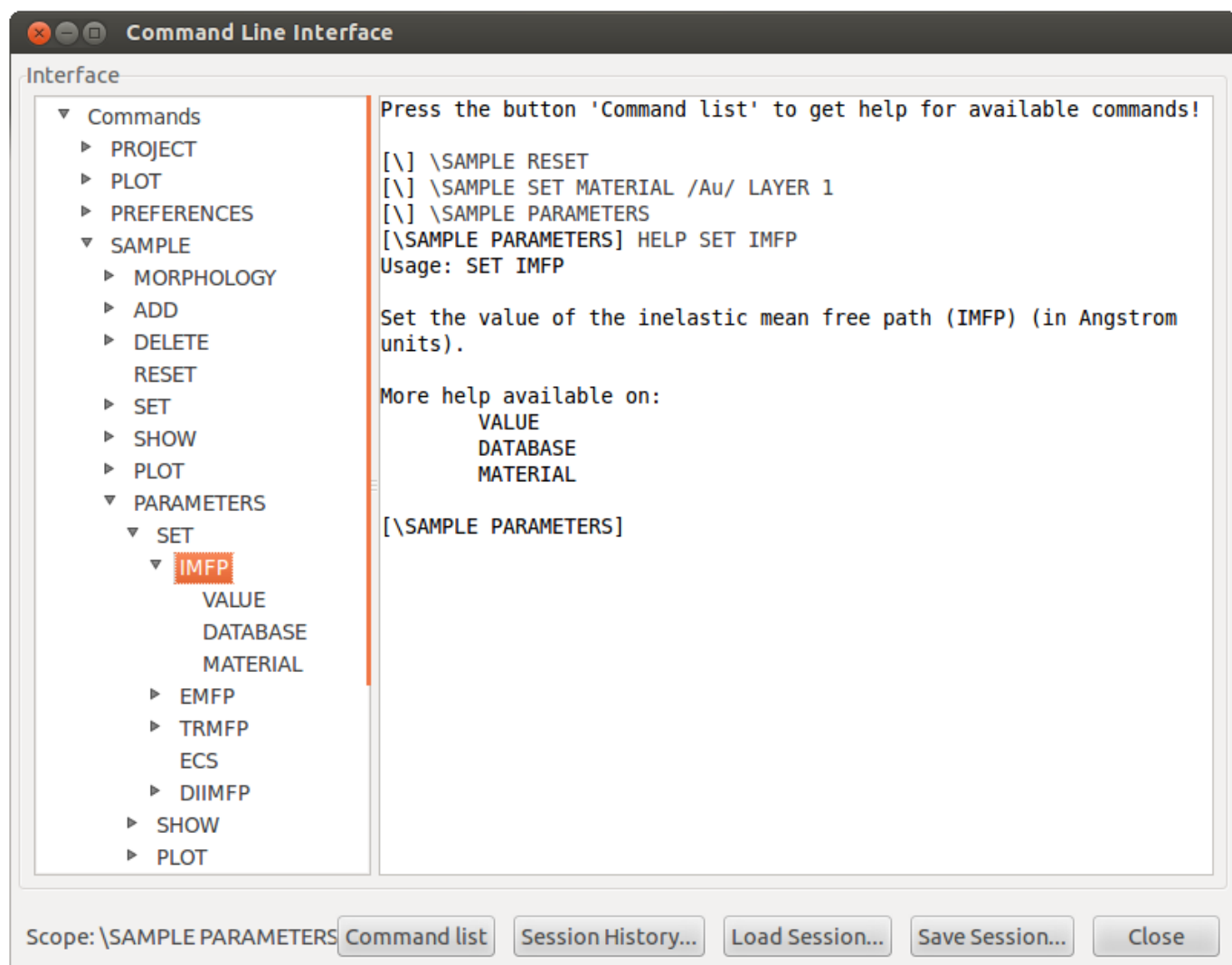


Figure 3.4: The command line interface console.

The CLI console can be opened by selecting the "Project/Command Line Interface" menu in the project menu or by pressing the shortcut key CTRL-9. The CLI console window is shown in Fig. 3.4. At the bottom of the CLI console, a number of buttons are seen. Clicking the "Command List" button opens a window within the CLI console that presents the structure of the commands

of the CLI. Clicking on any of these commands generates a text string on the CLI corresponding to the command in question preceded by HELP. As a result, the help text corresponding to the selected command is displayed in the CLI. In Fig. 3.4 the above is illustrated for the command SAMPLE PARAMETERS SET IMFP. Any command appearing in the CLI may be edited by using the up and down arrow and the delete key etc., and can be entered by pressing return. In this way, a command generated by clicking on the command list can be used to operate the software. Thus the command list provides a most useful reference guide for the CLI syntax.

In the command line interpreter, the modularity of the software is realized by the use of different scopes, each scope allowing a user to manipulate or inspect a certain subset of the relevant data and control parameters corresponding to a window in the GUI. Table 3.2 gives a survey of the scopes presently defined in SESSA¹. The acronyms shown and defined in Table 3.2 are frequently used in SESSA.

The active scope is indicated by the command prompt at the bottom left of the CLI console window. To set a scope from within the main scope, one simply has to enter the name of the scope, as provided by Table 3.2. Any command entered in the CLI that is preceded by a backslash ("\\") is interpreted as if it were entered in the main scope. In particular, to set the scope from within another scope, one can enter the name of the scope preceded by a backslash ("\\")-character. The exit command allows a user to move down one level in the hierarchy of scopes. The following example illustrates three alternative ways to set the scope to "Sample\Parameters":

1. directly from the main scope:

```
[>]sample parameters  
[> SAMPLE PARAMETERS]
```

2. in two steps from the main scope:

```
[>]sample  
[> SAMPLE] parameters  
[> SAMPLE PARAMETERS]
```

3. directly from within any other scope:

```
[> DATABASE]\ sample parameters  
[> SAMPLE PARAMETERS]
```

As an instructive example of the parallel operation of the GUI and CLI, press CTRL-5 to open the "Experiment/geometry" menu and change, say, the sample orientation azimuth (phi) to 45°. Now press CTRL-9 to open the CLI console. On the console, the command \GEOMETRY SET SAMPLE PHI 45 GEO 1 appears as it was generated by the GUI. By pressing the up, left and right arrows on the CLI console, the command can be edited and entered again, for example to set the sample azimuth to 30°. Bringing the "Experiment/geometry" menu to the front again by pressing CTRL-5 gives a graphical display of the new orientation of the sample surface normal. Scrolling through the list of commands processed by SESSA is possible by using the up and down arrow in the CLI console. Alternatively, an easily surveyable list of the processed CLI commands can be displayed by clicking on the "Session History" button in the CLI console. Any of the commands in this list

¹In the present implementation of SESSA there is an exception to the one-to-one correspondence between the GUI menus and the CLI scopes: the geometry, source and spectrometer scopes have been organized as submenus of an experiment menu in the GUI, but are separate scopes in the CLI. The scopes in the CLI will be modified later to match the menus in the GUI.

1	main
2	\ sample
3	\ \ peak
4	\ \ parameters
5	\ source
6	\ spectrometer
7	\ geometry
8	\ simulation
9	\ database
10	\ \ DIIMFP
11	\ \ SEP
12	\ \ IMFP
13	\ \ ECS
14	\ \ EMFP
15	\ \ TRMFP
16	\ \ PCS
17	\ \ PAP
18	\ \ EIICS
19	\ \ XPL
20	\ \ AEL
21	\ \ FY
22	\ \ ABF

Table 3.2: (Sub)-scopes of the CLI. The acronyms are defined in Table 3.3. Further information is given in Section 6

can be processed again by double clicking on it. The session history can be cleared by pressing the corresponding button in the session history command list. This is an important feature for producing CLI command files using the "Save session" command (see below).

The great advantage of this parallel CLI/GUI interface is that a set of CLI commands can be read from or written to a text file, using the PROJECT LOAD/SAVE SESSION commands or by pressing the "Load/save session" button on the CLI console. This makes it possible to process a large batch of commands. Such CLI command files can be produced in a simple way by a user without any knowledge of the CLI syntax. This can be done by a series of mouse clicks in the GUI and saving all previously entered commands by pressing the "Save session" button on the CLI console. The tutorials described in Section 7 are examples of CLI command files produced in this way. A "#" character at the beginning of a line in a CLI command file designates the line as a comment.

Another example of a SESSA CLI file is a file by the name of "SESSA_ini.ses" that resides in the directory where the SESSA-binary is located. This file is read whenever the software starts up and the commands contained in it are processed by the CLI. This may be advantageous for a user who commonly works on problems requiring settings that differ from the default settings in SESSA. This may concern the radiation type, the instrument settings, the sample composition, and so on.

A group of commands from the CLI can also be copied and pasted into word processing software and saved as a text file. Multiple files can be created in this way and loaded into SESSA to avoid the tedium and possible mistakes from using the GUI for multiple similar simulations. Similarly, a user can assemble desired setup files for a particular purpose by combining selected command lines from existing files. Finally, a user can assemble files for batch runs (e.g., for a series of XPS configurations or for a series of layer thicknesses). Each file can specify different file names to save spectra or peak intensities from a series of simulations. SESSA will create

IMFP	Inelastic Mean Free Path
DIIMFP	Differential Inverse Inelastic Mean Free Path
TECS	Total Elastic Cross Section
TRECS	Transport (Elastic) Cross Section
ECS	(Differential) Elastic Cross Section
EMFP	Elastic Mean Free Path
TRMFP	Transport Mean Free Path
PAP	Photoionization Asymmetry Parameter
PAG	Photoionization non-dipolar Asymmetry Parameter γ
PAD	Photoionization non-dipolar Asymmetry Parameter δ
EIICS	Electron Impact Ionization Cross Section
ABF	Auger Backscattering Factor
FY	Fluorescence Yield
PCS	Photoionization Cross Section
XPL	X-ray Photoelectron Lineshape
AEL	Auger Electron Transition Lineshape

Table 3.3: Acronyms for the physical quantities in the SESSA databases.

these files in the same directory as that from which setup files were loaded.

3.3 Representation of Data in SESSA

A CLI command as well as an input field in the GUI may comprise special data types as indicated in Table 3.4.

1. **integer:** an integer number whose range depends on the Operating System (OS) of the computer.
2. **real:** a real number with OS dependent range. The character "e" signifies exponentiation to a power of ten. For example, the expressions -0.0099, -99.0e-3 and -99e-3 are all valid expressions for the same real number.
3. **string:** a string of characters. A string may contain all alphanumerical characters and special signs ("% ", "*", etc.) in upper or lower case. If a string contains spaces, it must be enclosed in single quotes, e.g. "Au, 1000 eV".
4. **filename:** a string of characters designating a file of the operating system with a filename valid in the operating system.
5. **DBName:** a predefined string of characters designating a set of data within SESSA (see Section 4.8).
6. **material:** The material specifier is a special string of characters that allows the program to recognize the elements and stoichiometry in a given material. It identifies the elements present in the sample and their chemical state, allowing the software to retrieve the relevant information. For a user, there are two different ways to enter the material in the sample menu: one way is to enter the material specifier in the format used internally by SESSA, with a special syntax (e.g., "/SI/O2/" for silicon dioxide), as explained below. The alternative

$\langle \text{integer} \rangle$	an integer number
$\langle \text{real} \rangle$	a real number
$\langle \text{string} \rangle$	a string of characters
$\langle \text{filename} \rangle$	a string designating a file of the OS
$\langle \text{DBName} \rangle$	a string designating a set of data within SESSA
$\langle \text{material} \rangle$	a material specifier
$\langle \text{subshell} \rangle$	a subshell specifier

Table 3.4: Special data types for SESSA user interaction

method is to enter the material in a more intuitive syntax (e.g., “SiO₂” for silicon dioxide). If the material is specified in this simpler, more intuitive way, SESSA will translate this into the internal syntax that will be displayed in the material field in the GUI. Since the internal syntax is more powerful than the intuitive syntax, it will be described first and then the intuitive syntax.

The internal material specifier consists either of a number of compound specifiers, or a number of constituent specifiers, or both. The constituent specifier, enclosed in slashes “/” consists of an element identifier (the usual abbreviation of the element’s name from the periodic table of the elements), a chemical state attribute (an arbitrary string specified by the user enclosed in square brackets “[]”) and a real number describing the abundance of this species in a given layer of the compound or material:

$$\langle \text{constituent specifier} \rangle = / \langle \text{element identifier} \rangle [\langle \text{chemical state attribute} \rangle] \langle \text{abundance} \rangle /$$

Here

- $\langle \text{element identifier} \rangle$ represents a chemical symbol (H, He, Li, Be..) (case insensitive)
- $\langle \text{chemical state attribute} \rangle$ is an arbitrary string indicating the chemical state
- $\langle \text{abundance} \rangle$ is a positive real number indicating the relative abundance of the element in a given layer.

If the chemical state attribute is omitted, the software recognizes the constituent as the elemental form of the chemical species. If the relative abundance is omitted, it is taken to be unity.

A compound specifier consists of a number of constituent specifiers enclosed in parentheses “()” followed by the relative abundance of the considered compound, or by several compound specifiers. Nesting of compound specifiers is allowed. Again, if the abundance is omitted, it is taken to be unity.

$$\langle \text{compound specifier} \rangle = (A) x_A (B) x_B \dots$$

where A, B, ... are arbitrary combinations of compound or constituent specifiers and x_A , x_B are their relative atomic abundances. The concentration of compound A in this material is given by:

$$c_A = \frac{x_A}{x_A + x_B + \dots} \quad (3.1)$$

If the compound A is given by the constituents A_1, A_2, \dots etc. with abundances x_{A1}, x_{A2}, \dots etc., then A is specified as follows:

$$A = /A_1x_{A1}/A_2x_{A2}/\dots/, \quad (3.2)$$

and the concentration of the species A_i in the considered material is given by:

$$c_{A_i} = \frac{\left(\frac{x_{A_i}}{\sum_j x_{A_j}}\right)}{x_A + x_B + \dots} \quad (3.3)$$

The more intuitive syntax for the material specifier is a string of characters containing the chemical symbols of the elements and their abundances in the material without forward slashes. In this case the specification of the chemical symbols of the elements is case sensitive, e.g. "Si", "Fe", "Au" are valid chemical symbols for silicon, iron and gold, respectively, while "SI", "FE" and "AU" are invalid in the intuitive syntax. The reason is simply that case insensitive chemical symbols are not uniquely identifiable. For example "SI" might be interpreted as a sulfur–iodine compound or as silicon, "CO" might be interpreted as cobalt or carbon monoxide. The omission of the forward slashes and the case sensitivity is the main difference between the intuitive syntax and the internal syntax. The syntax for the chemical state attribute and the compound specifier is the same in both syntaxes.

Some examples:

- a) /S/I/O3.0e0/. A (very hypothetical) solid consisting of the three elements Sulfur, Iodine and Oxygen, all of them present in elemental form in relative amounts 1:1:3.
 - b) (/si[oxide]/O2/)99(/c/)1. A typical Silicon dioxide layer that contains Silicon bound to Oxygen, Oxygen and Carbon contamination. The relative amounts of the elements in the layer are 0.33:0.66:0.01.
7. **subshell:** a subshell may be specified by a string consisting of the principal quantum number n followed by the usual symbol for the angular momentum quantum number l (s for $l = 0$, p for $l = 1$, d for $l = 2$ and f for $l = 3$) and the usual symbol indicating the spin state e.g. "1/2", "3/2" etc. The subshell may be abbreviated to the unambiguous shortest form, e.g. "4f7" is equivalent to "4f7/2".

3.4 Output produced by SESSA

Information concerning the experimental settings specified by the user, the retrieved data corresponding to these settings, and the outcome of a model calculation can be written to a number of files by selecting the "Project/Save/Output" option in the GUI or by issuing the command PROJECT SAVE OUTPUT in the CLI. As a result a number of different files containing information in several categories are generated. For several categories, writing of the output can be (de)activated in the "Project/preferences" menu (see Section 4.3).

1. filenames ending with: "sam_lay.txt"

The sample structure

2. filenames ending with: "sam_peak.txt","sam_par.txt"

Signal electron generation and transport

3. filenames ending with: "exp.txt","prefs.txt"

The experimental settings and preferences settings

4. filenames ending with: "refs.txt","rems.txt"

References to works in the literature concerning the above and accompanying remarks

5. filenames ending with: ".spc",".pi",".adf",

These files are written if a model calculation was performed and contain the corresponding results. The output is divided into region data, corresponding to a certain energy-region setting for the spectrometer, and peak data, corresponding to a certain spectral line. The region data are written to files with names identified by the string "reg<region number>", where "<region number>" is an integer referring to the spectrometer region. The peak data are written to files identified by a peak identifier, consisting of the chemical symbol followed by the transition specifier. This is either the subshell abbreviation in case of an XPS peak (e.g. "2p3") or the Auger transition specifier (e.g. "L3M23M45").²

The filenames ending with ".spc" contain the energy spectra of the various peaks and regions for all selected geometries. The filenames ending with ".pi" contain the partial intensities for each peak and all geometries. If the number of geometries is larger than one, files ending with ".adf" are created that contain the partial intensities for the specified peak for all specified geometrical configurations. If ncol=0 is selected in the model menu (see Section 4.9) and the number of specified geometries is larger than one, it is assumed that the angular distribution of the peak intensities (zero-order partial intensities) is of main interest. In this case, the file "all.adf" is created and contains the peak intensities for *all* peaks as a function of the specified geometrical configurations.

6. filenames ending with: ".g"

Files that can be loaded into the Program GNUPLOT (see <http://www.gnuplot.info>) that has proven to be convenient for further graphical post-processing of the simulation data.

²An Auger spectrum may consist of many peaks. The Auger transitions for the more intense peaks can often be identified [3–5]. Other peaks are observed that arise from intrinsic excitations during the initial ionization or to extrinsic (energy-loss) processes as the Auger electrons travel in the material. We adopt a system here [5] in which a peak in an Auger spectrum is simply labeled with three letters indicating the shell and a number indicating the subshell (e.g., "L3M23M45"). The first letter (L) indicates the shell in which the initial ionization occurred, the second and third letter (M) indicate shells participating in the Auger transition, and the numbers designate the involved subshells.

An alternative quick and convenient means to produce output is to use the PLOT SHOW DATA option in the main plot window popup menu that displays the data contained in a plot in a separate read-only window (see Section 4.2), together with the relevant literature citation. The information in this window can be copied and pasted into another application for further processing.

4 Running SESSA

This chapter describes all commands utilized by the command line interface (CLI) in some detail. Since a close correspondence exists between the CLI and the graphical user interface (GUI), no detailed description of the latter is given. In most cases, it is evident which component of the GUI provides the equivalence to a certain CLI command. In the CLI, however, it is often necessary within a command to specify which peak, which geometry, which layer etc. one is addressing with the issued command. This situation can lead to awkward syntax such as “DO SOMETHING LAYER 1 PEAK 2 REGION 3”. In the GUI, the situation can be handled in a more elegant way within a submenu by means of one or more graphical selection tools. For example, there is an equivalence between the “Choose peak” and “Choose layer” selection boxes in the “Sample/parameters” menu in the GUI and the peak number and layer number in the equivalent CLI command (SAMPLE PARAMETERS PLOT ECS PEAK <PEAK#> LAYER <LAYER #>).

In the following sections concerning the CLI syntax of various scopes below, < > represents a parameter of the type indicated that has to be entered by the user, while [] is an optional parameter that may be omitted.

The energies displayed in and accepted by both the GUI and the CLI can be specified either on a kinetic-energy scale or, in the case of incoming photons, it may optionally be specified on a binding-energy scale. The user can set a preference in the “Project/preferences” menu. Depending on this setting, an energy referred to in the remainder of this Section is implied to be specified either on a kinetic- or a binding-energy scale.

4.1 The PROJECT Menu

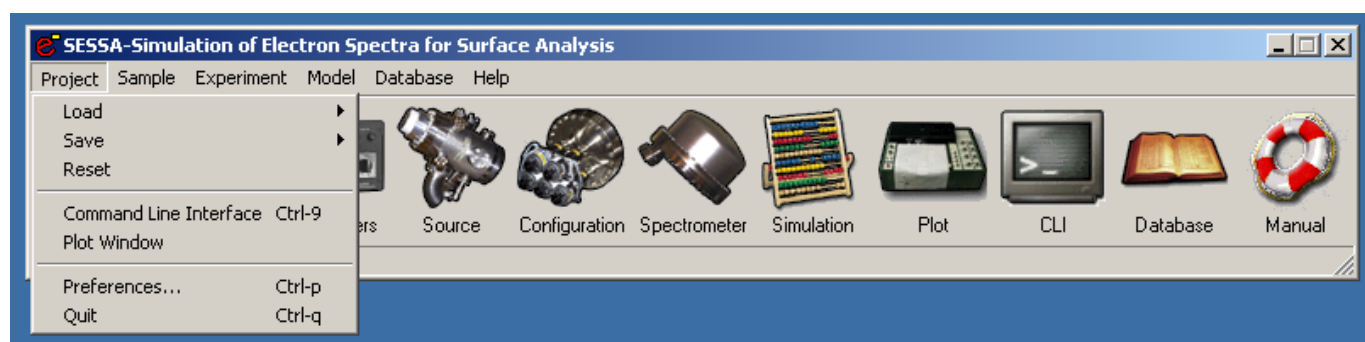


Figure 4.1: Graphical user interface for the PROJECT Menu.

The “Project” menu in the GUI is shown in Fig. 4.1. The CLI console, the separate plot window and the preferences dialog can be opened from within the project menu. The plot window, the CLI console and the preferences dialog are described below. Apart from that, the project menu is equivalent to the project menu in the CLI, as described in the next section.

4.1.1 Synopsis of CLI Commands.

1. PROJECT SAVE SESSION <string>

Save command history to the file <string >. Each command typed in during your session (or generated by clicking in the GUI) is written to a text file. This file may be later executed, but it can also be edited and modified to enable processing of a batch of commands. In this way, one can generate calibration curves of various kinds, angular distributions of peak intensities, etc.

2. PROJECT SAVE OUTPUT <string>

Save output to files beginning with the ID <string >.

3. PROJECT LOAD SESSION <string>

Load command history from the file <string >.

4. PROJECT RESET

Clear all data and reset everything to the default values.

4.2 The PLOT Menu

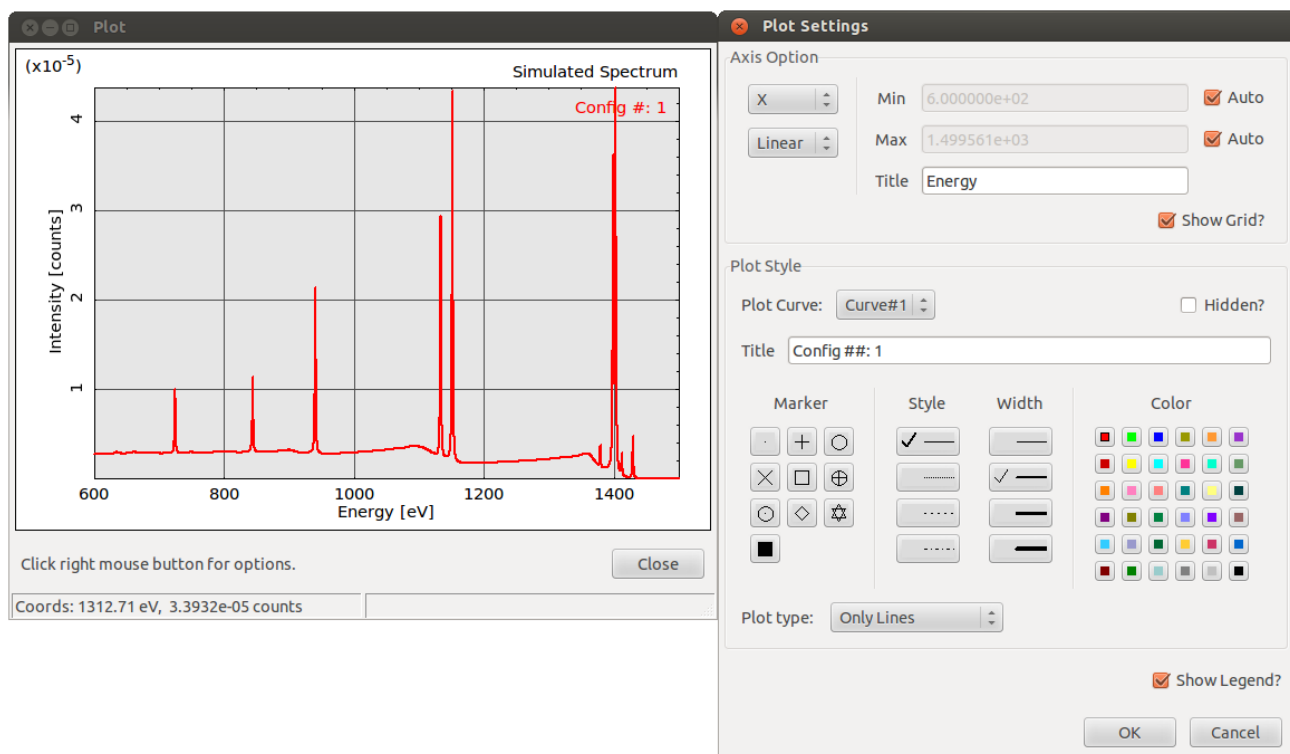


Figure 4.2: Graphical user interface for the PLOT and the PLOT/Settings Menu.

Data can be displayed in a separate window that allows full user access to the display parameters by double clicking on the window. Various quantities in SESSA can be graphically displayed. These displays can not in any way be changed by the user. However, by double clicking on any of these windows, a separate plot window is opened providing full user access to the plot settings, as



Figure 4.3: Read-only window displaying the data contained in the plot window. The data in this window can be transferred to other software by means of copy and paste operations for further processing.

shown in Fig. 4.2 as an example. This plot window is also accessible via the "Project/Plotwindow" command in the GUI and through appropriate commands (pertaining to the quantity on display) in the CLI. A right mouse click in the plot window activates a popup menu that opens the plot settings window (see Fig. 4.2), a comprehensive menu for manipulating the settings of the display. Alternatively, output of the graphical display in form of a postscript file may be selected in the plot popup menu, or a quick axis settings menu can be activated. The latter allows a user to set the axis range, and to turn on/off an axis grid or a logarithmic scaling of the axis. Furthermore, the user the popup menu can be utilized to open a read-only window displaying the data contained in the plot along with the corresponding references, as indicated in Fig. 4.3.

4.2.1 Synopsis of CLI Commands.

1. PLOT SET LOG X
Selects the x-axis for logarithmic scaling.
2. PLOT SET LOG Y
Selects the y-axis for logarithmic scaling.
3. PLOT SET NOLOG X
Selects the x-axis for linear scaling.
4. PLOT SET NOLOG Y
Selects the y-axis for linear scaling.
5. PLOT SET AUTO XRANGE
Selects the upper and lower limits of the x-axis for automatic scaling.
6. PLOT SET AUTO XLOW
Selects the lower limit of the x-axis for automatic scaling.
7. PLOT SET AUTO XHIGH
Selects the upper limit of the x-axis for automatic scaling.
8. PLOT SET AUTO YRANGE
Selects the upper and lower limits of the y-axis for automatic scaling.
9. PLOT SET AUTO YLOW
Selects the lower limit of the y-axis for automatic scaling.
10. PLOT SET AUTO YHIGH
Selects the upper limit of the y-axis for automatic scaling.
11. PLOT SET GRID X
Selects the x-axis grid for drawing.
12. PLOT SET GRID Y
Selects the y-axis grid for drawing.
13. PLOT SET NOGRID X
Disable drawing of the grid for the x-axis.
14. PLOT SET NOGRID Y
Disable drawing of the grid for the y-axis.

15. PLOT SET LEGEND

Activate drawing of a legend in the plot.

16. PLOT SET NOLEGEND

Deactivate drawing of a legend in the plot.

17. PLOT SET XRANGE <string>

Sets the x-axis range to <string >. Syntax to specify the range: 'xlo:xhigh'. Example: set xrange 1400:1500.

18. PLOT SET YRANGE <string>

Sets the y-axis range to <string >. Syntax to specify the range: 'ylo:yhigh'. Example: set yrange 1400:1500.

19. PLOT SET CURVETITLE <string> [CURVE <int>]

Sets the legend of the curve to <string >.

- CURVE: Number of the selected curve.

20. PLOT SET LTYPE <int> [CURVE <int>]

Sets the linetype of the selected curve (0- data points; 1- solid line; 2- data points and line).

- CURVE: Number of the selected curve.

21. PLOT SET COLOR <int> [CURVE <int>]

Sets the color of the selected curve (integer between 0 and 30).

- CURVE: Number of the selected curve.

22. PLOT SET WIDTH <int> [CURVE <int>]

Sets the linewidth of the selected curve (integer between 0 and 3).

- CURVE: Number of the selected curve.

23. PLOT SET DASH <int> [CURVE <int>]

Sets the dash style of the selected curve (integer between 0 and 10).

- CURVE: Number of the selected curve.

24. PLOT SET SYMBOL <int> [CURVE <int>]

Sets the symbol style of the selected curve (integer between 1 and 10).

- CURVE: Number of the selected curve.

25. PLOT SET VISIBLE CURVE <int>

Number of the selected curve.

26. PLOT SET VISIBLE ALL

Sets all curves to visible.

27. PLOT SET INVISIBLE CURVE <int>

Number of the selected curve.

28. PLOT SET INVISIBLE ALL

Selects all curves for hiding.

29. PLOT SET TITLE <string>
Sets the title of the plot to <string> .
30. PLOT SET XLABEL <string>
Sets the x-axis label of the plot to <string> .
31. PLOT SET YLABEL <string>
Sets the y-axis label of the plot to <string> .
32. PLOT SAVE DATA <string>
Save plot data of each curve to the text file <string> .
33. PLOT SAVE POSTSCRIPT <string>
Save plot as postscript to the file <string> .
34. PLOT SAVE PDF <string> [PAGESIZE <string>]
Save plot as pdf to the file <string> .
 - PAGESIZE: Set the page size. Allowed values are Letter, A3, A4, A5. A4 is the default page size.
35. PLOT SAVE PNG <string> [WIDTH <int>] [HEIGHT <int>]
Save plot as png to the file <string> .
 - WIDTH: Width of created image.
 - HEIGHT: Height of created image.
36. PLOT SAVE GIF <string> [WIDTH <int>] [HEIGHT <int>]
Save plot as gif to the file <string> .
 - WIDTH: Width of created image.
 - HEIGHT: Height of created image.
37. PLOT SAVE BMP <string> [WIDTH <int>] [HEIGHT <int>]
Save plot as bmp to the file <string> .
 - WIDTH: Width of created image.
 - HEIGHT: Height of created image.
38. PLOT SAVE JPG <string> [WIDTH <int>] [HEIGHT <int>]
Save plot as JPG to the file <string> .
 - WIDTH: Width of created image.
 - HEIGHT: Height of created image.
39. PLOT SAVE SVG <string>
Save plot as svg to the file <string> .
40. PLOT SHOW REFERENCE [CURVE <int>]
Show the refence of the selected curve.
 - CURVE: Number of the selected curve.
41. PLOT SHOW DATA
Display the data in the plot.

4.3 The PREFERENCES Menu

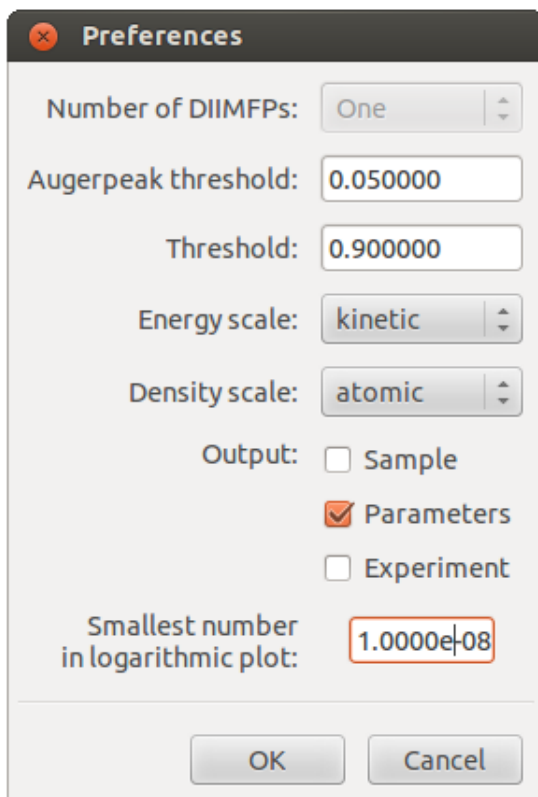


Figure 4.4: Graphical user interface for the PREFERENCES Menu.

The preferences menu allows a user to control various parameters determining the operation of SESSA as is shown in Fig. 4.4.

4.3.1 Synopsis of CLI Commands.

1. PREFERENCES SET NDIIMFP <int>

In a simulation, a user takes into account two different distributions of energy losses for the upper two layers in the sample. When the default value is chosen (NDIIMFP=1), it is assumed in a simulation that the differential inelastic mean free path is the same for all depths. This assumption usually provides a satisfactory approximation. However, if the electronic structures of the first two layers of the sample are substantially different, this difference may be observed in the loss features on the low-kinetic-energy side of the main peaks. In such cases it may be advisable to choose (NDIIMFP=2). Note that this may considerably increase the computation time for a simulation. Choosing yet another distribution of energy losses for deeper layers is not possible, but such effects will hardly ever be observable in an experimental spectrum.

2. PREFERENCES SET THRESHOLD <double>

Sets the threshold determining whether a peak retrieved from a database should actually be taken into account in any of the energy regions, as defined in the spectrometer menu. If the

fractional area of a peak within the region is below this threshold, the peak is rejected from the peak list. The default value is 0.9

3. PREFERENCES SET AES_THRESHOLD <double>

Sets the threshold determining whether an Auger peak retrieved from a database should actually be taken into account in any of the energy regions, as defined in the spectrometer menu. If the sensitivity factor is below this threshold, the peak is rejected from the peak list.

4. PREFERENCES SET PLOT_ZERO <double>

Sets the smallest positive number displayable in a logarithmic plot.

5. PREFERENCES SET ENERGY_SCALE KINETIC

Sets the energy scale to kinetic energy.

6. PREFERENCES SET ENERGY_SCALE BINDING

Sets the energy scale to binding energy if the excitation is with photons.

7. PREFERENCES SET DENSITY_SCALE ATOMIC

Sets the units for the density to atoms/cm³.

8. PREFERENCES SET DENSITY_SCALE MASS

Sets the units for the density to g/cm³.

9. PREFERENCES SET OUTPUT SAMPLE <string>

If < string >='true', information concerning the sample composition is included in the output.

10. PREFERENCES SET OUTPUT PARAMETERS <string>

If < string >='true', information concerning the parameters for electron generation and transport is included in the output.

11. PREFERENCES SET OUTPUT EXPERIMENT <string>

If < string >='true', information concerning the experimental settings is included in the output.

12. PREFERENCES SET OUTPUT GNUPLOT <string>

If < string >='true', special files for graphical post-processing with GNUPLOT are included in the output.

13. PREFERENCES SHOW

Show the values of the parameters in the PREFERENCES menu (only available in the CLI).

4.4 The SAMPLE Menu

This menu controls the parameters specifying the structure of the sample and the physical parameters of the sample of relevance for the particular experimental conditions, as shown in figures 4.5 to 4.10. The sample is conceived to consist of a number of non-crystalline and continuous layers each with a given composition, density and thickness. The interface between the various layers is assumed to be ideally flat, except for the vacuum-solid interface that may exhibit a particular type of roughness. The sample screen of SESSA allows the user to select five types of surface morphology:

1. Flat planar layered surfaces, as shown in Fig. 4.5

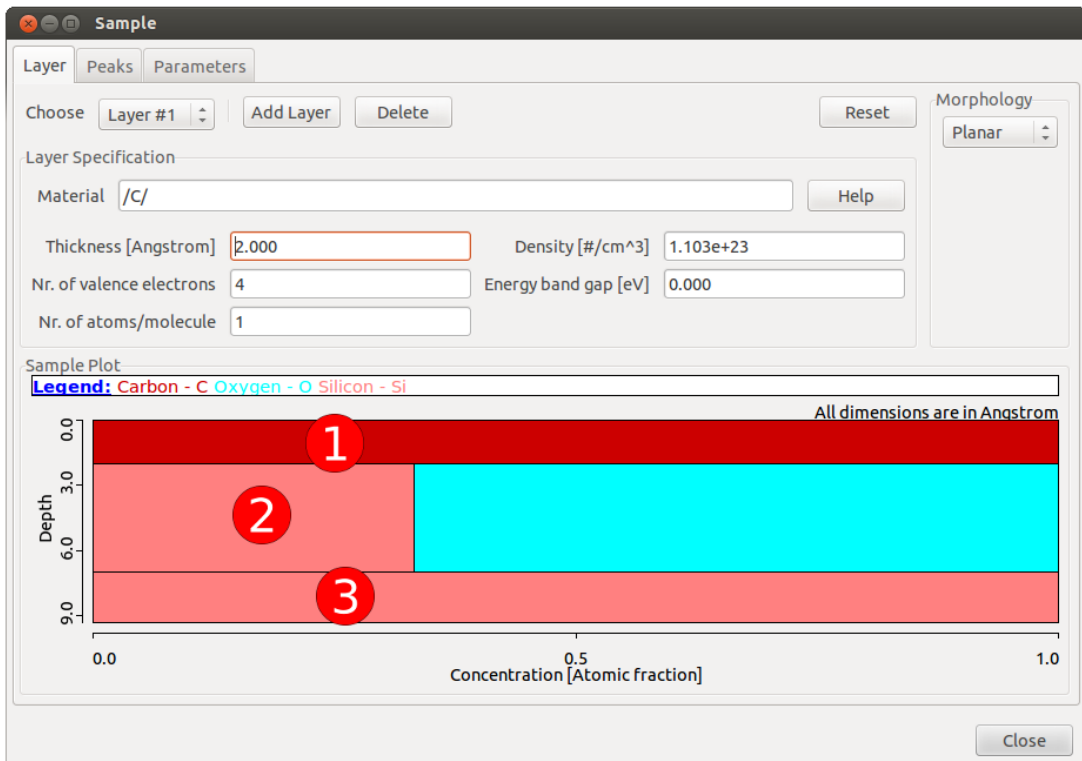


Figure 4.5: Graphical user interface for the SAMPLE Menu when the selected morphology is a planar sample. The white numbers in red circles designate layer numbers.

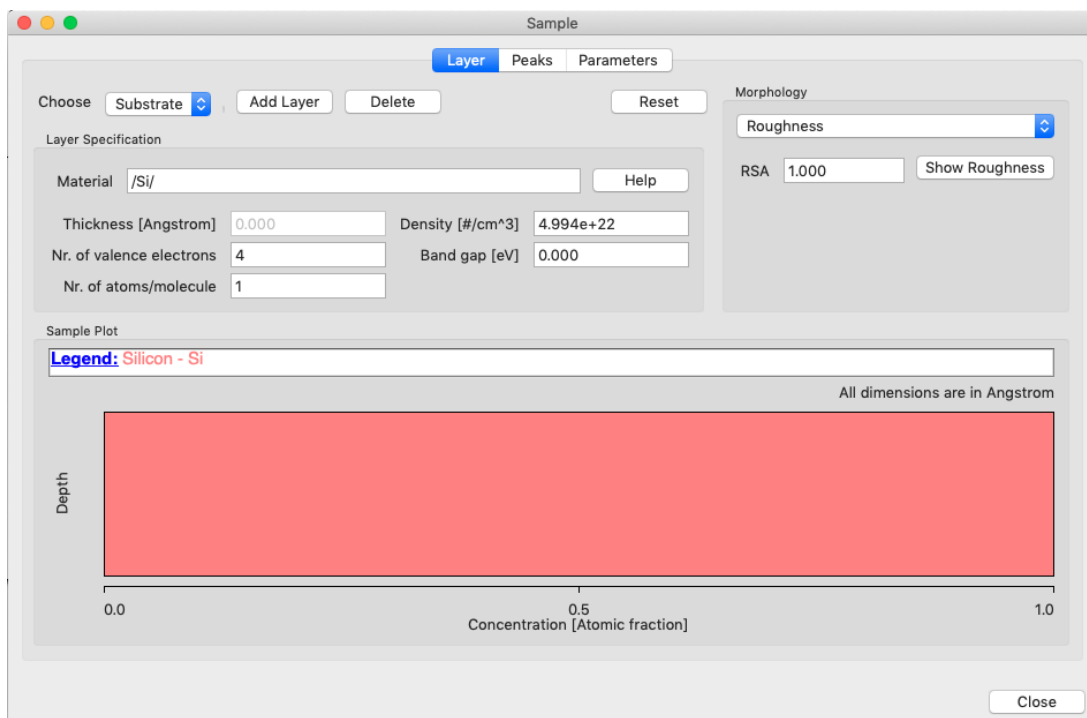


Figure 4.6: Graphical user interface for the SAMPLE Menu when the selected morphology is a surface with a specified roughness.

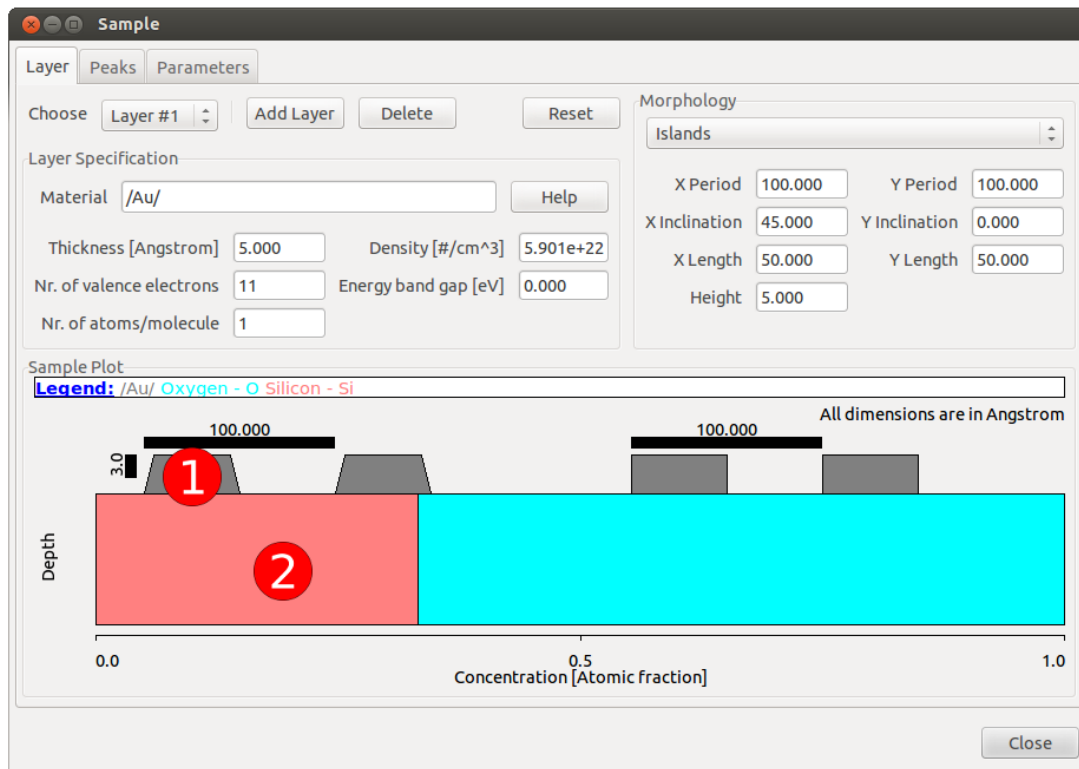


Figure 4.7: Graphical user interface for the SAMPLE Menu for morphology type “islands”. The white numbers in red circles designate layer numbers.

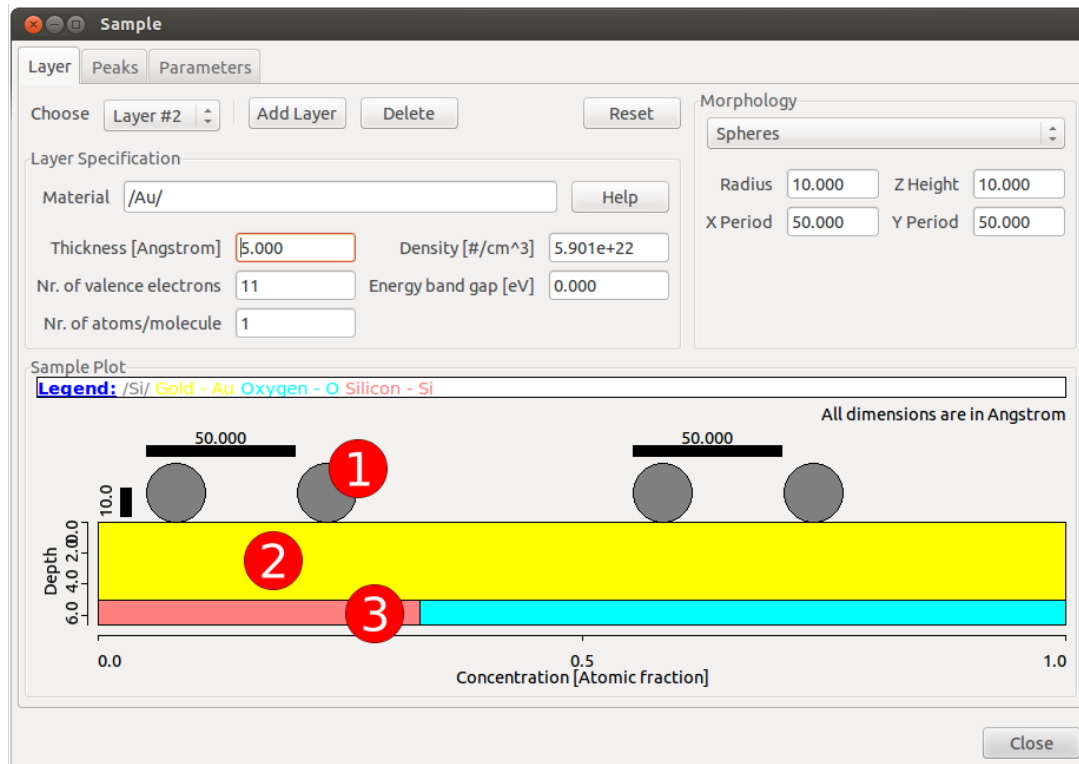


Figure 4.8: Graphical user interface for the SAMPLE Menu for morphology type “spheres”. The white numbers in red circles designate layer numbers.

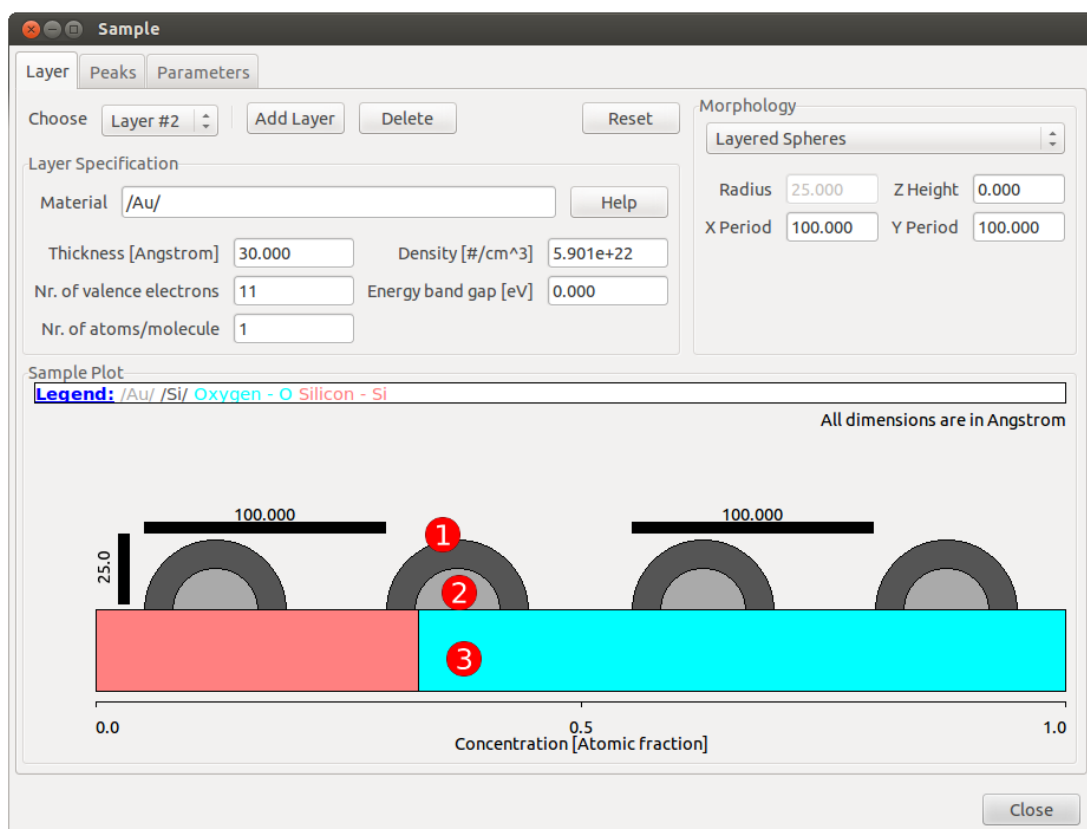


Figure 4.9: Graphical user interface for the SAMPLE Menu for morphology type “layered spheres”. The white numbers in red circles designate layer numbers.

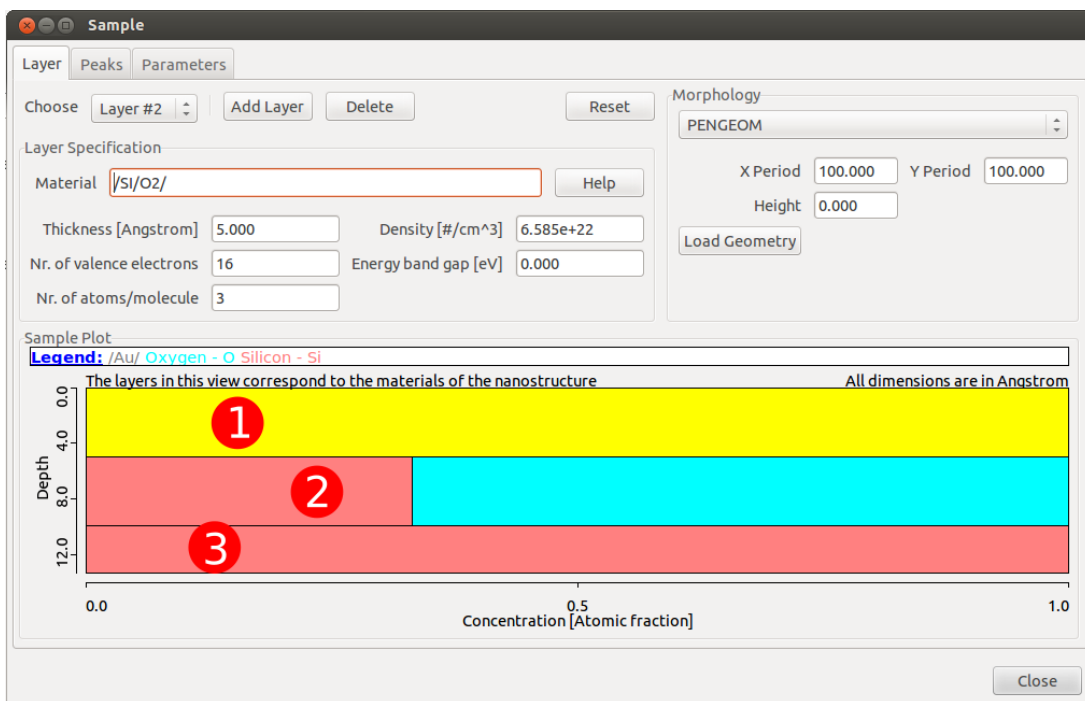


Figure 4.10: Graphical user interface for the SAMPLE Menu for morphology type “PENGEOmorphology”. The designated layer numbers should correspond with the “MATERIAL”-specifiers within the geometry file, as discussed in section 8.1.

2. Rough layered surfaces, as shown in Fig. 4.6
3. Islands (consisting of a single material) on top of a flat layered surface, as shown in Fig. 4.7
4. Spheres (consisting of a single material) on top of a flat layered surface, as shown in Fig. 4.8
5. Layered spheres on top of a flat layered surface, as shown in Fig. 4.9

Figures 4.5 to 4.9 are screenshots of the first five morphology types available for selection on the Sample screen. The substrate material is at the bottom, and other layers can be added by clicking the Add Layer button. Similarly, layers can be deleted by clicking the Delete button. For the Planar and Roughness morphologies, the relative composition of a layer containing two or more elements is shown as fractional regions that have two or more colors, with each color indicating an element, as shown in the legend. For the Islands, Spheres and Layered Spheres morphologies, there is no color to indicate composition.

Additionally, with the PENGEOmorphology-option (see Fig. 4.10), it is possible to load PENGEOmorphology-compatible geometry files. After selecting this option, a file dialog is opened where the geometry file can be selected. If the geometry file cannot be parsed correctly, an error dialog will open, informing the user that the selected file is corrupt. Otherwise, the file is accepted and the user can enter values for the X and Y periodicities and the nanomorphology height. The user is referred to Section 8 for guidelines for the creation of geometry files and examples of simulations.

It is also possible to perform simulations for a single nanoparticle or nano-island (i.e., as distinct from a periodic array of nanoparticles or nano-islands). This can be done by selecting the islands (Fig. 4.7), spheres (Fig. 4.8) or layered spheres (Fig. 4.9) morphology, specifying the relevant materials and particle or island dimensions, and entering MODEL SET SINGLE TRUE in the command

line interface (CLI), as described in Section 4.9. Note that this option cannot be selected from the GUI. Although the SESSA simulations will be performed for a single nanoparticle or island, the values of the X and Y periods here define the dimensions of the limiting body as described in Section 8. Simulating a single nanostructure (nanoparticle, nano-island or a different type defined by a PENGEOm geometry file) may result in large imprecisions of the simulation results since the majority of the simulated photoelectron trajectories will not originate from the nanostructure. It is therefore important to select values of the X and Y Periods (either through the GUI or with the corresponding commands in the CLI) to correspond to the total particle size (spheres, layered spheres) or to reproduce the desired surface coverage (islands). Doing otherwise may lead to inaccurate or erroneous results. The SINGLE option should not be used with the planar or roughness morphologies.

Another option is to perform a simulation for a nanoparticle (spheres, layered spheres) without a substrate. This is done by entering MODEL SET NOSUB TRUE in the CLI, as described in Section 4.9; this option is not available through the GUI. When using the NOSUB option, the substrate peaks must be deleted from the List of Peaks or otherwise the simulation will freeze. This option should not be used with the planar, roughness or islands morphologies.

Notes: Both the SINGLE and NOSUB options can be disabled using the same commands followed by ... FALSE (instead of ... TRUE). For nanoparticles (spheres, layered spheres), it is recommended to only use the SINGLE and NOSUB options in combination. The SINGLE and NOSUB options can be used in combination with external PENGEOm geometry files; for more details, the user is referred to Section 4.9 and particularly Section 8.4). The morphology modes Planar and Roughness should not be used with the SINGLE option or the NOSUB option. The morphology mode Islands can be used with the SINGLE option, but should not be used with the NOSUB option. The use of either the SINGLE or the NOSUB option (or both) can drastically reduce the computation times for otherwise equivalent simulations.

A desired sample morphology is selected from the morphology box in the top-right corner of each Sample screen (with the Layer tab) shown in Figs. 4.5 to 4.10. The user can then set parameters for the chosen nanomorphology, as shown in the relevant screens of Figs. 4.5 to 4.10. Commands for the control of individual morphology parameters are explained in detail in Section 4.4.3. The designation of layer numbers is indicated in all figures 4.5 to 4.10 as white numbers in red circles.

The material in a given layer is specified by a special string describing the elemental composition. All relevant parameters for a specified material are retrieved by the expert system and can be inspected and changed in the "Sample peak" menu (see section 4.4.7) and the "Sample parameter" menu (see section 4.4.5). A value for the density of each layer can also be determined for each layer individually. For elemental solids, this quantity is read from a database; for most other materials, it is estimated on the basis of elemental densities of the constituents in each layer. The estimated density may be in error by more than 100%. It is therefore recommended that the user should specify a more realistic value for the density in such cases.

4.4.1 The SAMPLE LAYER Menu

This menu (selected by the Layer tab in the Sample menus of figures 4.5 to 4.10) controls the parameters specifying the thickness, density, bandgap energy, number of valence electrons per atom or molecule, number of atoms per molecule, composition, thickness, and roughness of the surface. SESSA has a library of densities for elemental solids but only provides rough estimates for compounds, and the user should check these estimates. The default setting for density units is number of atoms per cubic centimeter but this can be changed to mass density (expressed in

g/cm³) using the Preferences menu (see Section 4.3). The bandgap energy E_g is needed for estimating IMFPs using the TPP-2M formula [6], and values for many compounds can be found in a number of sources[7–12]. If a value for the bandgap energy E_g cannot be found for the compound of interest, it is satisfactory to estimate this parameter because the IMFP is not a sensitive function of E_g [13, 14]. For highly ionic compounds such as the alkali halides, E_g is generally between 6 eV and 11 eV. For oxides, E_g values are often between 1 eV and 9 eV.

4.4.2 Synopsis of CLI Commands.

1. SAMPLE ADD LAYER <string> THICKNESS <double> [ABOVE <int>]
Adds a new layer above the selected layer. The material of the layer is specified by the material identifier <string > (see section 3.3).
 - THICKNESS: Specify the thickness (in Å) of the layer to be added (1 Å=0.1 nm).
 - ABOVE: Add the layer above the specified layer instead of above the layer that is selected in the "Choose layer" box.
2. SAMPLE DELETE LAYER <int>
Number of the selected layer.
3. SAMPLE RESET
Reset the complete sample structure to its default (a homogeneous Si sample).
4. SAMPLE SET ACTLAY <int>
Set the number of a given layer to which all following commands apply by default.
5. SAMPLE SET DENSITY <double> [LAYER <int>]
Set the density of a given layer (atoms/cm³)
 - LAYER: Number of the selected layer.
6. SAMPLE SET EGAP <double> [LAYER <int>]
Set the band gap energy (in eV) of a material in a given layer. This parameter is used to calculate the IMFP of non-conductors. Since no database exists for values of this quantity in SESSA, it must be manually set by a user. While the IMFP values do not sensitively depend on the bandgap, deviations of more than about 25% are possible if this parameter is not set and the default value $E_{gap} = 0$ eV is used.
 - LAYER: Number of the selected layer.
7. SAMPLE SET NVALENCE <int> [LAYER <int>]
Set the number of valence electrons per molecule of a material in a given layer.
 - LAYER: Number of the selected layer.
8. SAMPLE SET NATOMS <int> [LAYER <int>]
Set the number of atoms per molecule of a material in a given layer.
 - LAYER: Number of the selected layer.
9. SAMPLE SET MATERIAL <string> [LAYER <int>]
Set the material of a given layer by providing a material specifier <string >. For a user, there are two different ways to enter the material in the sample menu; One way is to enter the material specifier in a format used internally by SESSA, with a special syntax(e.g. "/SI/O2/" for

Silicon dioxide), as explained below. The alternative way is to enter the material specifier in a more intuitive syntax (e.g. "SiO₂" for Silicon dioxide). If the material is specified in this simpler, more intuitive way, SESSA will translate this into the internal syntax that will be displayed in the material field in the GUI. Below, the internal syntax, being a bit more powerful than the intuitive syntax will be described first, followed by an explanation of the intuitive syntax.

The material specifier consists either of a number of compound specifiers, or a number of constituent specifiers, or both, followed by their relative abundance. A constituent specifier consists of an element specifier and (optionally) by a chemical state attribute surrounded by slashes '/ /', followed by its abundance in the material: <constituent specifier>= /<element identifier>[<chemical state attribute>]/<abundance>. An element's specifier is the usual chemical symbol for an element, <element identifier>=H,He,Li,Be etc. (case insensitive). A chemical state attribute is needed when a peak in the spectrum is present in different chemical surroundings. It is an arbitrary string that allows identification of non-elemental chemical states of a given spectral line. <chemical state attribute>=[nonelemental], [oxide]...., etc. The abundance is a positive real number indicating the relative abundance of the element. If the abundance is omitted, it is taken to be unity. A compound specifier consists of a number of constituent specifiers enclosed in parentheses '()' followed by the relative abundance of the considered compound. Nesting of compound specifiers is allowed. For example, <compound-specifier> = (A)x(B)y,...,etc. Where A and B represent constituent or compound specifiers and x and y are their corresponding abundances. Examples:

S/i/O/: A solid consisting of Sulfur, Iodine and Oxygen, all of them present in elemental form.

/Si0.68/si[oxide]32e-2/O2/95 (/c)/5: The typical Silicon dioxide layer containing elemental silicon and silicon bound to oxygen in the ratio 68:32, oxygen and 5%carbon contamination. The more intuitive syntax for the material specifier is a string of characters containing the chemical symbols of the elements and their abundances in the material without forward slashes. In this case the specification of the chemical symbols of the elements is case sensitive, e.g. "Si", "Fe", "Au" are valid chemical symbols for Silicon, Iron and Gold, while "SI", "FE" and "AU" are invalid in the intuitive syntax. The reason is simply that case insensitive chemical symbols are not uniquely identifiable. For example "SI" might be interpreted as a sulfur-iodine compound or as Silicon, "CO" might be interpreted as Cobalt or Carbon monoxide. The omission of the forward slashes and the case sensitivity is the main difference between the intuitive syntax and the internal syntax. The syntax for the chemical state attribute and the compound specifier is the same in both syntaxes. (see section 3.3).

- LAYER: Number of the selected layer.

10. SAMPLE SET THICKNESS <double> [LAYER <int>]

Set the thickness (in Å) of a given layer.

- LAYER: Number of the selected layer.

11. SAMPLE SHOW SAMPLE

Show the parameters describing the sample structure in the CLI.

12. SAMPLE SHOW LAYER <int>

Show the parameters describing a single layer of the sample in the CLI.

13. SAMPLE PLOT SAMPLE

Graphical display of the concentration-depth profile of the sample.

4.4.3 The SAMPLE MORPHOLOGY Menu

This menu controls the nanomorphology of the sample surface

4.4.4 Synopsis of CLI Commands.

1. SAMPLE MORPHOLOGY SHOW

Displays information about the morphology of the sample as specified by the user

2. SAMPLE MORPHOLOGY SET PLANAR

Morphology of the surface is a planar surface with a number of parallel layers consisting of different materials

3. SAMPLE MORPHOLOGY SET ROUGHNESS

Morphology of the surface is a rough surface

4. SAMPLE MORPHOLOGY SET ISLANDS

Morphology of the surface is planar and layered with pyramid-shaped islands consisting of a single material on top

5. SAMPLE MORPHOLOGY SET SPHERES

Morphology of the surface is a planar and layered with spheres consisting of a single material on top

6. SAMPLE MORPHOLOGY SET LAYERED_SPHERES

Morphology of the surface is a planar consisting of a single material and with layered spheres on top

7. SAMPLE MORPHOLOGY SET PENELOPE <string>

An external PENGEOM file is used to specify the morphology of the specimen. While this choice allows a greater range of surface nanomorphologies to be specified by the user, (see section 8.1), there is no visualization of the structure within SESSA. This visualization can be achieved with the PENGEOM_VIEWER. See the Penetration and Energy LOss of Positrons and Electrons (PENELOPE) documentation (e.g. <http://www.oecd-nea.org/tools/abstract/detail/nea-1525>).

8. SAMPLE MORPHOLOGY SET RSA <double>

Set the roughness of the sample surface. A rough surface is assumed to consist of tilted surface segments with a certain distribution of tilt angles. The roughness is specified by the relative surface area (RSA)[15], that is, the mean value of the reciprocal of the cosines of the tilt angles. In other words, the relative surface area is the area of the surface when measured along the tilted surface segments, divided by the area of the surface segments projected onto the global surface. Consequently, RSA=1 represents an ideally smooth surface. Realistically rough surfaces are described by an RSA value between 1.05 and 1.2.

9. SAMPLE MORPHOLOGY SET X_LENGTH <double>

Set the length of the islands along the x-axis (in Å).

10. SAMPLE MORPHOLOGY SET Y_LENGTH <double>

Set the length of the islands along the y-axis (in Å).

11. SAMPLE MORPHOLOGY SET X_PERIOD <double>
Set the period of repetition of the selected nanostructure along the x-axis (in Å). If MODEL SET SINGLE TRUE is set(see Sec. 4.9) the x-dimension of the simulation bounding box is set instead (symmetric around the sphere or island).
12. SAMPLE MORPHOLOGY SET Y_PERIOD <double>
Set the period of repetition of the selected nanostructure along the y-axis (in Å). If MODEL SET SINGLE TRUE is set(see Sec. 4.9) the y-dimension of the simulation bounding box is set instead (symmetric around the sphere or island).
13. SAMPLE MORPHOLOGY SET X_INCLINATION <double>
For islands, set the inclination angle of the plane with the base perpendicular to the x-axis (in degrees).
14. SAMPLE MORPHOLOGY SET Y_INCLINATION <double>
For islands, set the inclination angle of the plane with the base perpendicular to the y-axis (in degrees).
15. SAMPLE MORPHOLOGY SET HEIGHT <double>
Set the height of the islands (in Å).
16. SAMPLE MORPHOLOGY SET Z_HEIGHT <double>
Set the height of the centre of the sphere above the planar surface (in Å). This value should be less than or equal to half the radius of the spheres.
17. SAMPLE MORPHOLOGY SET RADIUS <double>
Set the radius of the nanospheres (in Å).

4.4.5 The SAMPLE PARAMETERS Menu

This menu controls the parameters for the electron–solid interaction as shown in Fig. 4.11.

4.4.6 Synopsis of CLI Commands.

1. SAMPLE PARAMETERS SET SEP VALUE <double> LAYER <int>
Set the value of the surface excitation parameter (SEP) for a given layer.
 - LAYER: Number of the selected layer.
2. SAMPLE PARAMETERS SET SEP DATABASE <string> LAYER <int>
Select a database to retrieve the value of the surface excitation parameter (SEP) (see also 'help database sep show' for a list of available databases for this quantity).
 - LAYER: Number of the selected layer.
3. SAMPLE PARAMETERS SET SEP MATERIAL <string> LAYER <int>
Option to search the database of SEP values.
 - LAYER: Number of the selected layer.
4. SAMPLE PARAMETERS SET IMFP VALUE <double> PEAK <int> LAYER <int>
Set the value of the inelastic mean free path (IMFP) for a given peak in a given layer (in Å).

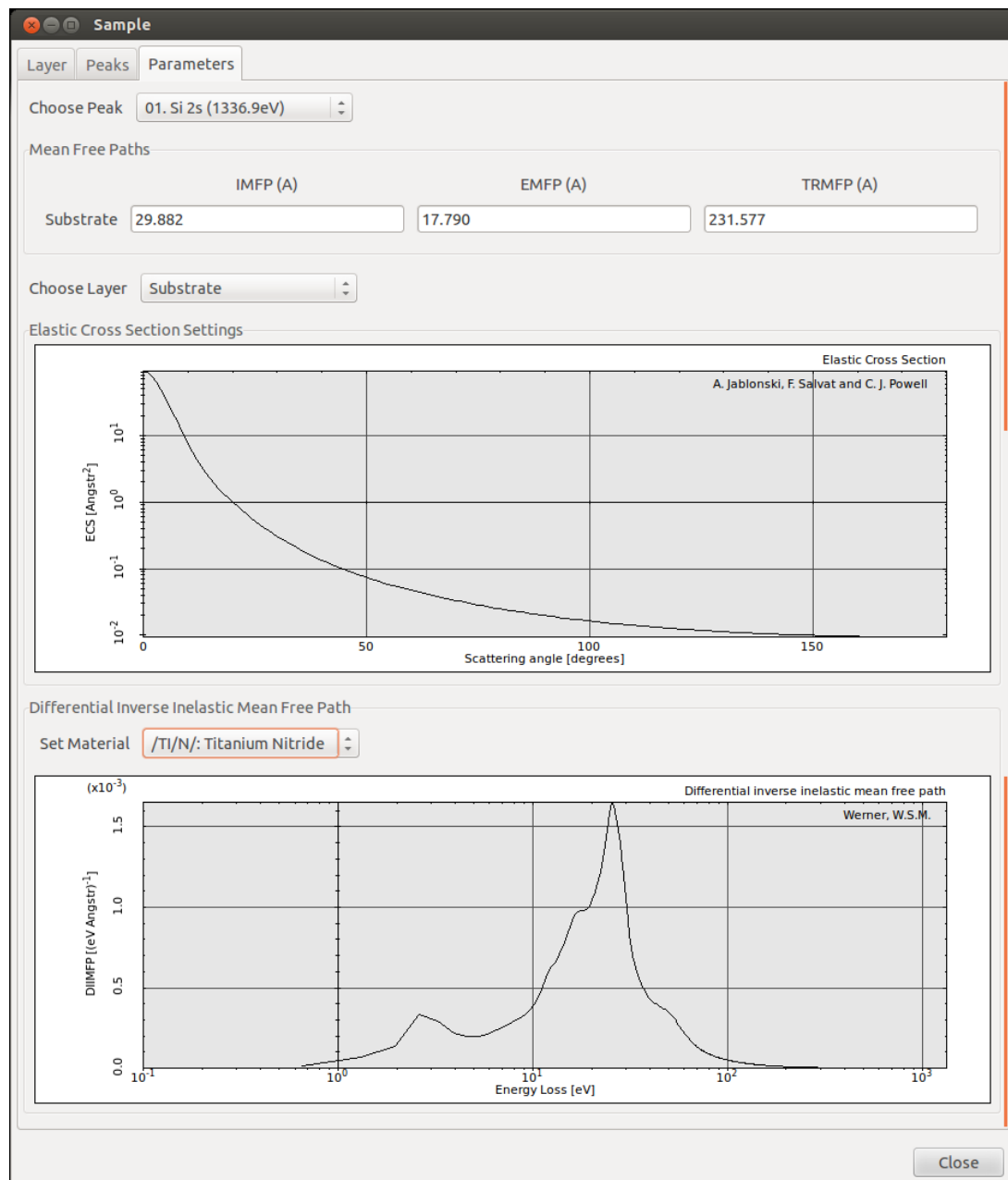


Figure 4.11: Graphical user interface for the SAMPLE PARAMETERS Menu.

- PEAK: Number of the selected peak.
- LAYER: Number of the selected layer.

5. SAMPLE PARAMETERS SET IMFP DATABASE <string> LAYER <int>
Select a database for retrieval of IMFP values.

- LAYER: Number of the selected layer.

6. SAMPLE PARAMETERS SET IMFP MATERIAL <string> LAYER <int>

Option to search the database of IMFP values derived from optical data. In this case the material identifier should be an ordinary (non-case sensitive) string (e.g. "Si", "SiO₂", "TiC", etc.). Note that optical data are only available for a limited number of materials. If the requested material is not found, a message is issued and the default database for the IMFP is automatically invoked. This default returns an estimate for the IMFP derived from the TPP-2M formula [6] (see also 'help database imfp show' for a list of available databases for this quantity).

- LAYER: Number of the selected layer.

7. SAMPLE PARAMETERS SET EMFP VALUE <double> PEAK <int> LAYER <int>

Set the value of the elastic mean free path (EMFP) (in Å) for a given peak in a given layer.

- PEAK: Number of the selected peak.
- LAYER: Number of the selected layer.

8. SAMPLE PARAMETERS SET EMFP DATABASE <string> LAYER <int>

Select a database to retrieve the value of the EMFP (see also 'help database emfp show' for a list of available databases for this quantity).

- LAYER: Number of the selected layer.

9. SAMPLE PARAMETERS SET TRMFP VALUE <double> PEAK <int> LAYER <int>

Set the value of the transport mean free path (TRMFP) (in Å) for a given peak in a given layer.

- PEAK: Number of the selected peak.
- LAYER: Number of the selected layer.

10. SAMPLE PARAMETERS SET TRMFP DATABASE <string> LAYER <int>

Select a database to retrieve the value of the TRMFP (see also 'help database trmfp show' for a list of available databases for this quantity).

- LAYER: Number of the selected layer.

11. SAMPLE PARAMETERS SET ECS DBNAME <string> PEAK <int> [LAYER <int>]

Select a database to retrieve the value of the ECS (see also 'help database ecs show' for a list of available databases for this quantity).

- DBNAME: Name of the database (see also 'help database ecs show' for a list of available databases for this quantity).
- PEAK: Number of the selected peak.
- LAYER: Number of the selected layer.

12. SAMPLE PARAMETERS SET DIIMFP DATABASE <string> LAYER <int>
Select a database to retrieve the value of the differential inverse inelastic mean free path (DIIMFP) (see also 'help database diimfp show' for a list of available databases for this quantity)
 - LAYER: Number of the selected layer.
13. SAMPLE PARAMETERS SET DIIMFP MATERIAL <string> LAYER <int>
Option requesting the program to search the database of optical data for evaluation of the DIIMFP. In this case the material identifier should be an ordinary (non-case sensitive) string (e.g. "Si", "Sio2", "TiC" etc.). Note that optical data are only available for a limited number of materials. If the requested material is not found, a message is issued and the default database for the DIIMFP is automatically invoked. This default returns Tougaard's universal DIIMFP [16].
 - LAYER: Number of the selected layer.
14. SAMPLE PARAMETERS SET DSEP DATABASE <string> LAYER <int>
Select a database to retrieve the value of the differential surface excitation parameter (DSEP) (see also 'help database dsep show' for a list of available databases for this quantity).
 - LAYER: Number of the selected layer.
15. SAMPLE PARAMETERS SET DSEP MATERIAL <string> LAYER <int>
Option requesting the program to search the database of optical data for evaluation of the DSEP. <edit this HELP text>
 - LAYER: Number of the selected layer.
16. SAMPLE PARAMETERS SHOW PEAK <int>
Show information about the electron-solid interaction for the selected peak in the CLI.
17. SAMPLE PARAMETERS PLOT ECS PEAK <int> [LAYER <int>]
Display the elastic cross section for given peak and layer. Note that for compound layers, the cross section is a weighted average of the elemental cross sections of the constituents of the layer.
 - PEAK: Number of the selected peak.
 - LAYER: Number of the selected layer.
18. SAMPLE PARAMETERS PLOT DIIMFP [LAYER <int>] [PEAK <int>]
Display the differential inverse inelastic mean free path for a given layer.
 - LAYER: Number of the selected layer.
 - PEAK: Number of the selected peak.
19. SAMPLE PARAMETERS PLOT DSEP [LAYER <int>] [PEAK <int>]
Display the differential surface excitation parameter for the simulation.
 - LAYER: Number of the selected layer.
 - PEAK: Number of the selected peak.

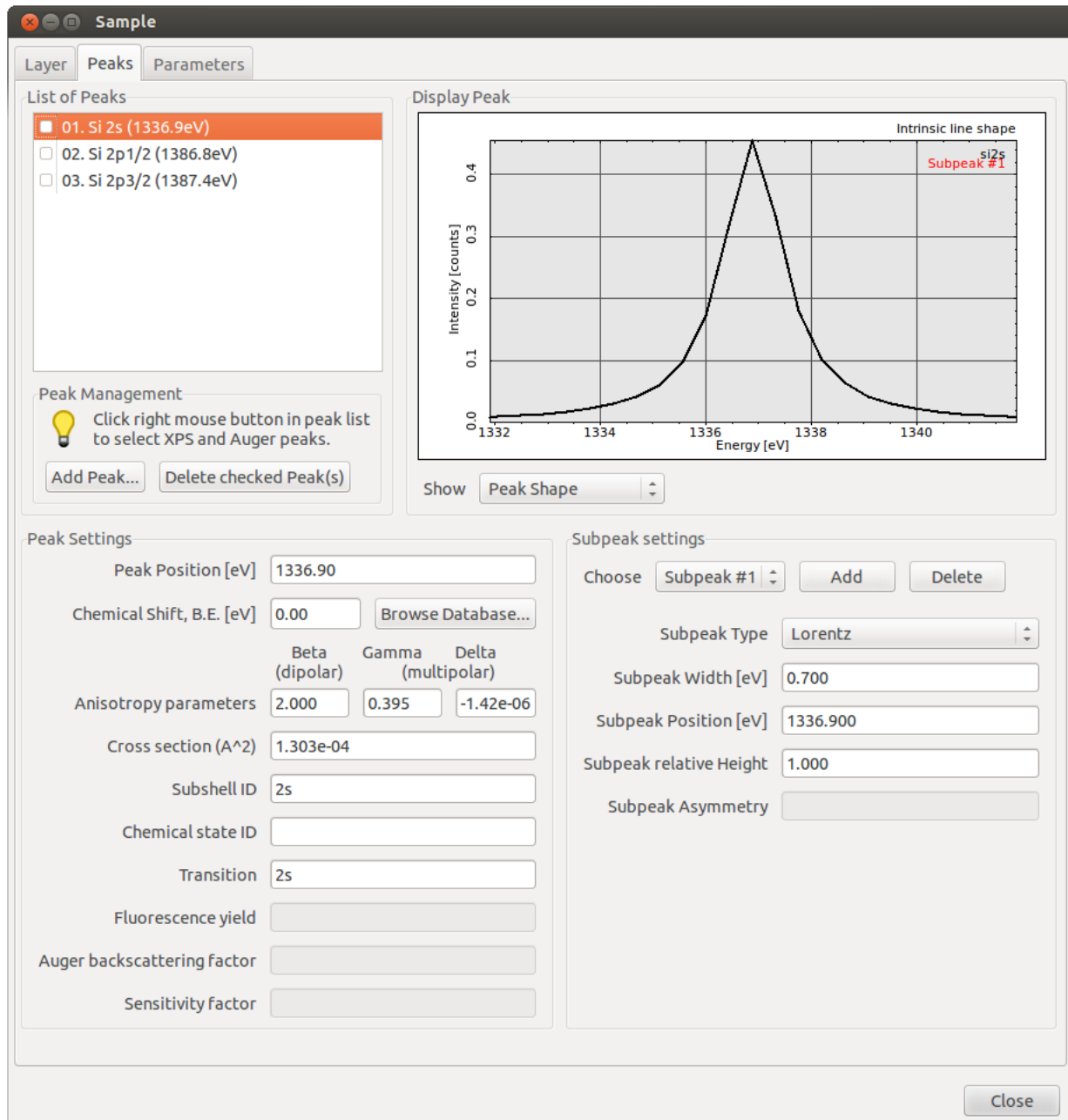


Figure 4.12: Graphical user interface for the SAMPLE PEAK Menu.

4.4.7 The SAMPLE PEAK Menu

This menu (selected by the Peaks tab in the Sample menu shown in the series of figures displaying the different sample settings, Figs.4.5 to 4.9) controls the attributes of the peaks in the sample that contribute to the specified energy regions, as shown in Fig. 4.12. The peaks of signal electrons that have a source energy distribution lying within the energy regions of the spectrometer, as specified by the user, can be inspected and modified in this menu. Note that, depending on the source energy and material of interest, it may happen that no peaks occur in the specified regions. In such cases, various data sets in SESSA are void that would otherwise contain information on the signal-electron peaks and parameters associated with them. A peak for an element may contain a number of subpeaks that are described by a functional form, relative height and width, or are given by an empirical peak shape read from a data file. Presently, SESSA does not contain detailed information on intrinsic peak shapes: the intrinsic peak is assumed to be described sufficiently well in terms of a Gaussian, Lorentzian or Doniach-Sunjic peak shape. Alternatively, a user can choose to load an empirical peak shape from a text file containing intensity as a function of energy (i.e. as a series of x,y pairs).

With each peak, there are associated a number of parameters such as the subshell identifier, cross section, fluorescence yield (only for Auger transitions), etc. The graphical display for the sample peak menu shows the intrinsic peak shape by default. By means of the "Choose data" box, a user can choose to change the display to the simulated spectrum or the simulated partial intensities. By double-clicking on the display, a new window opens with a display that can be modified by the user. A right mouse clicking the new window gives options for showing and saving the displayed data.

The angular distribution of photoelectrons emitted from an atom is calculated in SESSA using the formula given by Cooper [17]:

$$\frac{d\sigma}{d\Omega} = \frac{\sigma_{nl}}{4\pi} \left\{ 1 + \frac{\beta}{2} (3 \cos^2 \theta - 1) + (\delta + \gamma \cos^2 \theta) \sin \theta \cos \phi \right\} \quad (4.1)$$

where σ_{nl} is the total photoionization cross section, β is the dipole asymmetry parameter, δ and γ are the non-dipole asymmetry parameters, θ is the angle between the direction of photoelectron emission and the polarization direction, and ϕ is the angle between the direction of photoelectron emission and the plane defined by the X-ray and polarization directions.

The non-dipolar terms in Eq. (4.1) generally have a negligible effect on the angular distribution of emitted photoelectrons for typical laboratory X-ray sources with Al and Mg anodes (i.e., for Al K α and Mg K α X-rays). However, these terms can significantly affect the angular distributions for higher photon energies, such as for Ag L α X-ray sources or when using synchrotron radiation with energies higher than a few keV.

We note here that there is only one database in SESSA for the three photoelectron asymmetry parameters (i.e., the parameters β , γ and δ in Eq. (4.1)). This is the database PAP3 (described in Section 6) with the parameter values computed by Trzhaskovskaya, Nefedov, and Yarzhemsky[18, 19]. If a different database is selected for the dipolar parameter β , values of the non-dipolar parameters δ and γ will not be retrieved from this source. We note that Trzhaskovskaya *et al.* calculated photoionization cross sections and photoionization asymmetry parameters only for photon energies up to 5 keV above each photoionization threshold. Linear extrapolations were made to these values so that cross sections and asymmetry parameters would be available in SESSA for larger photon energies. These extrapolations could introduce uncertainties of more than 30% in the values of the derived parameters.

To enable a more realistic simulation of peak shapes in SESSA, a chemical shift may be specified which will appropriately modify the energy of a peak (which can be a specified peak or a

chemical component of a peak as indicated by the chemical state attribute). While the parameters of the sample peak menu can be manipulated in the GUI in the usual way, an additional feature was implemented in Version 1.2 of SESSA for the chemical shift. An appropriate value for the chemical shift may be entered by the user or the chemical shift database may be browsed by clicking the "browse database" button. A menu for selecting the chemical shift will pop up, as illustrated in Fig. 4.13.

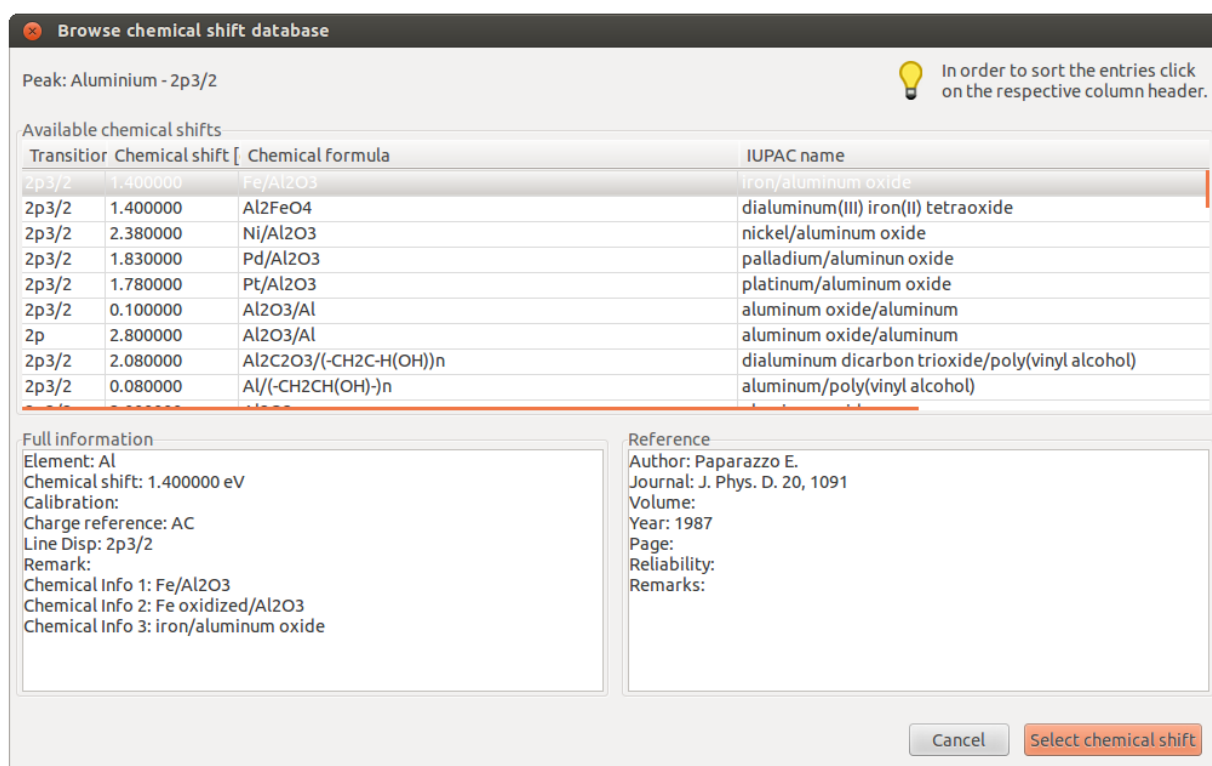


Figure 4.13: Graphical user interface for browsing the chemical shift database.

Here all entries from Version 4.0 of the NIST XPS Database (<http://srdata.nist.gov/xps>) for chemical shifts are displayed for the selected peak, together with some information about the chemical state and the source from which this information was taken. The listings in each column can be sorted alphabetically or numerically by clicking on the column heading. By double clicking on the most appropriate value, or by clicking the button "select chemical shift", the corresponding value is entered into the peak settings pane of the sample peak menu. The chemical shift database from the NIST XPS Database includes chemical shifts for the material that were measured on a single instrument and a larger number of calculated chemical shifts. The latter shifts were calculated as the difference of the binding energy for the line and compound that was reported in the particular data source and a reference binding energy for the same line of the elemental solid.

In the GUI, convenient peak list management tools are available as illustrated in Figs. 4.12 and 4.14. The main function of the peak list management tools is to facilitate deletion of a large number of peaks simultaneously in order to increase the simulation speed and to make it easier for a user to focus on a few selected peaks of special interest for the considered application. Selecting a peak for deletion is achieved by clicking the box to the left of a peak in the peak list. By means of a right mouse click anywhere in the peak list pane, it is possible to select all peaks,

to select all Auger peaks, all XPS peaks, or to uncheck all peaks (see Fig. 4.14). By clicking the “Delete checked peak(s)” button in the sample peak menu, the selected peaks can be deleted. To restore the peak list to the default set corresponding to the peaks retrieved by the expert system, the material of the corresponding layer needs to be entered again in the sample layer menu, e.g., by selecting the material in the material field and pressing enter. Individual peaks can be entered manually, if desired, by using the “add peak” button in the sample peak menu. Note that the peak for which the peak settings are displayed in the sample peak menu is indicated by a blue background in the peak list, while the checkboxes on the left of each peak merely indicate whether it has been marked for deletion.

Three types of data can be selected for graphical display in the SAMPLE PEAK menu by appropriate choice in the pull-down menu within the display peak window (top right region in Fig. 4.12). For each peak selected in the top left of Fig. 4.12, the user can choose one of the following displays:

1. the peak shape (default)
2. the peak spectrum
3. partial intensities

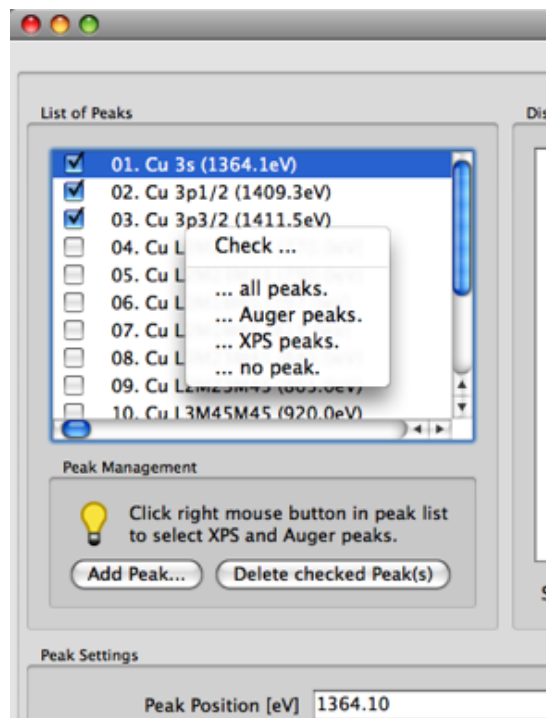


Figure 4.14: Portion of the graphical user interface for the SAMPLE PEAK Menu (Fig. 4.12) after a right mouse click in the peak list pane.

The peak shape represents the shape of the peak (i.e., the normalized energy distribution of the photoelectrons or Auger electrons emitted by the source atom) set by the user in the “peak settings” and “subpeak settings” menus shown in Fig. 4.12. The peak spectrum displays the simulated photoelectron or Auger-electron peak, i.e., the energy distribution of the photoelectrons

or Auger electrons as emitted from the sample surface and as seen by the analyzer. This spectrum includes energy losses as a result of single or multiple inelastic scattering (often referred to as the “inelastic tail”). The partial intensities represent the number of signal electrons that reach the detector (again for the given spatial distribution of signal-electron sources from a simulation) after participating in a given number of inelastic collisions.

4.4.8 Synopsis of CLI Commands.

1. SAMPLE PEAK SET ACTPEAK <int>
Set the peaks in the sample to which all of the following commands apply by default.
2. SAMPLE PEAK SET CHEMSHIFT VALUE <double> [PEAK <int>]
Set the value of the chemical shift in eV for a given peak.
 - PEAK: Number of the selected peak.
3. SAMPLE PEAK SET CHEMSHIFT DBENTRY <int> [PEAK <int>]
Select an entry from the chemical shift database.
 - PEAK: Number of the selected peak.
4. SAMPLE PEAK SET ABF VALUE <double> [PEAK <int>]
Set the value of the Auger backscattering factor (ABF) for a given peak.
 - PEAK: Number of the selected peak.
5. SAMPLE PEAK SET ABF DATABASE <string> [PEAK <int>]
Select a database to retrieve the value of the ABF (see also ‘help database ABF show’ for a list of available databases for this quantity).
 - PEAK: Number of the selected peak.
6. SAMPLE PEAK SET FY VALUE <double> [PEAK <int>]
Set the value of the fluorescence yield (FY) for a given peak.
 - PEAK: Number of the selected peak.
7. SAMPLE PEAK SET FY DATABASE <string> [PEAK <int>]
Select a database to retrieve the value of the FY (see also ‘help database FY show’ for a list of available databases for this quantity).
 - PEAK: Number of the selected peak.
8. SAMPLE PEAK SET ANISOTROPY <double> [DBNAME <string>] PEAK <int> [BETA] [GAMMA] [DELTA]
Set the asymmetry parameters (PAP) for the photoelectric cross section of a given peak. By default the dipolar asymmetry parameter will be set. Using the optional keywords GAMMA and DELTA will change the multipolar asymmetry parameters accordingly. Alternatively, this command can be used to set the database for retrieval of these quantities for a given peak.
 - DBNAME: If the DBNAME option is specified, the photoelectric asymmetry parameters are retrieved from the database indicated. See also ‘help database pap show’ for a list of available databases for this quantity).
 - PEAK: Number of the selected peak.

- BETA: Set the dipolar asymmetry parameter (default).
 - GAMMA: Set the multipolar asymmetry parameter gamma.
 - DELTA: Set the multipolar asymmetry parameter delta.
9. SAMPLE PEAK SET CROSS_SECTION <double> [DBNAME <string>] PEAK <int>
Sets the ionization cross section (in Å²) associated with the peak for the specified incoming radiation. When electrons are used as exciting radiation, the cross section is the electron-impact ionization cross section (EIICS). When photons are used, the cross section is the photoelectric cross section (PCS).
- DBNAME: Tells the software to retrieve the relevant cross section from the specified database (see also HELP DATABASE EIICS SHOW for a list of available databases for this quantity).
 - PEAK: Number of the selected peak.
10. SAMPLE PEAK SET TYPE <string> [PEAK <int>] SUBPEAK <int>
Set the subpeak type. The possible subpeak types are: GAUSS, LORENTZ, DONIACH_SUNJIC, EMPIRICAL (see section 4.4.7). Any peak in the spectrum may be described by a linear combination of several subpeaks, each with a position, width and relative intensity.
- PEAK: Number of the selected peak.
 - SUBPEAK: Number of the selected subpeak.
11. SAMPLE PEAK SET WIDTH <double> [PEAK <int>] SUBPEAK <int>
Set the width of the subpeak (in eV). The width is the value of the parameter describing the peak width for the selected subpeak type (e.g. for a Gaussian peak shape the width is the value of σ in the Gaussian distribution. (ignored for peaks described by empirical data)).
- PEAK: Number of the selected peak.
 - SUBPEAK: Number of the selected subpeak.
12. SAMPLE PEAK SET POSITION <double> [PEAK <int>] SUBPEAK <int>
Set the energy (in eV) of the subpeak position (ignored for peaks described by empirical data).
- PEAK: Number of the selected peak.
 - SUBPEAK: Number of the selected subpeak.
13. SAMPLE PEAK SET HEIGHT <double> [PEAK <int>] SUBPEAK <int>
Set the relative height of the subpeak (in arbitrary units).
- PEAK: Number of the selected peak.
 - SUBPEAK: Number of the selected subpeak.
14. SAMPLE PEAK SET ASYMMETRY <double> [PEAK <int>] SUBPEAK <int>
Set the asymmetry parameter for the Doniach-Sunjic formula (ignored for other peak types).
- PEAK: Number of the selected peak.
 - SUBPEAK: Number of the selected subpeak.

15. SAMPLE PEAK SET CHEMSTATID <string> [PEAK <int>]

Set the chemical state identifier of the peak. The chemical state identifier is an arbitrary string of characters that may be provided by a user to distinguish between the same atoms present in different states in the sample. The identifier is used to label peaks of the same element present in different chemical or physical states but is not interpreted by SESSA. In a simulation, all peaks of an element corresponding to the same transition but with a different chemical state identifier are treated as separate peaks.

- PEAK: Number of the selected peak.

16. SAMPLE PEAK SET SENSFAC <double> [PEAK <int>]

Set the sensitivity factor of the peak. This quantity is a correction factor for Auger peaks in cases for which the fluorescence yield and Coster-Kronig transition probability are not well known.

- PEAK: Number of the selected peak.

17. SAMPLE PEAK ADD AESPEAK ENERGY <double> TRANSITION <string> SUBSHELLID <string> ELEMENT <string> [CHEMSTATID <string>]

Add an Auger peak specified by the user to the list of peaks.

- ENERGY: Energy (in eV) of the peak.
- TRANSITION: The transition for the Auger peak.
- SUBSHELLID: The subshell that is ionized initially and leads to the considered Auger transition.
- ELEMENT: The element emitting the signal electrons.
- CHEMSTATID: Chemical state label for a peak.

18. SAMPLE PEAK ADD XPSPEAK ENERGY <double> SUBSHELLID <string> ELEMENT <string> [CHEMSTATID <string>]

Add a photoelectron peak specified by the user to the list of peaks.

- ENERGY: Energy (in eV) of the peak.
- SUBSHELLID: Subshell of the considered photoelectron peak.
- ELEMENT: Element emitting the signal electrons.
- CHEMSTATID: Chemical state of the peak.

19. SAMPLE PEAK ADD SUBPEAK PEAK <int> ENERGY <double>

Add a subpeak to the peak data structure.

- PEAK: Number of the selected peak.
- ENERGY: Specify the energy (in eV) for the subpeak.

20. SAMPLE PEAK DELETE PEAK <int> [SUBPEAK <int>]

Delete an attribute of the peak data structure

- PEAK: Number of the selected peak.
- SUBPEAK: Number of the selected subpeak.

21. SAMPLE PEAK SHOW [PEAK <int>] [SUBPEAK <int>]

Show information for the peak

- PEAK: Number of the selected peak.
 - SUBPEAK: Number of the selected subpeak.
22. SAMPLE PEAK LIST [PEAK <int>] [GEOMETRY <int>]
Shows brief information for all peaks.
- PEAK: Number of the selected peak.
 - GEOMETRY: Number of the selected geometry.
23. SAMPLE PEAK PLOT SPEC [PEAK <int>]
Graphical display of the partial spectrum emitted from the surface.
- PEAK: Number of the selected peak.
24. SAMPLE PEAK PLOT PART_INT [PEAK <int>]
Graphical display of the partial intensities of electrons emitted from the surface.
- PEAK: Number of the selected peak.
25. SAMPLE PEAK PLOT SHAPE [PEAK <int>] [SUBPEAK <int>]
Graphical display of the partial spectrum emitted at the location in the sample where the signal-electron excitation takes place.
- PEAK: Number of the selected peak.
 - SUBPEAK: Number of the selected subpeak.
26. SAMPLE PEAK OUTPUT SPEC FILE <string> [PEAK <int>]
Writes the spectrum for the selected peak to a file.
- FILE: Name of the file for output.
 - PEAK: Number of the selected peak.
27. SAMPLE PEAK OUTPUT PART_INT FILE <string> [PEAK <int>]
Writes the partial intensities for the selected peak to a file.
- FILE: Name of the file for output.
 - PEAK: Number of the selected peak.
28. SAMPLE PEAK LOAD DATA <string> [PEAK <int>] SUBPEAK <int>
Loads an ASCII file containing the peak shape of a given subpeak for an EXISTING peak. Before peak shape data can be loaded for a new peak, this peak has to be defined by adding it (see SAMPLE ADD PEAK). The expected format for each line of this file is: "energy (eV)/ one or more spaces/ intensity (arb. units)"
- PEAK: Number of the selected peak.
 - SUBPEAK: Number of the selected subpeak.

4.5 The SOURCE Menu

This menu specifies the source of exciting radiation for an experiment, as shown in Fig. 4.15. If an attribute of the source is changed, the expert system must start a new query for many relevant quantities. This means that previous user input for any of these quantities will be lost in such

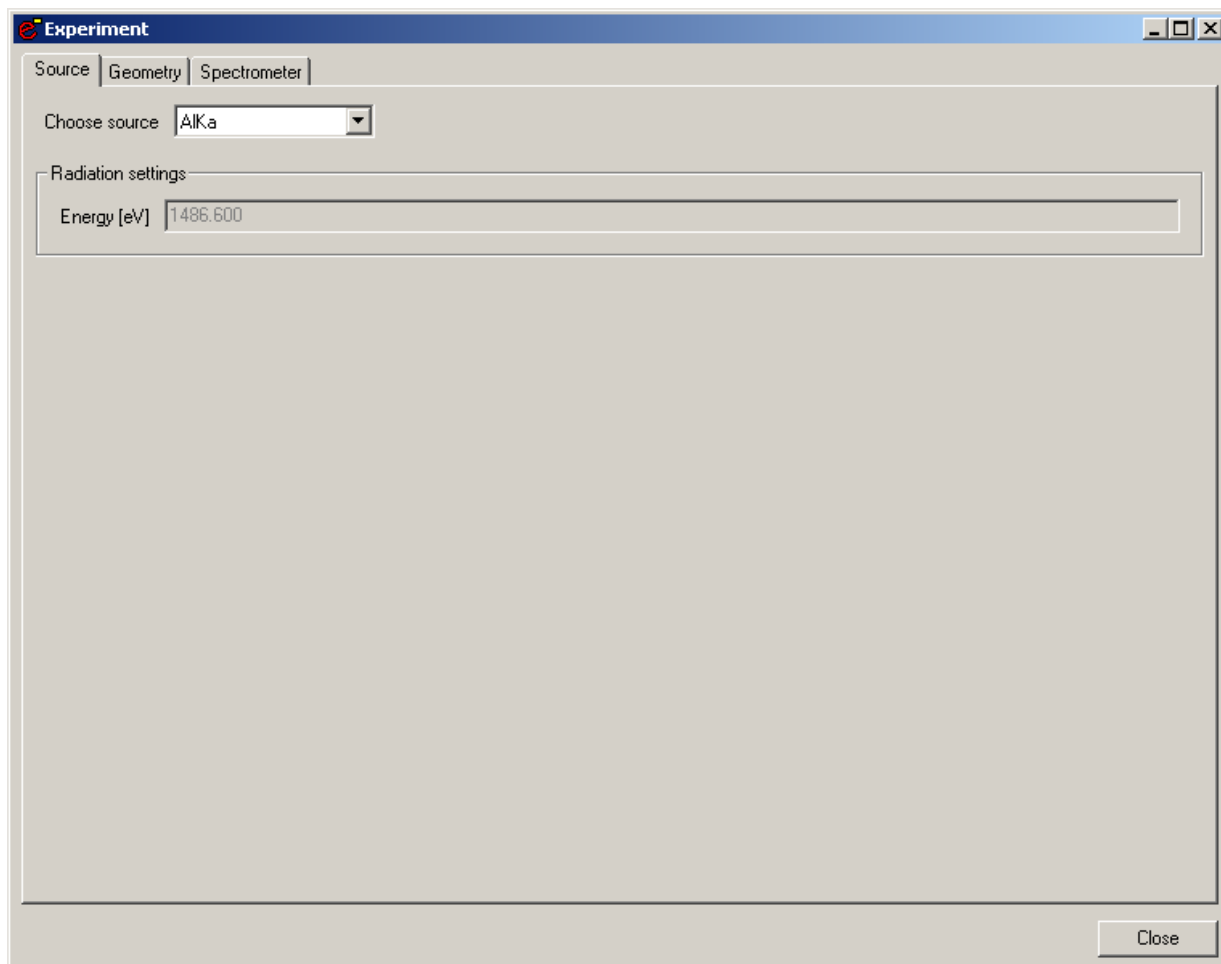


Figure 4.15: Graphical user interface for the SOURCE Menu.

cases. For example, definitions concerning the shape, position or relative intensities of a peak that were manually added by a user as well as the corresponding interaction parameters will be erased. To save such user settings, it is advisable to save the session (see "Project/save/session")

If the incoming radiation is chosen to be photons, their energy can be specified and their polarization can be specified to be circular or unpolarized by setting the linear polarization fraction to zero. If the incoming beam is partially linearly polarized, the fraction of the linearly polarized light P in the beam can be set with this command, as indicated in Fig. 4.15.

It is assumed that the remaining fraction (1-P) of the beam is circularly polarized or unpolarized. The polarization fraction only affects the angular distribution of photoelectrons in any calculation. For unpolarized or circularly polarized light, the angular distribution is rotationally symmetric around the polarisation vector [18, 20].

The polarization direction is chosen in the GEOMETRY menu (see Section 4.7).

If the incoming radiation is chosen to be electrons, the electron energy can be specified.

4.5.1 Synopsis of CLI Commands.

1. SOURCE SET ALKA
Sets the source to Al K α radiation.
2. SOURCE SET MGKA
Sets the source to Mg K α radiation.
3. SOURCE SET ZRMZ
Sets the source to Zr M ζ radiation.
4. SOURCE SET PHOTONS ENERGY <double>
Sets the source to photons with a specified energy.
 - ENERGY: photon energy (in eV).
5. SOURCE SET POLARIZATION FRACTION <double>
Set the fraction of linear polarization of the incoming light
6. SOURCE SET ELECTRONS ENERGY <double>
Sets the source to electrons with a specified energy.
 - ENERGY: electron energy (in eV).
7. SOURCE SHOW
Shows the parameters of the SOURCE menu.

4.6 The SPECTROMETER Menu

This menu specifies the energy ranges of interest as well as the parameters describing the spectrometer used to measure the spectrum, as shown in Fig. 4.16. A number of (non-overlapping) energy regions may be specified. A spectrometer region may not be more than 3000 eV wide. When retrieving the parameters needed to interpret an electron spectrum, the expert system looks for peaks of the specified sample that fall into one of the selected regions. At present, the simulated spectrum corresponds to electrons emitted from the sample. All effects of the instrumentation on an electron spectrum that may be observed in an experiment (analyzer transmission function, energy dependence of the energy resolution, etc.) are neglected in the present version of SESSA.

4.6.1 Synopsis of CLI Commands.

1. SPECTROMETER ADD REGION [RANGE <string>]
Add a new energy region for which the spectrum is to be simulated.
 - RANGE: Defines the range of the spectrometer energy window in eV. Example: SPECTROMETER ADD REGION RANGE 900:1400 will add a region with an energy window from 900 eV to 1400 eV.
2. SPECTROMETER DELETE REGION <int>
Delete the selected spectrometer region

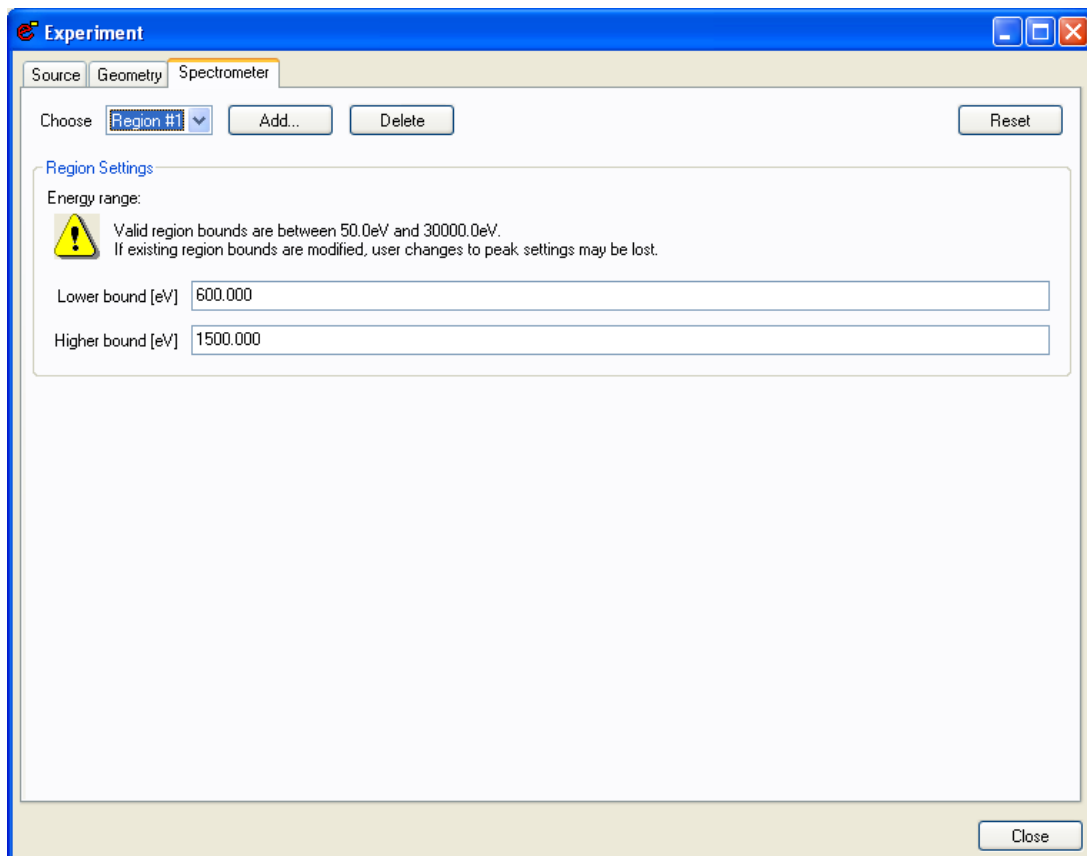


Figure 4.16: Graphical user interface for the SPECTROMETER Menu.

3. SPECTROMETER SET ACTREGION <int>

Set the number of the default spectrometer to which all following commands apply by default.

4. SPECTROMETER SET RANGE <string> [REGION <int>]

Set the range of the spectrometer energy window in eV. Example SPECTROMETER SET RANGE 900:1400 will set the energy window to (900:1400). SPECTROMETER SET RANGE 900: sets only the lower bound, SPECTROMETER SET RANGE :1400 sets only the upper bound.

- REGION: Number of the selected spectrometer region.

5. SPECTROMETER LIST

List all regions in the CLI.

6. SPECTROMETER RESET

Reset the spectrometer settings to default values.

7. SPECTROMETER SHOW SPECTROMETER

Show information about the spectrometer in the CLI.

8. SPECTROMETER SHOW REGION <int>

Show all information about the specified region in the CLI.

4.7 The GEOMETRY Menu

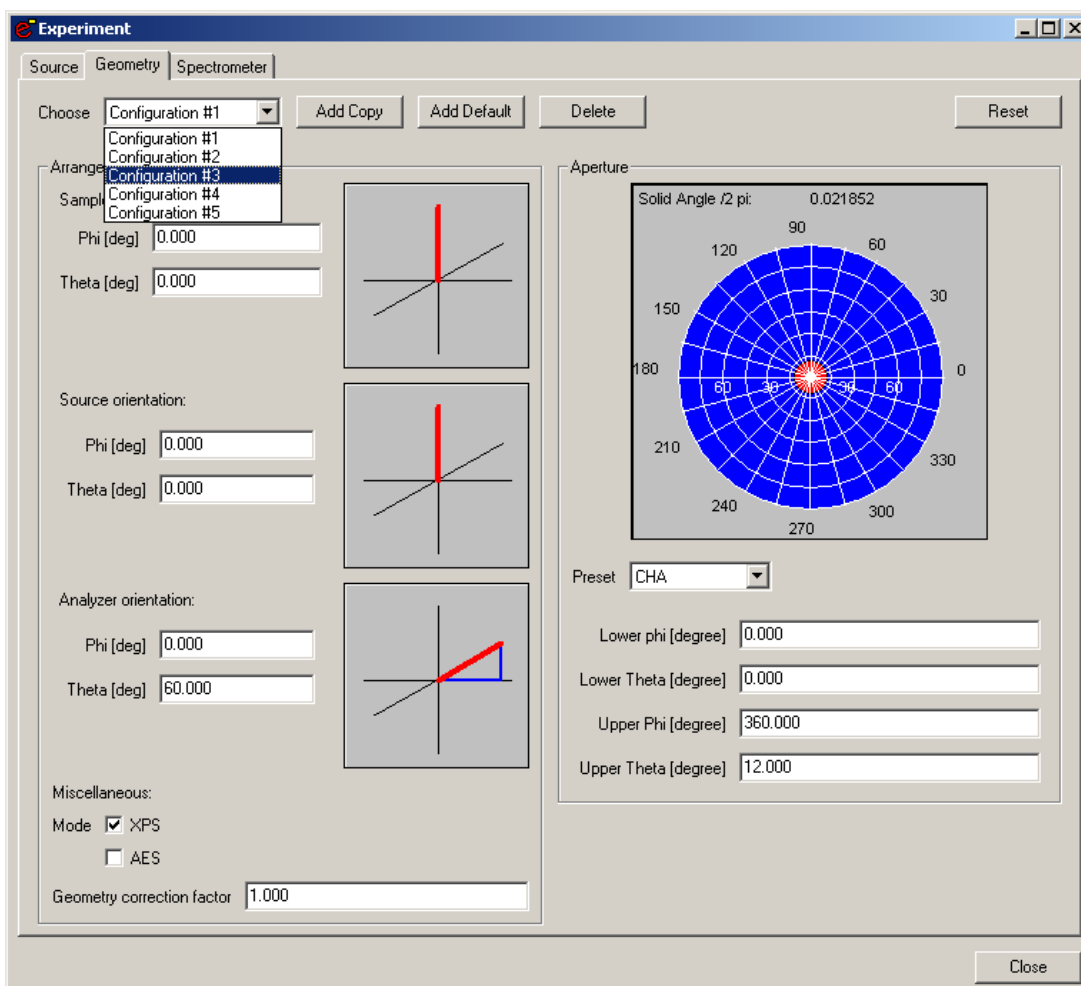


Figure 4.17: Graphical user interface for the GEOMETRY Menu.

This menu specifies the experimental geometry, as shown in Fig. 4.17. A number of geometries can be specified. When a model calculation is performed with SESSA (see section 4.9) a simulation is made for each geometry specified in this menu. For each geometry, the directions of the sample surface normal, the analyzer axis and the orientation of the source of exciting radiation are specified in spherical coordinates in a fixed frame of reference. The analyzer opening angle is specified in spherical coordinates in a frame of reference for which the z-axis is parallel to the analyzer axis. The azimuthal and polar angles of the polarization vectors are also set on this screen.

4.7.1 Synopsis of CLI Commands.

1. GEOMETRY SET ACTGEO <int>

Set the number of the default geometry to which all following commands apply by default.

When the optional parameter [geometry] is omitted in any command, it is assumed to apply to the default geometry set here.

2. GEOMETRY SET SAMPLE PHI <double> [GEOMETRY <int>]
Set the azimuthal angle for the sample normal.
 - GEOMETRY: Number of the selected geometry.
3. GEOMETRY SET SAMPLE THETA <double> [GEOMETRY <int>]
Set the polar angle for the sample normal.
 - GEOMETRY: Number of the selected geometry.
4. GEOMETRY SET SAMPLE ROTATION <double> [GEOMETRY <int>]
Set the azimuthal angle of rotation of the sample around its sample normal. Note that this command is only relevant for nanostructured surfaces; for surfaces with a planar or roughness morphology this command will have no effect whatsoever.
 - GEOMETRY: Number of the selected geometry.
5. GEOMETRY SET SOURCE PHI <double> [GEOMETRY <int>]
Set the azimuthal angle for the direction of the incoming radiation.
 - GEOMETRY: Number of the selected geometry.
6. GEOMETRY SET SOURCE THETA <double> [GEOMETRY <int>]
Set the polar angle for the direction of the incoming radiation.
 - GEOMETRY: Number of the selected geometry.
7. GEOMETRY SET SOURCE POLARIZATION PHI <double> [GEOMETRY <int>]
Set the azimuthal angle of the polarization vector.
 - GEOMETRY: Number of the selected geometry.
8. GEOMETRY SET SOURCE POLARIZATION THETA <double> [GEOMETRY <int>]
Set the polar angle of the polarization vector.
 - GEOMETRY: Number of the selected geometry.
9. GEOMETRY SET ANALYZER PHI <double> [GEOMETRY <int>]
Set the azimuthal angle for the analyzer axis.
 - GEOMETRY: Number of the selected geometry.
10. GEOMETRY SET ANALYZER THETA <double> [GEOMETRY <int>]
Set the polar angle for the analyzer axis.
 - GEOMETRY: Number of the selected geometry.
11. GEOMETRY SET ANALYZER CMA [GEOMETRY <int>]
Set the analyzer aperture to that of a cylindrical mirror analyzer (CMA).
 - GEOMETRY: Number of the selected geometry.
12. GEOMETRY SET ANALYZER CHA [GEOMETRY <int>]
Set the analyzer aperture to that of a concentric hemispherical analyzer (CHA).
 - GEOMETRY: Number of the selected geometry.
13. GEOMETRY SET ANALYZER RFA [GEOMETRY <int>]
Set the analyzer aperture to that of a retarding field analyzer (RFA).

- GEOMETRY: Number of the selected geometry.
14. GEOMETRY SET APERTURE LPHI <double> [GEOMETRY <int>]
Set the lower azimuthal angle for the analyzer aperture.
 - GEOMETRY: Number of the selected geometry.
15. GEOMETRY SET APERTURE UPHI <double> [GEOMETRY <int>]
Set the upper azimuthal angle for the analyzer aperture.
 - GEOMETRY: Number of the selected geometry.
16. GEOMETRY SET APERTURE LTHETA <double> [GEOMETRY <int>]
Set the lower polar angle for the analyzer aperture.
 - GEOMETRY: Number of the selected geometry.
17. GEOMETRY SET APERTURE UTHETA <double> [GEOMETRY <int>]
Set the upper polar angle for the analyzer aperture.
 - GEOMETRY: Number of the selected geometry.
18. GEOMETRY SET MODE XPS [GEOMETRY <int>]
Set the geometry mode to XPS. In this mode, the surface area seen by the analyzer changes as the inverse cosine of the polar detection angle with respect to the surface normal.
 - GEOMETRY: Number of the selected geometry.
19. GEOMETRY SET MODE AES [GEOMETRY <int>]
Set the geometry mode to AES. In this mode, the surface area seen by the analyzer is independent of the detection angle.
 - GEOMETRY: Number of the selected geometry.
20. GEOMETRY SET FACTOR <double> [GEOMETRY <int>]
Set a geometric correction factor for each geometry. Geometrical artifacts are often difficult to avoid in a real experiment, but are usually reproducible for a given instrument. Therefore a geometry-dependent overall correction factor can be defined here.
 - GEOMETRY: Number of the selected geometry.
21. GEOMETRY ADD GEOMETRY [COPY <int>]
Add a geometry to the list for angle-resolved experiments.
 - COPY: Add a geometry to the list and copies the parameter values for the previous geometry into the new geometry.
22. GEOMETRY DELETE GEOMETRY <int>
Delete the selected geometry from the list.
23. GEOMETRY LIST
List all different geometries.
24. GEOMETRY RESET
Reset the geometrical configurations to default.
25. GEOMETRY SHOW [GEOMETRY <int>]
Show all information about the specified geometry.
 - GEOMETRY: Number of the selected geometry.

IMFP	Inelastic Mean Free Path
DIIMFP	Differential Inverse Inelastic Mean Free Path
TECS	Total Elastic Cross Section
TRECS	Transport (Elastic) Cross Section
ECS	(Differential) Elastic Cross Section
SEP	Surface Excitation Parameter
DSEP	Differential Surface Excitation Parameter
PAP	Photoelectric Asymmetry Parameter beta, dipolar
PAD	Photoelectric Asymmetry Parameter delta, multipolar
PAG	Photoelectric Asymmetry Parameter gamma, multipolar
EIICS	Electron Impact Ionization Cross Section
ABF	Auger Backscattering Factor
FY	Fluorescence Yield
PCS	Photoelectric Cross Section
XPL	X-ray Photoelectron Lineshape
AEL	Auger Electron transition Lineshape
CS	Chemical Shift

Table 4.1: Acronyms for the physical quantities in the SESSA databases.

4.8 The DATABASE Menu

This menu selects the databases for the various physical quantities used in SESSA, as shown in Fig. 4.18. The default databases used for retrieval in the expert system can be selected in this menu. The acronyms used are shown in Table 4.1.

4.8.1 Synopsis of CLI Commands.

1. DATABASE IMFP SET <string>
Select a database for retrieval of IMFP values.
2. DATABASE IMFP SHOW
Show a list of available databases for the IMFP in the CLI.
3. DATABASE DIIMFP SET <string>
Select a database for retrieval of the DIIMFP.
4. DATABASE DIIMFP SHOW
Show a list of available databases for the DIIMFP in the CLI.
5. DATABASE TECS SET <string>
Select a database for retrieval of the TECS.
6. DATABASE TECS SHOW
Show a list of available databases for the TECS in the CLI.
7. DATABASE TRECS SET <string>
Select a database for retrieval of the TRECS.
8. DATABASE TRECS SHOW
Show a list of available databases for the TRECS in the CLI.

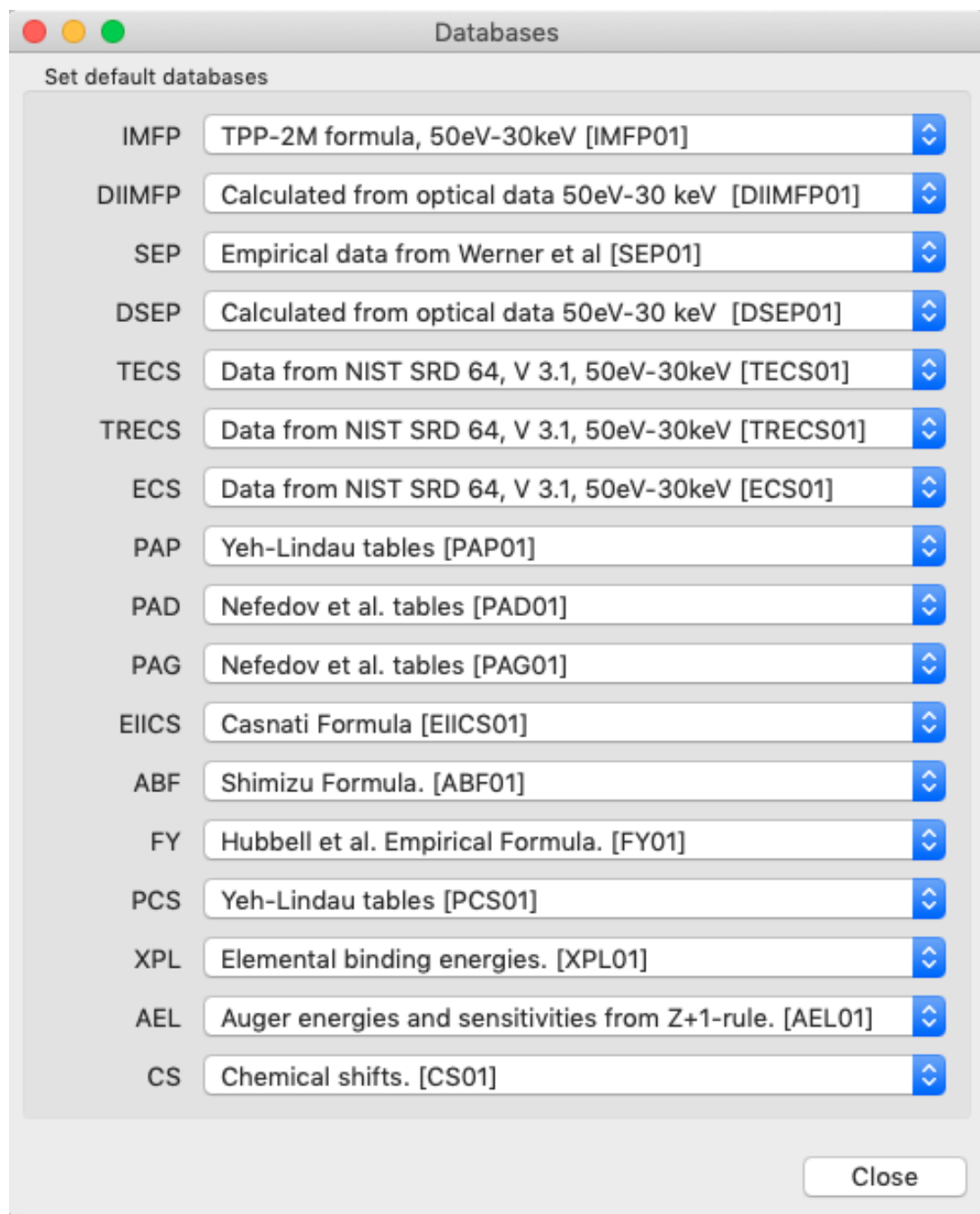


Figure 4.18: Graphical user interface for the DATABASE Menu.

9. DATABASE ECS SET <string>
Select a database for retrieval of the ECS.
10. DATABASE ECS SHOW
Show a list of available databases for the ECS in the CLI.
11. DATABASE SEP SET <string>
Select a database for retrieval of the SEP.
12. DATABASE SEP SHOW
Show a list of available databases for the SEP in the CLI.
13. DATABASE DSEP SET <string>
Select a database for retrieval of the DSEP.
14. DATABASE DSEP SHOW
Show a list of available databases for the DSEP in the CLI.
15. DATABASE PAP SET <string>
Select a database for retrieval of the PAP.
16. DATABASE PAP SHOW
Show a list of available databases for the PAP in the CLI.
17. DATABASE PAG SET <string>
Select a database for retrieval of the PAG.
18. DATABASE PAG SHOW
Show a list of available databases for the PAG in the CLI.
19. DATABASE PAD SET <string>
Select a database for retrieval of the PAD.
20. DATABASE PAD SHOW
Show a list of available databases for the PAD in the CLI.
21. DATABASE EIICS SET <string>
Select a database for retrieval of the EIICS.
22. DATABASE EIICS SHOW
Show a list of available databases for the EIICS in the CLI.
23. DATABASE ABF SET <string>
Select a database for retrieval of the ABF.
24. DATABASE ABF SHOW
Show a list of available databases for the ABF in the CLI.
25. DATABASE FY SET <string>
Select a database for retrieval of the FY.
26. DATABASE FY SHOW
Show a list of available databases for the FY in the CLI.

27. DATABASE PCS SET <string>
Select a database for retrieval of the PCS.
28. DATABASE PCS SHOW
Show a list of available databases for the PCS in the CLI.
29. DATABASE XPL SET <string>
Select a database for retrieval of the XPL.
30. DATABASE XPL SHOW
Show a list of available databases for the XPL in the CLI.
31. DATABASE AEL SET <string>
Select a database for retrieval of the AEL.
32. DATABASE AEL SHOW
Show a list of available databases for the AEL in the CLI.
33. DATABASE CS SET <string>
Select a database for retrieval of the CS.
34. DATABASE CS SHOW
Show a list of available databases for the CS in the CLI.
35. DATABASE SHOW DATABASE
Show a list of the databases selected for retrieval/simulation of XPS/AES spectra in the CLI.

4.9 The MODEL Menu

This menu controls parameters of the simulation, as indicated in Fig. 4.19. SESSA is able to perform a Monte Carlo simulation of an electron spectrum based on the parameters retrieved for the specified sample and for the specified experimental conditions, as described in Ref. [1]. For this purpose, a number of trajectories that mimic the physics of the electron transport are generated. The simulation algorithm is very efficient: each trajectory contributes to all energies in the spectrum. This is achieved by assigning an *a posteriori* likelihood for n -fold scattering to each trajectory. For each trajectory, a contribution to the so-called partial intensities is calculated. These quantities represent the probability that a given electron arrives at the detector after experiencing a given number of collisions. Multiplying this number with the distribution of energy losses after a given number of inelastic collisions gives the partial spectrum of n -fold inelastically scattered electrons. Adding up these contributions gives the total simulated spectrum. Furthermore, the trajectory reversal algorithm [21] is used by SESSA. This algorithm allows a user to perform simulations for a detector with an infinitely narrow opening angle of the analyzer (See Ref. [1] for more details about the simulation procedure). The maximum number of collisions ("Number of collisions") is either determined automatically or can be set by the user. The computation time required for a simulation increases with this maximum number: in particular, if $ndiimfp=2$ is chosen in the preferences menu, the required time will be greater (see section 4.3). If only the intensities of the peaks in the spectrum are of interest (electrons escaping without any inelastic collision), the maximum number of collisions can be set to zero. The simulated spectral shape will be then unrealistic, but the peak intensities will be realistic and generated very efficiently. The number of

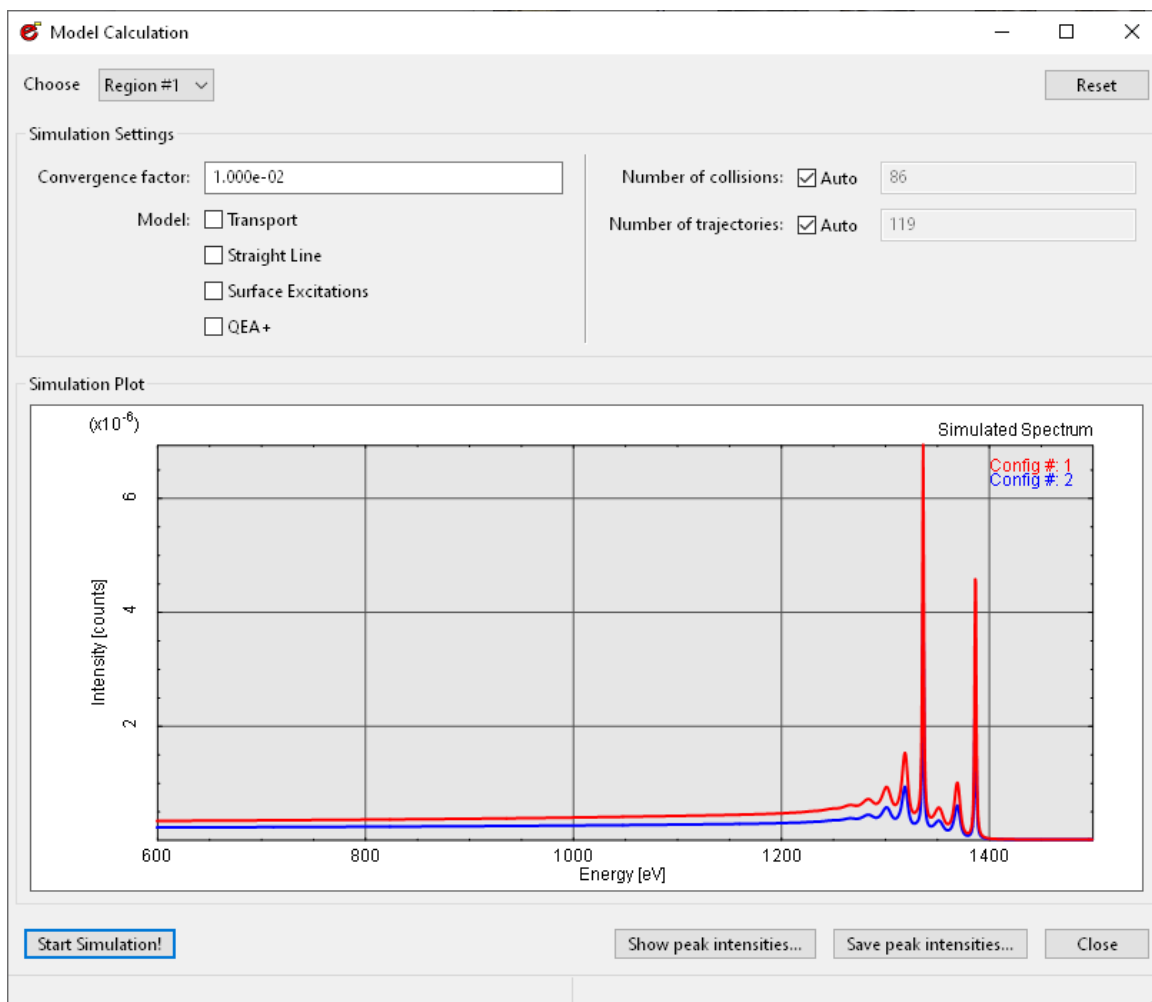


Figure 4.19: Graphical user interface for the MODEL Menu.

trajectories that is generated is either determined automatically by the convergence criterion, or can be specified by the user (typically 500 for a calculation with 1% precision.)

The user can choose to carry out a simulation in various approximations. It is presently possible to choose between five different approaches; the first three correspond to employing different distributions of scattering angles and associated mean free paths for successive collisions; the latter two concern the treatment of energy losses:

- (1) the usual "Mott" cross section for elastic scattering calculated from the relativistic plane-wave expansion method that is believed to provide a realistic description of elastic-scattering events of electrons in solids when used in conjunction with the elastic mean free path (EMFP) derived from it [21, 22].
- (2) Neglect of elastic deflections (straight line approximation, SLA, or rectilinear motion model), corresponding to an infinite elastic mean free path; and
- (3) an isotropic transport cross section taking the transport mean free path (TMFP) as the characteristic length for elastic deflections.
- (4) Surface Excitations can optionally be accounted for in the model calculations (SE)
- (5) A model in which the energy dependence of the inelastic mean free path is approximately taken into account (QEA+) (see section 5.2.5 for details)

The third approach is essentially equivalent to the so-called transport approximation (TA), see Ref. [1] and Ref. [23].

The latter four options for the simulation approach can be selected by checking the corresponding boxes labelled "Transport" "Straight Line" "Surface Excitations" and "QEA+" in the GUI (Fig. 4.19). The Show Peak intensities and Save Peak intensity buttons provide a convenient means of displaying and/or saving the zero-th order partial intensities for the peaks in the spectrum.

As described in Section 4.4, simulations can be made for a single nanoparticle or island. After selecting spheres, layered spheres or islands for the sample morphology and specifying the relevant materials and dimensions, the user can enter MODEL SET SINGLE TRUE or ... FALSE in the CLI to enable or disable the option. Note that this option cannot be selected from the GUI. Although the SESSA simulations will be performed for a single nanoparticle or island, the values of the X and Y periods here define the dimensions of the limiting body as described in Section 8. It is then important to select values of the X and Y periods (either through the GUI or the CLI) to correspond to the total particle size (spheres, layered spheres) or to reproduce the desired surface coverage (islands). Doing otherwise may lead to inaccurate or erroneous results.

Another option is to perform a simulation for a nanoparticle (spheres, layered spheres) without a substrate. This is done by entering MODEL SET NOSUB TRUE or ... FALSE in the CLI to enable or disable the option. This option is not available through the GUI. When using the NOSUB option, the substrate peaks must be deleted from the List of Peaks or otherwise the simulation will freeze. The morphology modes Planar and Roughness should not be used with the SINGLE option or the NOSUB option. The morphology mode Islands can be used with the SINGLE option, but should not be used with the NOSUB option. The use of either the SINGLE or the NOSUB option (or both) can drastically reduce the computation times for otherwise equivalent simulations.

Notes: For nanoparticles (spheres, layered spheres), it is recommended to only use the SINGLE and NOSUB options in combination. The SINGLE and NOSUB options can be used in combination with external PENGEOOM geometry files; for more details, the user is referred to Section 8.4.

4.9.1 Synopsis of CLI Commands.

1. MODEL SET NCOL <int> [REGION <int>]

Set the maximum number of inelastic collisions to a fixed value.

- REGION: Number of the selected spectrometer region.

2. MODEL SET NTRAJ <int> [REGION <int>]

Set number of trajectories used in the simulation to a fixed value.

- REGION: Number of the selected spectrometer region.

3. MODEL SET TA <string>

Set TA (transport approximation) to 'true' or 'false'. If TA is set to 'true', an isotropic distribution of polar deflection angles is used in the simulation.

4. MODEL SET SLA <string>

Set SLA (straight line approximation) to 'true' or 'false'. If SLA is set to 'true', deflections of the electrons by elastic scattering during their escape from the surface will be completely neglected.

5. MODEL SET SE <string>
Set SE (surface excitations) to 'true' or 'false'. If SE is set to 'true', surface excitations are taken into account in the simulation.
6. MODEL SET QEAPLUS <string>
Set QEAPLUS (quasi elastic approximation plus) to 'true' or 'false'. If QEAPLUS is set to 'true', the energy dependence of the IMFP is taken into account in the simulation via the so-called QEA+ approximation (see section 5.2.5 for details)
7. MODEL SET CONVERGENCE <double>
Set the convergence criterion for the MC simulation. The simulation for a given peak terminates when the relative change in the sum of all requested partial intensities drops below the criterion for ten successive trajectories. So, for example, if the user has set number of collisions=0, and the convergence criterion is 0.01, then the simulation terminates if the intensity of the no-loss peak changes by less than 1% for 10 successive trajectories. Then, the precision of the calculation for the peak intensity will be better than 1%. Note that when an entire spectrum is simulated (number of collisions>0), the sum of all partial intensities (to which the termination criterion applies) is actually the total spectral intensity (area under the spectrum) for the considered transition.
8. MODEL SET SINGLE <string>
If this parameter is 'true' simulation of a single nanoparticle on the surface is performed instead of a periodic array of nanoparticles.
9. MODEL SET NOSUB <string>
If this parameter is 'true', the simulation is truncated at the substrate. ATTENTION: Remove the substrate material peaks or the simulation will freeze.
10. MODEL AUTO NCOL [REGION <int>]
Maximum number of inelastic collisions will be automatically calculated by the simulation module.
 - REGION: Number of the selected spectrometer region.
11. MODEL AUTO NTRAJ [REGION <int>]
Number of trajectories will be automatically calculated by the simulation module.
 - REGION: Number of the selected spectrometer region.
12. MODEL PLOT [REGION <int>]
Graphical representation of the simulated spectrum for a given spectrometer region in the separate plot window.
 - REGION: Number of the selected spectrometer region.
13. MODEL SIMULATE
Perform a Monte Carlo simulation of the spectral shape using the given settings for all relevant parameters.
14. MODEL SHOW
Show information on parameters controlling the simulation.
15. MODEL RESET
Reset model settings to the default values.

16. MODEL SAVE SPECTRA <string>

Save the simulated spectra of all regions into a file whose filename begins with <string>. This will write the angular distribution for all spectra if more than one geometrical configuration was specified.

17. MODEL SAVE INTENSITIES <string>

Save the peak intensities (zero order partial intensities) of all peaks to a file with filename <string>. This will write the angular distribution of all peaks to a file if more than one geometrical configuration was specified.

5 Retrieval strategy and simulation model

5.1 Retrieval strategy of the expert system

In a first step, the expert system establishes the relevant peaks in accordance with the user's specification of the sample composition and the selected excitation source and spectrometer settings. This is done by looking up the source energy and the type of exciting radiation (photons, electrons) and querying the databases for the peak shapes for each element in all layers of the sample. When a peak is found that is not present in the internal peak list, and it falls within any of the specified spectrometer regions, the peak is added to the peak list. This peak list is on display in the "Sample/Peaks" menu in the GUI and can be listed via the corresponding command in the CLI.

The energy distribution for a useful peak in an AES or XPS spectrum for a solid is known to be sharply peaked with respect to the nearby background. However, the total energy range where the emission probability assumes non-vanishing values can generally be very broad. In order to decide whether a peak should be taken into account in a given spectrometer region, it is therefore necessary to invoke some meaningful criterion. In the SESSA expert system, this is done by comparing the fraction of the peak *area* that falls within the considered spectrometer energy region with the threshold parameter. If this fraction exceeds the threshold value specified by the user (see Section 4.3), the peak is included; otherwise it is discarded from the peak list.

If a given element is present in more than one chemical state, each peak for this material is added in duplicate to the peak list, and is accordingly labelled. While the main purpose of the chemical-state label is indeed to indicate the chemical states of a given element in order for the software to be able to differentiate between different them, it is to be noted that the chemical state label is nothing but an *arbitrary* label allowing such a distinction to be made. In other words, it can just as well be used for an entirely different purpose, e.g. to simulate the excitation depth distribution in some special applications of electron spectroscopy (see for example Section 7.3.1).

After the relevant peaks have been established in this way, the parameters for the generation of the associated signal electrons are retrieved from the corresponding databases together with the parameters describing the characteristics of the electron-solid interaction (or, in other words, the surface sensitivity).

As mentioned before, an essential aspect of the expert system, in particular in conjunction with a simulation module, is that for each considered electronic transition leading to the emission of signal electrons, *all* parameters concerning their generation and interaction with the solid *must* be known; otherwise the software will eventually be unable to take meaningful decisions and to provide meaningful results (i.e., the software would cease to run). This situation is, of course, completely unacceptable, and the databases must therefore be able to return at least a credible estimate for each queried quantity. As explained in Section 3.1, SESSA is designed always to provide a backup database that is extensive. The reliability of the returned datum from the backup

database is, of necessity, not always comparable to the typical reliability of the other databases. Nevertheless, the fact that each datum is traceable to its source in the scientific literature (see also Section 6) makes the individual reliability of any datum accessible to the user, while the overall reliability of, for example, the outcome of a simulation of SESSA can be assessed in survey form by inspection of the files ending with "rems.txt" and "refs.txt" (see Section 3.4).

5.2 Algorithm for spectrum simulation

When all required parameters have been retrieved from the databases, a simulation of the expected outcome of the specified experiment can be performed with SESSA. The simulation algorithm is based on the partial intensity approach for the electron-solid interaction [1, 24–27]. The key quantities in this approach are the so-called partial intensities that describe the number of electrons arriving at the detector after having participated in a given number of inelastic collisions in the solid between their point of generation and escape from the surface. In SESSA, the partial intensities are calculated with a very efficient Monte Carlo calculation based on the so-called trajectory reversal algorithm [21] that benefits from a symmetry property of the (linearized) Boltzmann kinetic equation which forms the basis of the surface sensitivity of electron-beam techniques for non-crystalline solids. In the following sections, the simulation algorithm is described in some detail. The user can thus better understand and interpret the results of a simulation.

In the range of medium energies (50 eV to 20 keV) for which SESSA is designed, the characteristics of the electron–solid interaction allow some drastic simplifications to be made leading to a convenient starting point of the theory. In particular, a clear distinction can be made between multiple inelastic scattering and multiple elastic scattering. While inelastic scattering can be treated in a straightforward manner by means of an analytic theory, elastic scattering is most conveniently tackled by means of a numerical approach. The Monte Carlo technique employed by SESSA is the most flexible numerical technique with respect to the boundary conditions of the considered problem.

5.2.1 The electron spectrum in AES/XPS

The objective of SESSA is to facilitate interpretation of the spectra of electrons that are generated by means of electron or photon bombardment in the near-surface region of a solid, escape from the surface, and are analyzed and detected by a spectrometer. Obviously, the quantities relevant for the mentioned processes, and in particular any eventual relationship between them, need to be studied before establishing a theory describing the phenomenon. A detailed discussion on the physical quantities describing the signal electron generation and transport is beyond the scope of this guide and the reader is referred to reviews in the literature (e.g. Refs. [1, 2, 28]).

The most important facts may be summarized as follows:

- For any given electronic transition, the energy and angular distributions are uncorrelated; i.e., the energy distribution of electrons liberated at an atom in a solid is the same for all emission directions. Since the depth distribution of the emitting sources is determined by the compositional depth profile of the specimen, we expect that the source angular, energy and depth distributions will be uncorrelated, and the source distribution $S_0(E, z, \vec{\Omega})$ can be factored into energy- ($f_0(E)$), angular- ($g_0(\vec{\Omega})$) and depth- ($c_0(z)$) dependent terms:

$$S_0(E, z, \vec{\Omega}) = f_0(E) \times c_0(z) \times g_0(\vec{\Omega}) \quad (5.1)$$

Here $\vec{\Omega} = (\theta, \phi)$ is a shorthand notation for the electron emission direction, specified by the polar angle θ and the azimuthal angle ϕ .

- The electron–solid interaction characteristics for the electron transport (mean free paths, cross sections, etc.) are not strongly energy dependent. More precisely, the change in any interaction characteristic is small compared to the value of that quantity when the energy changes by an amount ΔE corresponding to a typical energy loss $\langle T \rangle \sim e^2/a_0 = 27.2$ eV (also corresponding to 2 Ry = 1 Hartree) in an inelastic collision, where e is the electron charge and a_0 the Bohr radius. We then have:

$$\frac{\Delta\lambda}{\lambda} \ll \frac{\Delta E}{\langle T \rangle} \quad (5.2)$$

where λ stands for any of the interaction characteristics. This condition is the basis for the so-called quasi-elastic approximation (QEA) in which it is assumed that the interaction characteristics of a photoelectron are constant in between the photoionisation process inside the solid and its emission from the surface. An approximate means to account for the energy dependence of the interaction characteristics is described in Section 5.2.5.

- The width of the energy distribution for any useful peak in an AES or XPS spectrum is small compared to the typical energy loss in an inelastic collision.
- Energy losses and deflections can be regarded as independent processes.

The above conditions are generally fulfilled in AES and XPS [1] and allow one to immediately understand the so-called partial intensity approach for the theoretical description of an electron spectrum, without resorting to complicated mathematical derivations. Readers interested in a rigorous mathematical treatment of the problem are referred to Ref. [28].

The source term in Eq. 5.1 is evaluated as follows: the energy dependent factor, $f_0(E)$, is entirely determined by user specification in the peak menu (see section 4.4.7), i.e. the parametrisation of a peak shape specified by a user is used, or, alternatively, an empirical peak shape can be read in. The depth dependent factor, $c_0(z)$, is entirely determined by the sample morphology as set in the sample morphology menu (see section 4.4.3). Note that only if a planar morphology is selected in the morphology menu, this is actually a function depending only on the depth (and not on the lateral coordinates). In all other cases it also depends on the lateral coordinates. In the following, we will nonetheless maintain the notation $c_0(z)$, adopted above, but the reader should keep in mind that the distribution of sources may in general be a three-dimensional one. In particular, this implies that the integrals over the depth in the formulae below, run over all Space. Finally, the angular source distribution $g_0(\vec{\Omega})$ is taken to be isotropic in the case of Auger electron emission, while for photoelectrons it is generally highly anisotropic and is determined by the experimental configuration, through the angle θ_k between the incident radiation and the emission direction of the photoelectron, and, in the case of (partially) linear polarisation of the incoming beam, by the angle θ_ε between the direction of emission of the photoelectron and the direction of the polarisation vector of the incident photon beam. The corresponding directions can be set by a user in the geometry menu (see section 4.7). Denoting the fraction of linearly polarised light of the beam by P , the differential photoelectric cross section is taken to be [20]:

$$\begin{aligned} \frac{4\pi}{\sigma_x} \frac{d\sigma_x}{d\Omega} &= 1 + \frac{\beta}{4} \left[1 - 3P + 6P \cos^2 \theta_\varepsilon + 3(P-1) \cos^2 \theta_k \right] \\ &+ \left[\delta + \gamma P \cos^2 \theta_\varepsilon - \frac{\gamma}{2}(P-1) \right] \cos \theta_k + \frac{\gamma}{2}(P-1) \cos^3 \theta_k \end{aligned} \quad (5.3)$$

where β is the dipolar asymmetry parameter, γ and δ are the non-dipolar parameters and σ_x is the total cross section for the considered shell. The latter parameters are all automatically retrieved from databases in SESSA.

It is obvious that each electron leaving the surface has experienced a given number, say $n = 0, 1, 2, \dots$ of inelastic collisions. In other words, the emerging spectrum consists of groups of electrons that have experienced a certain number of inelastic processes. Since the energy and angular distribution in the source function $S_0(E, z, \vec{\Omega})$ factorize into energy and angular terms, and since elastic (deflections) and inelastic collisions (energy losses) may be assumed to occur independently, it follows that each of the groups of n -fold inelastically scattered electrons is also a product of a function $F_n(E)$ depending only on the energy and a function $C_n(\vec{\Omega})$ that depends only on the emission direction. Taking the energy distribution of the n -th group, the so-called partial energy distribution, to be normalized, $\int F_n(E)dE \equiv 1$, the partial intensities $C_n(\vec{\Omega})$ are identified as the *number* of electrons in the corresponding group.

Since the energy dependence is assumed to be sufficiently weak, it follows that the interaction characteristics within each group can be taken to be the same and, furthermore, since the energy distribution at the source is narrow compared to the typical energy loss, the transfer processes determining the surface sensitivity are the same for all electrons within a given peak.

Summing up the different groups gives the spectrum $Y(E, \vec{\Omega})$:

$$Y(E, \vec{\Omega}) = \sum_{n=0}^{n_{max}} C_n(\vec{\Omega}) F_n(E) \quad (5.4)$$

In the above expression, n_{max} is the largest order of inelastic scattering considered. In SESSA, this parameter can be automatically determined, by clicking the "Auto" box in front of the "number of inelastic collisions" field in the simulation menu, or can be set by the user. The latter option is convenient, e.g., when only the intensity of the peak of no-loss electrons is of interest since this intensity can then be calculated very efficiently (see Section 5.2.3). The remaining problem is to find a convenient means of evaluating the partial intensities and energy distributions. This is discussed in the next sections.

5.2.2 Multiple inelastic scattering: the partial energy distributions

Since the transport equation is linear, it is straightforward to express the distribution of energy losses after a given number of inelastic collisions in terms of the source energy distribution $f_0(E)$ if the energy-loss distribution in a single inelastic collision $w(T)$ is known. The latter quantity is of course identical to the (normalized) differential inelastic inverse mean free path for which a database is available in SESSA.

Let us assume that the source energy distribution $f_0(E)$ is normalized to unity area. The probability that an Auger- or photoelectron is emitted by an atom with an energy between $E + T$ and $E + T + dT$ is then given by $f_0(E + T)dT$. Multiplying this probability with the probability $w(T)$ for an energy loss in the interval $(T, T + dT)$ gives the probability that the electron has the energy E after it experienced a single inelastic collision. Integrating over all different possible values of the energy loss T gives the energy distribution after one energy loss as:

$$F_1(E) = \int f_0(E + T)w(T)dT \quad (5.5)$$

In exactly the same way, the higher-order loss distributions may be established. The whole procedure may be summarized by the recurrence relations:

$$\begin{aligned} F_n(E) &= \int F_{n-1}(E + T)w(T)dT \\ &= \int f_0(E + T)L_{n-1}(T)dT \end{aligned} \quad (5.6)$$

In the second line of this equation, the partial loss distributions $L_n(T)$, i.e., the distribution of energy losses after n inelastic collisions, is introduced.

When more than one type of inelastic-scattering distribution is of relevance for the considered problem (e.g., when the inelastic-scattering properties are significantly different in the two topmost layers of the sample), the above equation can be generalized as follows:

$$\begin{aligned} F_{n_1,n_2,n_3,\dots}(E) &= \int F_{n_1-1,n_2,n_3,\dots}(E + T)w_1(T)dT \\ &= \int F_{n_1,n_2-1,n_3,\dots}(E + T)w_2(T)dT \\ &= \dots \end{aligned} \quad (5.7)$$

Where $w_1(T)$ is the distribution of energy losses for the first layer, etc. In the present version of SESSA, it is possible to distinguish between two different inelastic-scattering distributions, $w_1(T)$ and $w_2(T)$, by setting the parameter NDIIMFP to two. One inelastic-scattering distribution ($w(T)$) is set as the default (NDIIMFP=1) (see Section 4.3).

5.2.3 Multiple elastic scattering: the partial intensities.

The partial intensities $C_n(\vec{\Omega}_i, \vec{\Omega}_e)$ (the number of signal electrons arriving at the detector that have experienced n inelastic collisions) depend on several experimental parameters such as the flux of exciting radiation, the spectrometer transmission, etc., as well as on the source depth distribution of the emitting species $c_0(z)$ (where $c_0(z)$ represents the atomic fraction at a given depth z), the probability that a transition takes place at a certain depth, the so-called excitation depth distribution function $\phi_x(z, \vec{\Omega}_i, \vec{\Omega}_x)$ and the probability for escape after n inelastic collisions, that is described by the emission depth distribution functions $\phi_{e,n}(z, \vec{\Omega}_x, \vec{\Omega}_e)$:

$$C_n(\vec{\Omega}_i, \vec{\Omega}_e) = DAFTN_a \int_{\Delta\Omega} \int_{4\pi} \int_0^\infty \phi_x(z, \vec{\Omega}_i, \vec{\Omega}_x)c_0(z)\phi_{e,n}(z, \vec{\Omega}_x, \vec{\Omega}_e)dzd\vec{\Omega}_xd\vec{\Omega}_e \quad (5.8)$$

The subscripts "x" and "e" are used again to denote the excitation and emission processes respectively, and $\vec{\Omega}_x$ and $\vec{\Omega}_e$ are the emission direction of the signal electron at the source and the direction of emission from the surface. Furthermore, D denotes the detector efficiency, T is the spectrometer transmission, F is the flux of the exciting radiation, N_a is the atomic density, and A is the analyzed area.

The latter is obviously determined by the experimental geometry and, in particular, depends on whether the area seen by the analyzer exceeds the excitation area on the sample. In this case, the analysed area is independent of the emission angle, whereas in the opposite case when the illuminated area is much larger than the area seen by the analyzer, the analyzed area varies with the polar emission angle as $A \propto 1/\cos\theta_e$. The latter situation corresponds to the XPS-mode in

the Geometry menu of SESSA (see Section 4.7), while the former corresponds to the AES mode; note, however, that the AES mode could be applicable to XPS instruments in which the incident X-rays are focused to a relatively small area. It is also important to recognize that perfect alignment of the beam of primary radiation and the analyzer is not always achievable in measurements of angular distributions, in which case geometrical artifacts can arise in the measured angular distributions. Sometimes, measurements can be made of the relevant calibration factors. These calibration factors, if known, can be entered for a given geometry in the geometry correction factor box of the Geometry menu.

The quantity $\Delta\Omega$ represents the solid angle of the analyzer, over which the emitted spectrum needs to be integrated. The magnitude of the solid angle is indicated in the geometry menu on the panel showing the acceptance angle of the spectrometer. The factors D , F and T in front of the integral in Eq. 5.8 are taken to be unity in the present implementation of SESSA.

A further simplifying assumption made in the simulation is that the excitation depth distribution function $\phi_x(z, \vec{\Omega}_i, \vec{\Omega}_x)$ varies only very slowly with the depth. This quantity can then be taken outside the depth integral and replaced by the production cross section $\sigma_{ex}(\vec{\Omega}_i, \vec{\Omega}_x)$. In an XPS experiment, this production cross section is equal to the photoelectric cross section $\sigma_{ph}(\vec{\Omega}_i, \vec{\Omega}_x)$. In AES the production cross section is independent of Ω_x and is given by the product of electron impact ionization cross section σ_{ei} , the Auger backscattering factor $(1 + r_A(\Omega_i))$ that accounts for the additional ionization of the considered subshell through backscattered primary electrons, and the probability that the core hole is filled via the considered Auger electron transition, indicated here with ω_A : $\sigma_{ex} = \sigma_{ei}\omega_A(1 + r_A(\Omega_i))$.

In the present version of SESSA, the angular dependence of the excitation depth distribution is also simplified. In the case of AES, the dependence on $\vec{\Omega}_i$ is assumed to follow Shimizu's expression [29], while the emission angular distribution at the source is taken to be isotropic. For XPS, it is assumed that the direction of incidence at the location of signal-electron generation is identical to the incident direction of the X-rays on the surface, i.e., deflections of photons in the solid and at the surface are neglected. Taking into account the above assumptions and collecting all constant terms into a new constant K , the partial intensities can be written as:

$$C_n(\vec{\Omega}_i, \vec{\Omega}_e) = K \int_{\Delta\Omega} \int_{4\pi} \int_0^{\infty} \sigma'_{ex}(\vec{\Omega}_i, \vec{\Omega}_x) c_0(z) \phi_{e,n}(z, \vec{\Omega}_x, \vec{\Omega}_e) dz d\vec{\Omega}_x d\vec{\Omega}_e \quad (5.9)$$

where $\sigma'_{ex}(\vec{\Omega}_i, \vec{\Omega}_x)$ represents the normalized angular part of the production cross section.

The emission depth distribution functions $\phi_{e,n}(z, \vec{\Omega}_x, \vec{\Omega}_e)$ represent the probability for signal-electron escape from a given depth after experiencing a given number of inelastic collisions n . The probability for n -fold scattering, on the other hand, depends on the pathlength travelled inside the solid. Due to elastic scattering, not all electrons travel the same pathlength; rather, the pathlengths s are distributed according to a function $Q(z, s, \vec{\Omega}_x, \vec{\Omega}_e)$. In other words, the depth distribution function can be expressed in terms of this pathlength distribution function and the probability for n -fold scattering as a function of the travelled pathlength $W_n(s)$ [24] that is given by the Poisson distribution when the interaction characteristics are assumed to be independent of the energy. The latter approach, known as the quasi-elastic approximation [1,2,24,30], is adopted in SESSA and is valid when the considered energy loss range is small compared to the primary energy. The emission depth distribution can be written as:

$$\phi_{e,n}(z, \vec{\Omega}_x, \vec{\Omega}_e) = \int_0^{\infty} Q(z, s, \vec{\Omega}_x, \vec{\Omega}_e) W_n(s) ds \quad (5.10)$$

Using this result, Eq. (5.9) can be transformed as follows:

$$C_n(\vec{\Omega}_i, \vec{\Omega}_e) = K \int_{\Delta\Omega} \int_{4\pi} \int_0^\infty \int_0^\infty \sigma'_{ex}(\vec{\Omega}_i, \vec{\Omega}_x) c_0(z) Q(s, z, \vec{\Omega}_x, \vec{\Omega}_e) W_n(s) ds d\vec{\Omega}_x d\vec{\Omega}_e dz \quad (5.11)$$

The distribution of pathlengths represents a quantity that is ideally suited for calculation with the Monte Carlo (MC) technique since in this approach a large set of trajectories is simulated. By making a histogram of the lengths of such a set of trajectories, the pathlength distribution is immediately obtained. In SESSA, the integral in Eq. (5.11) is therefore calculated by means of the Monte Carlo (MC) technique. The MC simulation is based on the very efficient trajectory reversal algorithm [21], which in turn is based on a symmetry property of the Boltzmann kinetic equation, the so-called reciprocity theorem (see e.g. Ref. [31]).

This theorem states that, for a quasi-elastic trajectory, the source point and the terminal point of a trajectory are equivalent. In other words, instead of simulating a trajectory from its source point through the solid and hoping that this electron is emitted from the surface with the correct direction to be detected by the analyzer (which, depending on the magnitude of the acceptance solid angle of the analyzer, is not likely to be the case for the overwhelming majority of all trajectories), one can also start the simulation at the analyzer and trace back the path of the electron inside the solid. In this way a significant increase in the efficiency of a MC calculation is obtained that makes it possible to perform simulations of this kind on a personal computer.

The generation of trajectories proceeds in the usual way by means of the Monte Carlo technique. More details can be found in Ref. [1]. It is only noted here that the user has a choice among three different types of elastic-scattering cross sections in the simulation:

1. The “Mott” cross section for elastic scattering derived from the relativistic plane-wave expansion method. This choice is believed to give the most reliable results [32], and is recommended for most applications.
2. The isotropic transport cross section. This choice (made by checking the Transport box in the Model menu of Fig. 4.17) allows a faster simulation of the trajectories and gives excellent results when the conditions of the so-called generalized radiative field principle are met [23]. The use of the transport cross section corresponds to making the transport approximation that is often used in the analytic treatment of such problems [1]. The transport cross section is one of a few types of cross section for which the transport equation can be solved analytically.
3. A forward-peaked delta-function-shaped “cross section” representing the rectilinear motion model or straight-line approximation (SLA). This choice (made by checking the Straight Line box in the Model menu of Fig. 4.19) allows a user to study the magnitude of elastic-scattering effects in a given application (i.e., by comparing results from this choice with results of a similar simulation made using the Mott cross section).

In SESSA, the efficiency of the trajectory-reversal algorithm is further enhanced by directly calculating the partial intensities, rather than first calculating the pathlength distribution and then integrating this distribution. Furthermore, the method of statistical weights is used to account for the angular and depth dependences of the source function. To appreciate the former statement, note that the integrals in Eq. (5.10) and Eq. (5.11) can be calculated immediately along each trajectory, instead of first making a histogram and then later performing the integrations. The integral

Eq. (5.11) can thus be solved by directly summing up the contributions to the partial intensities $(\Delta C_n)_k$ corresponding to the k -th linear step between two deflections in the MC algorithm as follows:

$$(\Delta C_n)_k(\vec{\Omega}_i, \vec{\Omega}_e) = K \int_{s_k}^{s_k + \Delta s_k} W_n(s) \sigma'_{ex}(\vec{\Omega}_i, \vec{\Omega}_{x,k}) c_0(z(s)) ds \quad (5.12)$$

Here s_k is the pathlength travelled in the solid before the k -th step and Δs_k is the length of the k -th step. The second and third factor in the integral account for the angular and depth dependence of the source function. Assigning the appropriate weight factors for the source distribution in this way in an MC algorithm is known as the method of statistical weights. The integral in Eq. (5.12) can be evaluated analytically, leading to an additional enhancement of computational speed.

After a sufficiently large set of trajectories has been established in this way, the partial intensities are finally obtained as:

$$C_n(\vec{\Omega}_i, \vec{\Omega}_e) = \frac{1}{N_{traj}} \sum_{j=0}^{N_{traj}} \sum_{k=0}^{N_k} (\Delta C_n)_{k,j}(\vec{\Omega}_i, \vec{\Omega}_e) \quad (5.13)$$

The number of steps per trajectory, N_k , is determined by the termination criterion. When the total pathlength of a trajectory exceeds a pathlength given by the IMFP and the considered order of partial intensities n_{max} :

$$s > 2 \times \lambda_i \times (n_{max} + 5), \quad (5.14)$$

the trajectory is terminated. The total number of trajectories, N_{traj} , is determined by the convergence criterion. If the fractional change of the sum of all considered partial intensities is below the convergence factor, generation of trajectories is terminated. The sum of all partial intensities is of course identical to the total spectral intensity of a peak (i.e., the area of the peak and the inelastic background). Note that for, e.g., a thin layer on top of a substrate, the partial intensities decrease rapidly with the order of inelastic scattering. Then, on a logarithmic display, the dependence of the simulated partial intensities on the number of inelastic collisions may exhibit oscillations. These are caused by the fact that the higher-order partial intensities only contribute negligibly to the total spectral intensity and such oscillations are thus an artifact of the convergence of the simulation. As an alternative means to control the convergence behavior of the algorithm, the user may directly specify the number of trajectories in the simulation menu.

A further aspect of the simulation that deserves to be mentioned here is the fact that the vacuum-solid interface is generally assumed to be atomically flat in SESSA. The only other surface morphology, apart from this idealized concept of an atomically flat surface, is a rough surface. The surface roughness can be specified by a user in SESSA by setting the value of the relative surface area (RSA, see Section 4.4). The relative surface area is a measure of the surface roughness in terms of the ratio of the real surface area divided by the projected surface area, i.e., the area of the idealized flat surface.

5.2.4 Modeling surface excitations in electron spectra

A simple model for surface excitations induced by Auger or photoelectrons escaping from semi-infinite solids with planar surfaces and energy losses suffered as a consequence has been implemented in SESSA [33, 34]. Surface excitations are additional modes of the inelastic scattering process in the bulk of a material and are a consequence of the boundary conditions of Maxwell's equations near an interface between media with a different dielectric constant, in the present case the sample and vacuum. The starting point of this model is the observation that the depth range

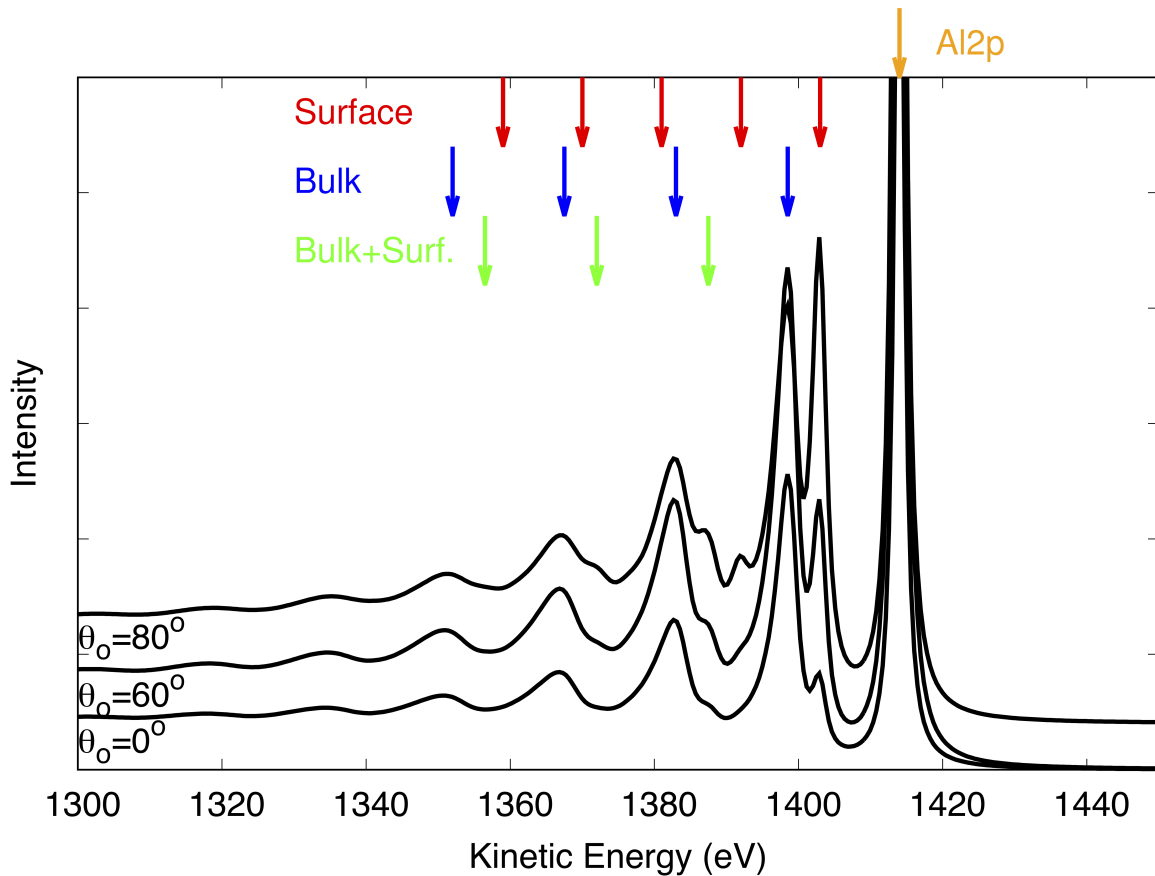


Figure 5.1: Simulation results for the Al-K α excited Al2p photoelectron peak taking into account surface excitations using the database "SEP03" for different photoelectron emission angles θ_0 with respect to the surface normal. Red arrows indicate surface plasmons, blue arrows indicate bulk plasmons, and green arrows indicate combination bulk and surface plasmons (see text).

where surface excitations take place is very shallow inside the solid, while surface excitations also take place in vacuum when the probing electron still interacts with the solid state electrons. When the pathlength of escaping electrons inside the surface scattering zone is sufficiently small compared to the characteristic mean free path for deflections, the passage through the surface scattering zone is approximately rectilinear, and the partial intensities for bulk and surface scattering are uncorrelated [27, 33, 35]:

$$C_{n_b, n_s} = C_{n_b} \times C_{n_s} \quad (5.15)$$

where n_b and n_s are the collision numbers for bulk and surface scattering, respectively. Rectilinear passage also implies that the probability for plural surface scattering is governed by the Poisson stochastic process:

$$C_{n_s}(E, \theta) = \frac{\langle n_s(E, \theta) \rangle^{n_s}}{n_s!} e^{-\langle n_s(E, \theta) \rangle}, \quad (5.16)$$

where $\langle n_s(E, \theta) \rangle$ is the average number of surface excitations during a single surface crossing with energy E and angle θ (with respect to the surface normal). Different physical models have

Name	Eqn.	SEP(a_{DB})	#SE for Al2p	Ref.
SEP01	(5.17)	Empirical	0.121	[34]
SEP02	(5.18)	Empirical	0.243	[38]
SEP03	(5.17)	$0.039\hbar\omega_p + 0.4$	0.175	[34]
SEP04	(5.18)	$\sqrt{32a_0e^2/\pi^2}$	0.345	[39]
SEP05	(5.17)	$\sqrt{8a_0/\pi^2e^2}$	0.173	[36]

Table 5.1: Survey of databases for the surface excitation parameter (SEP) and employed equation used in conjunction to calculate the average number of surface excitations. The quantity $\hbar\omega_p$ in the universal guideline to calculate the SEP in Ref. [34] is the plasmon energy, which is calculated in SESSA from the density of the material, a_0 is the Bohr radius and e the elementary charge. Note that for user-defined values of the SEP, Eqn. 5.17 is always used to calculate the surface partial intensities. The column headed #SE Al2p shows the average number of surface excitations retrieved from the corresponding SEP databases for the spectra shown in Fig. 5.1. In that particular example, the database "SEP01" was selected.

been proposed in the literature for the average number of surface excitations, qualitatively expressing the fact that $\langle n_s(E, \theta) \rangle$ should roughly be proportional to the time the electron spends in the surface scattering zone. The result by Oswald [36], based on the work by Stern and Ferrell [37] is given as:

$$\langle n_s(E, \theta) \rangle = \frac{1}{a_{DB}\sqrt{E} \cos \theta + 1} \quad (5.17)$$

The alternative mathematical form for $\langle n_s(E, \theta) \rangle$ is [38, 39]:

$$\langle n_s(E, \theta) \rangle = \frac{1}{a_{DB}\sqrt{E} \cos \theta} \quad (5.18)$$

Note that the material parameter a_{DB} in Eqn. 5.18 is generally defined differently in the literature. Here the reciprocal value is used to ensure consistency with Eqn. 5.17. Following the convention in the literature [34], the quantity a_{DB} will be referred to as "surface excitation parameter" (SEP) in the following. Databases for the SEP have been implemented in SESSA, from which the average number of surface excitations is calculated as indicated in table 5.1, see also section 4.

In analogy to the case of bulk excitations (see Eqn. 5.5) the distribution of energy losses in a single surface excitation, $w_s(T)$ (which will be denoted as differential surface excitation parameter, DSEP, in the following) is introduced. To account for the passage through the surface scattering zone, the spectrum in the partial intensity approach is given by:

$$Y(E, \vec{\Omega}) = \sum_{n_s=0}^{\infty} C_{n_s}(E, \theta) \int_0^{\infty} Y_{Bulk}(E + T, \Omega) L_{n_s}(T) dT, \quad (5.19)$$

where $Y_{Bulk}(E, \Omega)$ is the bulk spectrum, given by Eqn. 5.4 and the partial loss distributions for surface excitations $L_{n_s}(T)$ are calculated from a self-convolution of $w_s(T)$ in analogy to the bulk values (Eqn. 5.6).

An example of application of the above algorithm to account for surface excitation for electrons escaping from flat planar surfaces is shown in Fig. 5.1. The result shows the simulated Al-K α excited XPS spectrum of the Al 2p-photoelectron peak for several different emission angles using the database SEP03. A comparison of values for the average number of surface excitations in a single surface crossing (NSE) is given in table 5.2 for the different databases.

$\theta(^{\circ})$	SEP01	SEP02	SEP03	SEP04	SEP05
0	0.18	0.11	0.13	0.08	0.13
60	0.31	0.22	0.23	0.15	0.24
80	0.56	0.63	0.47	0.44	0.47

Table 5.2: Comparison of the values of the average number of surface excitations for the different databases available in SESSA for the Al $2p$ peak (see Fig. 5.1).

It is seen that in addition to the bulk plasmon replicas of the main photoelectron peak (blue arrows), surface plasmon replicas also appear, although only the first two are appreciable in size (those at energies of ≈ 1403 eV and 1392 eV, first two red arrows left of main peak), since higher order surface partial intensities decrease rapidly by virtue of the Poisson stochastic process when $\langle n_s(E, \theta) \rangle < 1$ (see Eqn. 5.16). The bulk plasmons themselves are also replicated by the surface plasmons as indicated by the green arrows, reflecting the fact that the partial intensities $C_{n_b, n_s=1}$ always assume appreciable values, while for $n_s \geq 2$ surface excitations are practically negligible.

It is emphasized that the above algorithm has been shown to realistically describe surface excitations for semi-infinite planar surfaces [27, 33, 35], giving rise to energy losses in the UV-regime of energies. However, it is well known that nanostructured surfaces may lead to characteristic surface losses, their spectral form depending on the exact nanomorphology [40] which typically appear in the visible range of energy losses. The above model, which is incorporated in SESSA, may then not appropriately describe the resulting experimental spectra. For this reason the simulation of surface excitations can be deactivated by the command 'MODEL SET SE false'.4.9

5.2.5 Spectrum modeling beyond the quasi-elastic approximation

The main interest in simulating XPS data is usually concerned either with peak intensities for the purpose of quantitation of experimental spectra, or the inelastic background in the vicinity of a peak. This is the reason why in the literature the quasi-elastic approximation is commonly invoked (see Eqn. 5.2), which yields the exact result for the zero-loss peak, often referred to as elastic peak or simply photoelectron "peak". If a significant energy loss range is of interest, as for example for inelastic background analysis to obtain information about the sample morphology, the quasi-elastic approximation may become invalid and it would be desirable to account for the energy dependence of the interaction characteristics in the simulation in some way. In principle, this can be achieved by employing the so-called direct simulation approach in a Monte Carlo simulation [42]. However, this comes at the cost of increased complexity and a severe decrease in computational efficiency and, moreover, it is strictly not possible to combine a direct simulation approach with the trajectory reversal algorithm since the latter is based on Case's reciprocity theorem [31] for *one speed* transport.

In his Masters thesis, Hronek proposed a simple and effective workaround, which has become known as the Hronek approximation [41]. He observed that the partial intensity approach is conceptually similar to the multi-speed approximation employed in numerical solution of the transport equation in neutron physics [43], in which the particle flux is divided into groups within a certain speed interval. In a statistical sense, the n -th order partial intensities correspond to the group of particles within a certain speed range. Since their intensity is governed by the Poisson distribution after n collisions (see Eqn. 5.10) and, therefore, by the inelastic mean free path after n inelastic collisions, a simple, yet effective, way to account for the energy dependence of the interaction characteristics is to multiply the peak spectrum $Y_{QEA}(E)$ by the energy dependence of

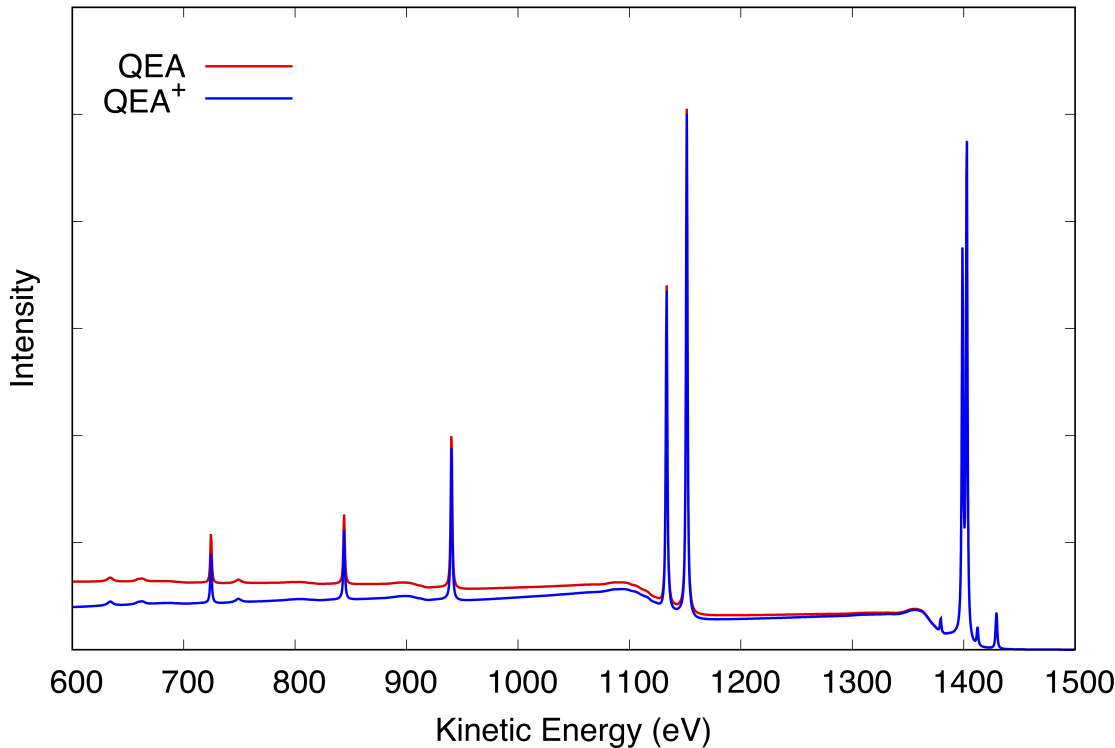


Figure 5.2: Comparison of a simulated Al- $K\alpha$ excited XPS spectrum of Au in the quasi-elastic approximation (QEA) (red curve) and using the so-called Hronek-approximation [41] or QEA-plus approximation (blue curve), which accounts for the change in the interaction characteristics with the energy of a photoelectron as it escapes from the surface in an approximate way (see text)

the inelastic mean free path:

$$Y_{QEA^+}(E) = Y_{QEA}(E) \times \frac{\lambda(E)}{\lambda(E_0)}, \quad (5.20)$$

where E_0 is the energy of the photoelectron peak.

One of the underlying implications of this type of approximation is that the energy dependence of the elastic interaction is negligible. For sufficiently smooth initial angular distributions at the source, where the photoionisation takes place, the so-called generalized radiative field similarity principle [23] states that the details of the elastic cross section do not essentially affect the pathlength distribution and hence the partial intensities will mainly change due to the energy dependence of the inelastic mean free path, which is accounted for by the approximate equation 5.20. Indeed the distribution of pathlengths for Auger- or photoelectrons is not significantly affected by the energy dependence of the elastic scattering cross section. This makes the QEA^+ -approximation an effective approach in true slowing down problems even for a sharply peaked initial angular distribution, such as for reflection of a focussed beam of electrons from a surface [24].

A comparison between the QEA (red curve) and QEA^+ (blue curve) approximation is shown in Fig. 5.2. It is seen that the quasi-elastic approximation is excellent for energy losses ΔE less than about 10% of the initial energy and the effect of the change in the interaction characteristics

becomes noticeable only if a very broad energy region of the spectrum is considered.

5.3 Modeling of nanostructured surfaces in SESSA

There are generally three aspects of the photoelectron (or Auger-electron) emission process that can be affected by the nanomorphology of a surface:

1. The photoionization process itself may be different from that for an ideal flat surface. The intrinsic peak shape, i.e., the energy distribution of the photoelectrons directly after photoionization, could be modified due to possible differences in the screening response in the local region compared to a semi-infinite surface.
2. The inelastic-scattering processes near the surface may exhibit additional modes related to the morphology and composition of a nanostructured surface [40].
3. The distribution of pathlengths of specific photoelectrons created in a material A that travel in another material, say B, depends on the geometric boundaries of the considered morphology. As a consequence, the relative peak intensities (and the shape of the inelastic background) will be influenced by inelastic scattering along the trajectory and can also be affected by the morphology and composition of the nanostructure.

Some evidence for the existence of nano-structure-induced changes in the photoelectron peak shape exists, but is not included in the present version of the software. It should be noted that, even for planar surfaces, the intrinsic peak shapes used for spectrum modeling are not generally realistic; they are assumed to be a single Lorentzian with a width of 0.7 eV by default. However, more realistic peak shapes can be imported using empirical data from a text file (see Section 4.4.7). This strategy should work equally well in simulations for nanostructured surfaces.

The additional modes of inelastic-scattering processes near nanostructured surfaces are obviously of paramount importance for the optical properties of nanostructures and their study has become an important subfield of nanophotonics and plasmonics [40]. Such modes can most easily be studied by electron energy-loss spectroscopy (EELS) in the transmission electron microscope (TEM) and can be observed in EELS spectra as clearly distinguishable features extending from the near infrared to the near ultraviolet regime of wavelengths.

However, on the scale of loss features important for understanding the attenuation of photoelectrons, these effects are believed to be of minor importance and are in fact expected to be nearly impossible to detect in typical XPS spectra. The reason is that the overwhelming majority of processes attenuating the outgoing photoelectrons (and thereby affecting the relative intensities, extrinsic peak shapes, etc.) take place inside the solid, since the surface scattering zone, where additional modes due to the nanomorphology come into play, is at least about an order of magnitude smaller than the relevant mean free paths for inelastic scattering inside the solid. As a result, the most effective experimental means for studying such effects in the TEM is to use an aloof scattering geometry in which the beam does not actually penetrate the specimen; alternatively, a supporting substrate that is (almost) completely transparent to the beam (such as mica) can be used. With these techniques, inelastic scattering inside the solid can be minimized and the spectral features of interest can be observed. For simulation of nanostructured surfaces with SESSA, one has just the opposite situation since the signal always originates from within the surface, making the phenomena addressed above difficult to distinguish in experimental spectra. On the other hand, theoretically explaining such spectral features is very difficult in general:

one either has to resort to semi-classical theories or to full quantum-mechanical treatment of the many-body problem involving the nearly free solid-state electrons [44, 45]. This type of analysis is obviously beyond the scope of general-purpose software such as SESSA. Moreover, since these effects are expected to be weak in photoelectron spectra, they are not incorporated in the present version of SESSA.

The spatial distribution of matter (i.e., the three-dimensional geometric distribution of matter inside a sample) near a nanostructured surface is known to have a major effect on features of the energy and angular distributions of emitted photoelectrons [17, 46, 47]. This result is not surprising since typical dimensions of nanostructures are of the same order as the inelastic mean free paths of the detected photoelectrons in typical XPS experiments. It is therefore to be expected that details of the morphology should have a strong effect on the attenuation of photoelectrons in a spectrum and therefore on the relative photoelectron intensities, angular distributions, and inelastic backgrounds. In fact, the influence of morphology on spectra is sometimes so pronounced that significant information on the nanomorphology of a surface can be derived from XPS spectra. The effects of nanostructure morphology is taken into account in the present version of SESSA by keeping track of the pathlengths of electron trajectories within each of the regions of the sample that form the boundary of the nanostructure. With this information, the partial intensities of the relevant peaks in the spectrum are calculated according to the formalism outlined in Section 5.2.3.

In the present implementation of SESSA, the nanomorphology of the surface is defined and traced using the PENGEOm code system [48]¹. When a user starts a simulation, the information concerning the nanomorphology of the surface entered in the SESSA expert system (either using the GUI or the CLI), is written to an internal file, following the syntax prescribed by the PENGEOm package. This is then used to initialize a PENGEOm data structure which is used during the simulation to check in which material the electron is located, whether it has crossed a boundary between two adjacent regions consisting of different materials, and to locate the point of intersection. If an intersection took place, the position of the electron is updated to the location of intersection and simulation of the trajectory is continued from there in the usual manner.

5.4 Current limitations of databases and simulation

It was shown in the previous section that three quantities need be known for a realistic simulation of the energy and angular distributions: (1.) the partial intensities; (2.) the source energy, angular and depth distributions; and (3.) the differential inelastic inverse mean free path (see Eqns. (5.4) and (5.6)). The additional parameters needed for a simulation of the partial intensities are: the total inelastic mean free path, the differential elastic-scattering cross section, the total elastic-scattering cross section (or, alternatively the transport cross section if the transport approximation is used), the photoionization cross section, the photoionization asymmetry parameter, the electron–impact ionization cross section, the fluorescence yield and the Auger-electron backscattering factors. For all of these quantities, SESSA contains reasonably reliable data in its databases, while the simulation algorithm for the partial intensities, described above, has also proven to be satisfactory. Comparisons of peak intensities with experimental results exhibit a quite close agreement (see Section 7.1.1-7.1.5). This situation is generally the case for the intensity of those electrons that escape without being inelastically scattered. It should be emphasized again that the area of the no-loss peak is identical to the zero-order partial intensity, while the higher-order partial intensities

¹The authours would like to thank Prof. Salvat-Galvada (University of Barcelona) for his kind permission to use the PENELOPE code in SESSA

describe the spectral intensity in the inelastic background.

For the distribution of energy losses in an inelastic process (i.e., the DIIMFP), there exist a limited number of materials for which optical data are available that allow a detailed calculation of this quantity. For all other materials, Tougaard's universal cross section [16] is used as a backup data source that gives a reasonable estimate of the overall shape of the loss distribution, but does not describe the fine details of the inelastic excitation probability of a solid. Furthermore, surface and intrinsic excitations [1, 2] are entirely neglected in the present version of SESSA.

The main limitation in the simulation of the spectral *shape* (as opposed to spectral *intensity*) is the fact that the shape of the energy distribution for inelastic scattering in solids is generally quite complex and a comprehensive database for this quantity, that *must* be based on empirical data, is presently not available within SESSA, nor, for that matter, anywhere else in convenient form. Presently, the lineshape of an XPS peak is approximated. After looking up the specified binding energy in a database for elemental binding energies (containing accepted values for binding energies), a default lineshape is chosen for each peak. This default lineshape is a Lorentzian with a full width at half-maximum (FWHM) of 1.4 eV. For AES, the situation is much more complex, since AES peaks can be very broad and consist of many subpeaks.

At present, lineshape information for a limited number of Auger peaks is available in the AEL database in SESSA. The only stored data for these peaks are the kinetic energy of the transition, the subshell where the initial ionization took place, and an empirical sensitivity factor. The latter is needed since extensive knowledge of the probability for emission of the considered Auger electrons requires knowledge not only of the relevant fluorescence yields but also of applicable Coster-Kronig transition probabilities. Sufficient data for Coster-Kronig probabilities of the needed reliability are not now available. An empirical sensitivity factor is therefore used to estimate the peak intensity of an Auger transition. The lineshape is again chosen by default to be a Lorentzian with a FWHM of 6.0 eV. The default choice of a Lorentzian lineshape is reasonable in many cases for XPS but is hardly ever a realistic choice for an Auger transition.

These considerations indicate that a user interested in directly comparing experimental line-shapes with results of a SESSA simulation should provide information about the source energy distribution in the 'SAMPLE/PEAK' menu of Fig. 4.12. An example further clarifying this problem is given as a tutorial in Section 7.2.2.

Summarizing, the main limitations of the simulation algorithm are that surface and intrinsic excitations are neglected and that the excitation depth distribution function is assumed to be constant inside the specimen. Furthermore, the assumption of an atomically flat surface restricts the applicability of SESSA to practical cases where the surface morphology is not expected to influence the spectral intensities. As far as the databases are concerned, the most important lack of data concerns the empirical peak shapes of photoelectron and Auger-electron transitions and comprehensive data on the Coster-Kronig transition probabilities.

6 Physical Data in SESSA

A large amount of data is needed to quantitatively interpret an Auger-electron or photoelectron spectrum quantitatively. The required data include basic physical information on the solid in question (density, atomic number of the constituent atoms, etc.), information on the process of creating the signal electrons (photoelectric effect and Auger-electron emission) as well as on the various parameters governing the interaction of the signal electrons with the solid on their way out of the specimen. The number of required physical parameters can therefore be large for a particular situation. The SESSA databases provide an extensive and fully traceable dataset for these parameters. The energy range for which data are available extends from 50 eV up to 20 keV.

An extensive dataset for all relevant physical parameters is a strict prerequisite for proper operation of the expert system. On the other hand, it is obvious that not all physical parameters are available for all materials with the same accuracy or, for that matter, are available at all for any arbitrary material. This situation implies that in cases where there are gaps in the data sets, these must be complemented by some credible estimate for the quantity in question. This in turn means that it is generally impossible to make an overall statement on the reliability of the data retrieved by SESSA. It is therefore essential for the data to be fully traceable. Every individual datum retrieved by SESSA is accompanied by a full reference to the literature and in many cases also contains a statement concerning its reliability. The easiest way for the user to assess the overall quality of the retrieved data is to copy these data to disk and to perform an output of these data. Two of the files produced in this way (filenames ending with `refs.txt` and `rems.txt`) contain a list with statements on the reliability of the retrieved data (see Section 3.4).

The physical quantities for a particular spectrum generally depend on a number of parameters (material, atomic number, energy, etc.). The range of these parameters for which each quantity is available is determined by the selected choice for the data source. For example, the DIIMFP from optical data can only be provided by Penn's algorithm [49] (which is generally regarded as providing the most reliable results for this quantity) for those materials for which energy-loss functions are available in the literature. However, the backup source in this parameter, Tougaard's empirical DIIMFP [16], provides a *universal* approximate description for the energy-loss probability in a single inelastic collision. The primary and backup sources for this quantity together are generally extensive in that they cover the entire range of parameters of relevance for electron spectroscopy. This strategy is generally also followed for other parameters: For each quantity for which the primary (most reliable) source does not completely cover the relevant range, the backup source (usually an approximate empirical expression) is extensive, or vice versa.

6.1 Databases used in SESSA

The quantities available in the SESSA databases as well as their sources are indicated in the following list.

1. Elemental data. (Chemical symbol, chemical name, elemental density (if available), number of valence electrons, atomic weight, atomic electronic configuration, etc.) Source: Refs. [50, 51]
 - Keys: Atomic number.
 - Range: Atomic Number 1-94.
2. Differential inverse inelastic mean free path (DIIMFP).
 - a) Source: Calculated [52] using linear response theory with the algorithm developed by Penn [49] and using optical data in Refs. [53–55]¹.
 - Keys: Material, Energy (eV), Energy Loss(eV).
 - Range: Material: restricted by availability in source; Energy: 50 eV-30 keV.
 - b) Source: Universal curve proposed by Tougaard [16].
 - Keys: Energy Loss (eV).
 - Range: Universal.

/Li/	/Be/	/C/	/C[diamond] /	/Na/
/Na/	/Mg/	/Al/	/Si/	/Sc/
/Sc/	/Ti/	/V/	/Cr/	/Co/
/Co/	/Ni/	/Cu/	/Ge/	/Nb/
/Nb/	/Mo/	/Ru/	/Rh/	/Ag/
/Ag/	/In/	/Sn/	/Cs/	/Tb/
/Tb/	/Dy/	/Hf/	/Ta/	/Re/
/Re/	/Os/	/Ir/	/Pt/	/Bi/
/Bi/	/Ag/Br/	/Ag/Cl/	/Ag/I/	/Al/As/
/Al/As/	/Al/N/	/Al/Sb/	/B[cubic]/N/	/Cd/S/
/Cd/S/	/Cd/Se/	/Cd/Tel	/Ga/As/	/Ga/P/
/Ga/P/	/Ga/Sb/	/Ga/Se/	/In/As/	/In/Sb/
/In/Sb/	/K/Br/	/K/Cl/	/Mg/F2/	/Na/Cl/
/Na/Cl/	/Nb/C0.712/	/Nb/C0.844/	/Nb/C0.93/	/Pb/Se/
/Pb/Se/	/Pb/Te/	/Si/C/	/Si/O2/	/Ti/C0.7/
/Ti/C0.7/	/Ti/C0.95/	/V/C0.76/	/V/C0.86/	/Zn/S/
/Zn/Se/	/Zn/Te/	/H2/O[liquid] /		

Table 6.1: List of identifiers to specify materials in the IMFP02 database

3. Total inelastic mean free path (IMFP).
 - a) Source: Empirical expression (TPP-2M) [56–58].
 - Keys: Material, Energy (eV).
 - Range: Material: Universal; Energy: 50 eV–200 keV.

¹The authors would like to thank Dr. S. Tanuma (National Institute for Materials Science, Tsukuba, Japan) for providing his set of optical loss functions for use in SESSA.

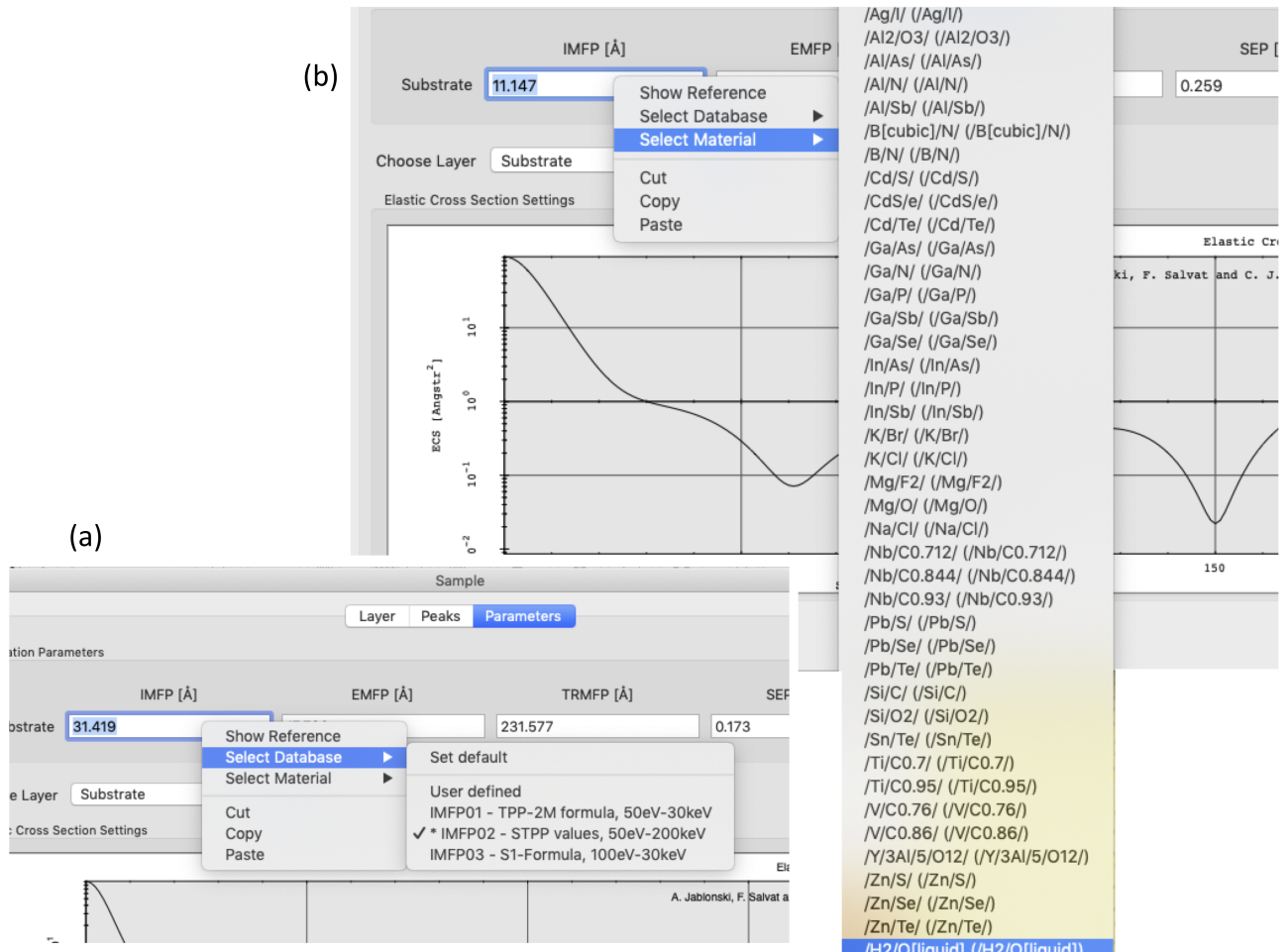


Figure 6.1: (a) Detail of the Sample/Parameters menu in the GUI highlighting the pop-up-menu after a right mouse click in the box containing the IMFP value. After selecting the IMFP02 database, a third option, "select material" appears, which can be used to conveniently select any of the materials available in the IMFP02-database. Note that user selection of this database is indicated by the check-mark in front of "IMFP02 - STPP values..", the asterisk indicates that the requested datum for the IMFP could indeed be successfully retrieved. (b) Illustration of the right-click pop-up menu to select the material for the IMFP calculation with the database IMFP02. In the particular example on display, the material being selected is liquid water. After a repeated pop-up is prompted by a user this material will be indicated be a check mark in front of the identifier.

The IMFP from the TPP-2M equation is calculated using the parameters in the Sample Layer menu, in particular the number of valence electrons, the density, the number of atoms per molecule, the band gap (see Fig. 4.5ff.) and the atomic masses of the constituents. The latter item is not displayed in the Sample Layer GUI but this and the former two items are retrieved from internal SESSA databases. However, there is no database in SESSA for the band gap and it is necessary for a user to manually enter a reasonable estimate of the band gap energy for non-conductors in order to get a useful value for the IMFP value in question. Otherwise, the default value ($E_{gap} = 0$ eV) is used, which may lead to deviations from realistic IMFP values of up to about 25%. While bandgap energies are available for many compounds [59–64], evaluations of the earlier TPP-2 formula showed only a weak dependence on the bandgap [64]. That is, only rough estimates of the bandgap are needed if specific data for the material of interest are not available. For example, the bandgap is generally between 6 eV and 11 eV for highly ionic compounds such as the alkali halides and is often between 1 eV and 9 eV for oxides.

- b) Source: IMFP values for 41 elemental solids, 42 inorganic compounds, and liquid water calculated by Shinotsuka, Tanuma, Powell, and Penn [56–58] using optical data.
- Keys: Material ID, Energy (eV).
 - Range: Material: Selected materials for which optical data are available; Energy: 50 eV–30 keV.

It should be noted that the IMFP values in this database were calculated not only for simple materials such as mono-elemental metals, but also for compounds, for example, and most importantly for near ambient pressure XPS, *liquid* water [57]. In order to retrieve the data specifically for such a compound, the material specifier must be entered in the material box in the sample menu *to the letter* corresponding to the symbol in the database (see Table 6.1). In addition, the default database for the IMFP should be set to "IMFP02" (see section 4.8).

Alternatively, the right click pop-up menu in the parameter menu displaying the IMFP as indicated in Fig. 6.1 may be utilized. It is important to note that this will change the database for retrieval of the IMFP value *only* for the considered peak and layer, neither the material of the layer in question will be changed (as verifiable by inspecting the sample/layer menu, see Fig. 4.5ff.), nor will the database for the IMFP values for any of the other peaks be changed. The above is one example of a number of possible pitfalls associated with the selection of some of the more special materials in Table 6.1, such as a simple typo in the identifier. This makes it imperative for a user to verify that the IMFP value used is indeed retrieved from the desired database. This is achieved by a right mouseclick in the box containing the value of the IMFP and verifying that the correct database is indeed used for the IMFP retrieval. As explained in section 3.1, the database from which any given datum is retrieved in SESSA is indicated by an asterisk in front of the database name upon a right mouse click in the box containing the datum in question, as illustrated in Fig. 6.1.

- c) Source: Empirical expression (S1) of Seah [65].
- Keys: Material ID, Energy (eV).
 - Range: Material: Universal ; Energy: 50 eV–30 keV.

The IMFP according to the S1-equation is calculated on the basis of the parameters

in the sample menu. The same remark as in paragraph 3a applies to the value of the band gap, which must be entered by a user in the case of non-conducting materials.

4. Surface excitation parameter (SEP).

- a) Source: Empirical values from Ref. [34] to be used in conjunction with Eqn. (5.17)
 - Keys: Material ID, Energy (eV), Surface crossing angle
 - Range: Material: Selected materials in Ref. [34]; Energy: universal; Angle: universal
- b) Source: Values calculated from available optical constants as described in Ref. [38] to be used in conjunction with Eqn. (5.18)
 - Keys: Material ID, Energy (eV), Surface crossing angle
 - Range: Material: Selected materials for which optical data are available; Energy: universal; Angle: universal
- c) Source: Values calculated from empirical formula in Ref. [34] to be used in conjunction with Eqn. (5.17)
 - Keys: Material ID, Energy (eV), Surface crossing angle
 - Range: Material: universal ; Energy: universal; Angle: universal
- d) Source: Values calculated from theoretical formula in Ref. [39] to be used in conjunction with Eqn. (5.18)
 - Keys: Material ID, Energy (eV), Surface crossing angle
 - Range: Material: universal ; Energy: universal; Angle: universal
- e) Source: Values calculated from theoretical formula in Ref. [36] to be used in conjunction with Eqn. (5.17)
 - Keys: Material ID, Energy (eV), Surface crossing angle
 - Range: Material: universal ; Energy: universal; Angle: universal

5. Differential surface excitation parameter (DSEP).

- a) Source: Values calculated from available optical constants as described in Ref. [38].)
 - Keys: Material ID, Energy (eV), Surface crossing angle
 - Range: Material: Selected materials for which optical data are available; Energy: universal; Angle: universal
- b) Source: Values calculated from available optical constants as described in Ref. [34].)
 - Keys: Material ID, Energy (eV), Surface crossing angle
 - Range: Material: Selected materials for which optical data are available; Energy: universal; Angle: universal

6. Differential elastic scattering cross section (ECS).

- a) Source: Values computed by the program of Yates [66] using the relativistic partial-wave expansion method based on atomic Thomas-Fermi-Dirac (TFD) potentials [67].
 - Keys: Atomic Number, Energy (eV).
 - Range: Atomic number: 1-99; Energy: 50 eV–20 keV.

b) Source: NIST SRD 64, V 3.1, Electron elastic-scattering cross-section database. Values computed using the relativistic partial wave expansion method based on atomic Dirac-Hartree-Fock (DHF) potentials [32, 68] as used for the NIST Electron Elastic-Scattering Cross-Section Database (SRD 64) [69]. The cross sections obtained from DHF potentials are believed to be more reliable than those obtained from TFD potentials[32].²

- Keys: Atomic Number, Energy (eV).
- Range: Atomic number: 1-92; Energy: 50 eV–20 keV.

7. Total elastic scattering cross section (TECS).

a) Source: Values computed by the program of Yates [66] using the relativistic partial-wave expansion method based on atomic Thomas-Fermi-Dirac potentials [67].

- Keys: Atomic Number, Energy (eV).
- Range: Atomic number: 1-99; Energy: 50 eV–20 keV.

b) Source: NIST SRD 64, V 3.1, Electron elastic-scattering cross-section database. Values computed using the relativistic partial wave expansion method based on atomic Dirac-Hartree-Fock (DHF) potentials [32, 68] as used for the NIST Electron Elastic-Scattering Cross-Section Database (SRD 64) [69]. The cross sections obtained from DHF potentials are believed to be more reliable than those obtained from TFD potentials [32].³

- Keys: Atomic Number, Energy (eV).
- Range: Atomic number: 1-92; Energy: 50 eV–20 keV.

8. Transport scattering cross section (TRECS) that is used to determine transport mean free paths (TRMFPs) for simulations using the transport approximation.

a) Source: Values computed by the program of Yates [66] using the relativistic partial-wave expansion method based on atomic Thomas–Fermi–Dirac potentials [67].

- Keys: Atomic Number, Energy (eV).
- Range: Atomic number: 1-99; Energy: 50 eV–20 keV.

b) Source: NIST SRD 64, V 3.1, Electron elastic-scattering cross-section database. Values computed using the relativistic partial wave expansion method based on atomic Dirac-Hartree-Fock (DHF) potentials [32, 68] as used for the NIST Electron Elastic-Scattering Cross–Section Database (SRD 64) [69]. The cross sections obtained from DHF potentials are believed to be more reliable than those obtained from TFD potentials [69].⁴

- Keys: Atomic Number, Energy (eV).
- Range: Atomic number: 1-92; Energy: 50 eV–20 keV.

²The authors would like to thank Prof. A. Jablonski (Institute of Physical Chemistry, Polish Academy of Sciences, Warsaw, Poland) for providing calculated differential elastic-scattering cross sections, total elastic-scattering cross sections, and transport scattering cross sections for use in SESSA.

³The authors would like to thank Dr. S. Tanuma (National Institute for Materials Science, Tsukuba, Japan) for providing his set of optical loss functions for use in SESSA.

⁴The authors would like to thank Dr. S. Tanuma (National Institute for Materials Science, Tsukuba, Japan) for providing his set of optical loss functions for use in SESSA.

c) Source: Tilinin's quasiclassical expression [70].

- Keys: Atomic Number, Energy (eV).
- Range: universal.

9. Photoionization cross section (PCS).

a) Source: Values computed by Scofield for Mg and Al K α x-rays [71].

- Keys: Atomic Number, Subshell ID, Photon Energy (eV).
- Range: Atomic number: 1-96; Subshells: extensive; Photon Energy: Mg and Al K α x-rays.

b) Source: Values computed by the program of Yeh and Lindau [72].

- Keys: Atomic Number, Subshell ID, Photon Energy (eV).
- Range: Atomic number: 1-96; Subshells: extensive; Photon Energy: extending from just above the ionization threshold energy to 20 keV.

c) Source: Values tabulated by Trzhaskovskaya, Nefedov, and Yarzhemski [18, 19]⁵.

- Keys: Atomic Number, Subshell ID, Photon Energy (eV).
- Range: Atomic number: 1-99; Subshells: extensive; Photon Energy: extending from just above the ionization-threshold energy to 5 keV above threshold. For higher photon energies, linear extrapolations were made to the calculated values. These extrapolations may introduce an uncertainty of more than 30% in the derived cross sections for energies more than 5 keV above threshold.

10. Photoelectric asymmetry parameter (PAP).

a) Source: Calculations of Reilman *et al.* [73] for Mg, Al K α and Zr M ζ -X-rays.

- Keys: Atomic Number, Subshell ID, Photon Energy (eV).
- Range: Atomic number: 1-96; Subshells: extensive; Photon Energy: Mg and Al K α and Zr M ζ .

b) Source: Values computed by the program of Yeh and Lindau [72].

- Keys: Atomic Number, Subshell ID, Photon Energy(eV).
- Range: Atomic number: 1-96; Subshells: extensive; Photon Energy: extending from just above the ionization threshold energy to 30 keV.

c) Source: Values tabulated by Thrzhaskovskaya, Nefedov, and Yarzhemski [18, 19]⁶.

- Keys: Atomic Number, Subshell ID, Photon Energy (eV).
- Range: Atomic number: 1-99; Subshells: extensive for atomic numbers \leq 54 but limited to subshells with binding energies less than 2 keV for atomic numbers \geq 55; Photon Energy: extending from just above the ionization-threshold energy to 5 keV above threshold. For higher photon energies, linear extrapolations were made to

⁵The authors would like to thank the late Prof. V. I. Nefedov (Institute of General and Inorganic Chemistry, Russian Academy of Sciences, Moscow, Russia) for providing his calculated photoionization cross sections for use in SESSA.

⁶The authors would like to thank the late Prof. V. I. Nefedov (Institute of General and Inorganic Chemistry, Russian Academy of Sciences, Moscow, Russia) for providing his calculated photoelectric asymmetry parameters for use in SESSA

the calculated values. These extrapolations may introduce an uncertainty of more than 30% in the derived asymmetry parameters for energies more than 5 keV above threshold.

It should be noted that the database of Trzhaskovskaya, *et al.* [18, 19] is not extensive for some subshells in atoms with atomic numbers ≥ 55 . For example, this database might not provide a datum for a certain peak in the considered energy range (as specified by a user through setting the photon energy and the spectrometer energy window). Unfortunately, this database is the only database for non-dipolar asymmetry parameters within SESSA, and the authors know of no other database for these quantities that could avoid this deficiency. There are two possible ways that the expert system could handle such a situation:

(1) the expert system could conclude that the information for the peak in question is not complete and therefore decides to delete this peak altogether; or
(2) the simulation is performed with neglect of the non-dipolar contribution to the photoelectric cross section. The former alternative is believed to be undesirably restrictive since it does not seem reasonable to delete a peak due to a lack of non-dipolar asymmetry parameters. It would be particularly undesirable to delete a peak arising from common laboratory x-ray sources (such as Al K α or Mg K α) for which the non-dipolar terms are generally small enough for these effects to be neglected. Therefore, the second alternative was adopted in the present version of SESSA, i.e., the non-dipolar terms are set to zero. Note that no corresponding warning is issued if this occurs.

11. Electron impact ionization cross section (EIICS).

- a) Source: Empirical expression of Casnati *et al.* [74].
 - Keys: Atomic Number, Subshell, Electron Energy (eV).
 - Range: Universal.

- b) Source: Semiclassical expression of Gryzinski [75].
 - Keys: Atomic Number, Subshell, Electron Energy (eV).
 - Range: Universal.

- c) Source: Empirical expressions and parameter values of Bote *et al.* [76].
 - Keys: Atomic Number, Subshell, Electron Energy (eV).
 - Range: Universal.

12. Photoelectron line shape (XPL).

Source: Binding energies of the elements [77].

- Keys: Atomic Number, Subshell.
- Range: Atomic Number, Subshell: extensive.

13. Auger electron line shape (AEL).

Source: Energies and sensitivities calculated according to the " $Z + 1$ " rule, as described in the Appendix of Ref.[5].

- Keys: Atomic Number, Subshell.
- Range: Atomic Number: 3-92, Subshells: limited by the availability in the data source.

14. Fluorescence yield (FY).

- a) Source: Polynomial fit to empirical data for K-, L-, and M-shell fluorescence yields due to Hubbell *et al.* [78]
 - Keys: Atomic Number, Subshell.
 - Range: Universal.
- b) Source: Semi-empirical expression for the K-shell fluorescence yield of Bambynek [79]
 - Keys: Atomic Number, Subshell.
 - Range: Universal.
- c) Source: Burhop's semi-empirical expression for the K-shell fluorescence yield [80]
 - Keys: Atomic Number, Subshell.
 - Range: Universal.

15. Auger backscattering factor (ABF).

Source: Shimizu's formula for normal incidence of an electron beam on a homogeneous solid [81].

- Keys: Atomic Number, Subshell.
- Range: Universal.

16. Chemical Shifts (CS).

Source: Measured and calculated chemical shifts from Version 4.0 of the NIST X-ray Photoelectron Spectroscopy Database [82]

- Keys: Atomic Number, Subshell.
- Range: Limited by availability of data in source [82] .

7 Tutorials

In the present chapter, a small collection of SESSA CLI–files are presented and discussed. These files should help the reader to get acquainted with the most important features of operating SESSA. In addition, the tutorial sessions might be helpful to better understand some aspects of the surface sensitivity of electron spectroscopy for practical applications. These tutorials consist of a number of files residing in the indicated directories. In each of these directories, there is one file that has the same name as the directory and ends with the extension .ses. Loading this file will perform the tasks specified in all individual files in the directory in one operation. The estimated computation times specified in the sections below are clock times measured when running the simulations on a 1.2 GHz Pentium PC.¹

¹A commercial product is identified to specify conditions for an experimental test. Such identification does not imply recommendation or endorsement by the National Institute of Standards and Technology, nor does it imply that the product concerned is the best available for the purpose

7.1 Peak Intensities

7.1.1 Angular distribution of photoelectrons emitted from a homogeneous Au sample: Chandrasekhar's H -function.

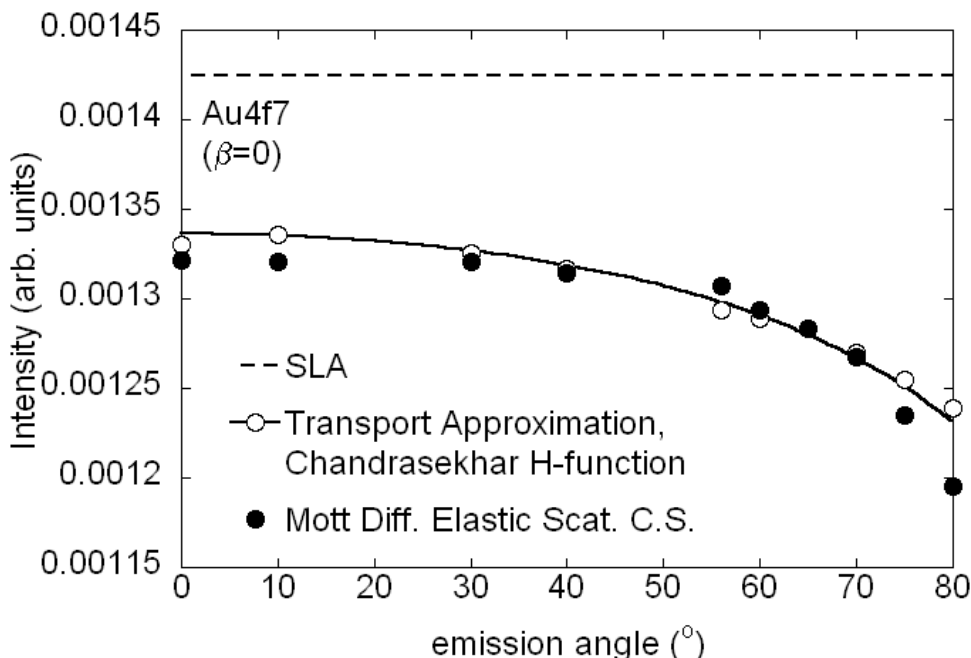


Figure 7.1: Angular distribution of the $\text{Au4f}_{7/2}$ photoelectron peak intensity excited by $\text{Al-K}\alpha$ x-rays as a function of the emission angle (that is, as the sample is tilted). For model purposes, the photoelectric asymmetry parameter was set to zero (isotropic emission). It can be seen from the open symbols, that the SESSA results obtained in the transport approximation coincide with Chandrasekhar's H -function [83] represented by the solid line. This result is expected since the H -function is the exact analytic distribution for isotropic scattering. The solid circles represent the result obtained using the more realistic Mott cross section for elastic scattering, the dashed line is the result in the rectilinear motion model or straight-line approximation (SLA).

- **Purpose:** Getting acquainted. Performing a calculation of a photoelectron angular distribution and showing a comparison of results arising from different cross sections for elastic scattering.
- **Time required for simulation:** ~ 30 s.
- **Directory:** tutorials\au-homo
- **CLI-files (.ses):** ini.ses, sample.ses, spectr.ses, geo.ses, sla.ses, ta.ses, mott.ses, auhomo.ses
- **GNUPLOT-files (.g):** compare.g

- **Output-files** (`output*.*`): `sla_all.adf`, `ta_all.adf`, `es_all.adf`

- **Procedure:**

1. Start SESSA.
2. Open the CLI-console window (CTRL-9 or choose Project/Command Line Interface from the Main menu). Click on the button Load Session and select the file ... \tutorials\au-homo\ini.ses. SESSA reads a number of commands from this file that initialize the software and sets a few preferences. Press CTRL-p to open the preferences menu. It is seen that the options Output/sample and Output/experiment have been deselected. This means that when SESSA writes output to a file, the corresponding information will not be included (see Section 4.3).
3. Load the file `sample.ses` and open the “Sample/peak” menu (CTRL-1). It is seen that the sample is now assumed to consist of a semi-infinite piece of gold. The Sample/peak menu (CTRL-2) displays information on the signal electrons emitted from this sample for the given spectrometer and source settings. The “Sample/Parameter” menu (CTRL-3) displays the corresponding parameters describing the electron-solid interaction. A right-mouse click on any of the numbers displayed here allows the user to change the database or view the reference for the value on display. Furthermore, the numbers can be changed by entering any value within a meaningful range. The database selection menu and reference dialog can also be invoked for a graphical representation of the differential elastic-scattering cross section and the differential inverse inelastic mean free path by means of a right mouse click. Furthermore, a double click on any of the graphical displays in SESSA transfers their contents to a separate plot window that provides features allowing a user to change the display, to plot the contents of the window to a postscript file, etc.
4. Load the file `geo.ses` and open the Experiment/geometry menu (CTRL-5). By choosing one out of the defined eight geometries from the Choose Configuration box, the selected information can be displayed or changed. SESSA will later do a separate calculation for each of the geometrical configurations shown here.
5. Load the file `spectr.ses` and open the Experiment/spectrometer menu (CTRL-6) to see that the spectrometer region has been set to a rather narrow energy range. Consequently, only the $\text{Au}4f_{7/2}$ peak is within the spectrometer energy window, as can be verified by pressing CTRL-2. It is seen that the $\text{Au}4f_{5/2}$ peak is also missing and that the asymmetry parameter for the $\text{Au}4f_{7/2}$ peak was set to zero for purpose of a model calculation. This choice was achieved by explicit commands in the file `spectr.ses` (press CTRL-9 to return to the CLI console and view these commands there).
6. Load the file `sla.ses` and open the Model Calculation menu (CTRL-7). A peak is on display here and the Straight Line Approximation box is checked. Furthermore the Auto box for number of collisions is deselected (and n_{col} is set to zero). The reason for setting n_{col} to zero is that we are presently only interested in the peak intensity of electrons that escape without inelastic scattering. By checking the Auto box for number of collisions, an entire spectrum is simulated instead of only the no-loss peak (although the spectrometer range would also have to be extended to lower kinetic energies in order to see any effect). The fact that the Straight Line Approximation box is checked means that SESSA assumes that the paths of the electrons in the solid are straight lines (i.e., elastic scattering of the signal electrons is neglected).

7. Load the file `ta.ses` and note that the simulation takes longer to converge now. Furthermore, the Transport Approximation box is now checked instead of the Straight Line Approximation box. This choice implies that elastic scattering is assumed to be isotropic and that the distance between successive elastic deflections is taken to be equal to the transport mean free path. Use of the transport approximation enables an analytic solution to be given for the angular distribution of photoemitted electrons (for emitters homogeneously distributed in a semi-infinite solid): the Chandrasekhar H–function [83]. Whenever the maximum number of collisions is set to zero and more than one geometrical configuration is defined, the partial intensities are displayed as a function of the configuration number (instead of the collision order) in the Sample/peak menu (CTRL-2) when Partial Intensities is selected for graphical display in the Sample/Peaks window. The partial intensities are seen to decrease monotonically (within the precision of the calculation) when going to more oblique emission. This is the expected behavior for the H–function. To increase the precision of the calculation, decrease the convergence factor in the simulation menu (see Section 4.9).
8. Load the file `mott.ses`. Another simulation is performed that takes considerably longer. In this simulation, realistic (Mott) cross sections are used for the differential elastic-scattering cross sections [14, 22, 32, 66, 67, 84].
9. Start `GNUPLOT` and load the file `compare.g`. The result should resemble Fig. 7.1.
10. When working with CLI files, the order in which the commands are issued is important. For example, when `sample.ses` is loaded after `spectr.ses`, there will be two peaks in the considered region since the material is set in `sample.ses` and the command deleting the peak (and issued before in `spectr.ses`) will therefore be overruled. For user convenience, a file `au-homo.ses` has been included that runs all tests described in this section and should lead to the result shown in Fig. 7.1.

- **Discussion:**

The results shown in Fig. 7.1 provide a test for correct operation of a Monte Carlo simulation of electron transport in that the Chandrasekhar function represents the exact analytic solution of the emission problem for isotropic sources in a semi-infinite homogeneous medium and isotropic scattering. The H–function may be approximated by

$$H(\mu, \omega) = \frac{1 + \mu\sqrt{3}}{1 + \mu\sqrt{3}(1 - \omega)} \quad (7.1)$$

In this expression, $\mu = \cos\theta$, when θ is the electron emission angle with respect to the surface normal and ω is the single-scattering albedo given in terms of the inelastic (λ_i) and transport (λ_{tr}) mean free paths as $\omega = \lambda_i / (\lambda_i + \lambda_{tr})$. The test is seen to be successful for SESSA. It is furthermore seen that the difference with the more realistic Mott cross section is not very significant. This result is explained by the so-called generalized radiative-field similarity principle [23] that specifies conditions for this similarity between isotropic and non-isotropic scattering to occur. It is also seen that the intensity at normal emission is decreased compared to the rectilinear-motion model where elastic deflections are completely neglected (SLA, Straight Line Approximation). See Ref. [85] for a more detailed discussion.

7.1.2 Angle-resolved XPS for a homogeneous Al sample.

- **Purpose:** Examine the effects of elastic scattering and the acceptance angle of the analyzer.
- **Time required for simulation:** ~30 s.
- **Directory:** tutorials\al-anisotropy
- **CLI-files (*.ses)** : ini.ses, sample.ses, spectr.ses, geo.ses, sim.ses, al-anisotropy.ses, infinite.ses
- **GNUPLOT-files (*.g)** : compare.g
- **Output-files (output*.*):** sla_all.adf, ta_all.adf, es_all.adf

- **Procedure:**

The only difference from the procedure of Section 7.1.1 is that the three simulation steps are now executed in one file (sim.ses). The difference in the calculations is that the anisotropy of the photoionization cross section is not switched off: on the contrary, it is of main interest here. The specified geometries correspond to perpendicular irradiation of the back of a thin Al foil; the analyzer is again rotated around the sample covering a range of polar emission angles between -80° and 80°. Note that a polar angle in SESSA is always specified by a positive number in the range 0°–180°, as is usual in a spherical coordinate system; “negative” polar emission angles are obtained by changing the azimuthal angle by 180° (see the file geo.ses for details).

- **Discussion:**

When core-level photoelectrons are liberated from an atom, the emitted intensity along the direction of the incident photons vanishes. In solids, however, a finite contribution in the forward direction is always seen. This is illustrated by the open symbols in Fig. 7.2 that represent the experimental data acquired by Baschenko *et al.* [86]. There are two reasons why a finite intensity is always observed in the forward and backward directions: first, the acceptance solid angle of the analyzer is finite, and, second, photoelectrons are scattered elastically by atoms in the solid. As a result, the elastic mean free path length may become comparable to the inelastic mean free path. Consequently, the signal electrons are efficiently scattered inside the solid and even for an infinitely small analyzer acceptance angle, a non-vanishing intensity is expected in the forward and backward directions.

The simulation results shown in Fig. 7.2 are consistent with the above interpretation in that, even in the rectilinear motion model (curve labelled SLA), there is a finite probability for detecting electrons along the surface normal when the analyzer acceptance angle is finite. For an infinitely small acceptance angle, the intensity along the surface normal should be zero in the rectilinear-motion model, but not when elastic scattering is considered. SESSA is able to perform a simulation for an *infinitely* small acceptance angle of the analyzer by

employing a symmetry property of the kinetic equation. Instead of simulating the trajectory from its generation point, tracing it through the solid, and hoping that it is emitted in the direction of the detector, its path is started in the analyzer and traced back in reverse in the solid. In this way, every simulated trajectory contributes to the intensity simulated with the Monte Carlo method. This procedure was devised by Gries and Werner and has become known as “trajectory reversal” [21]. With the conventional MC calculation methods, it is strictly impossible to perform a simulation for an infinitely small acceptance angle. The reader may load the file `infinite.ses` to see how long it takes SESSA to converge to the same precision in such a case. Even for a moderately (but realistically) large polar opening angle of 6°, conventional MC calculations take of the order of weeks to converge to the precision of the data displayed in Fig. 7.2.

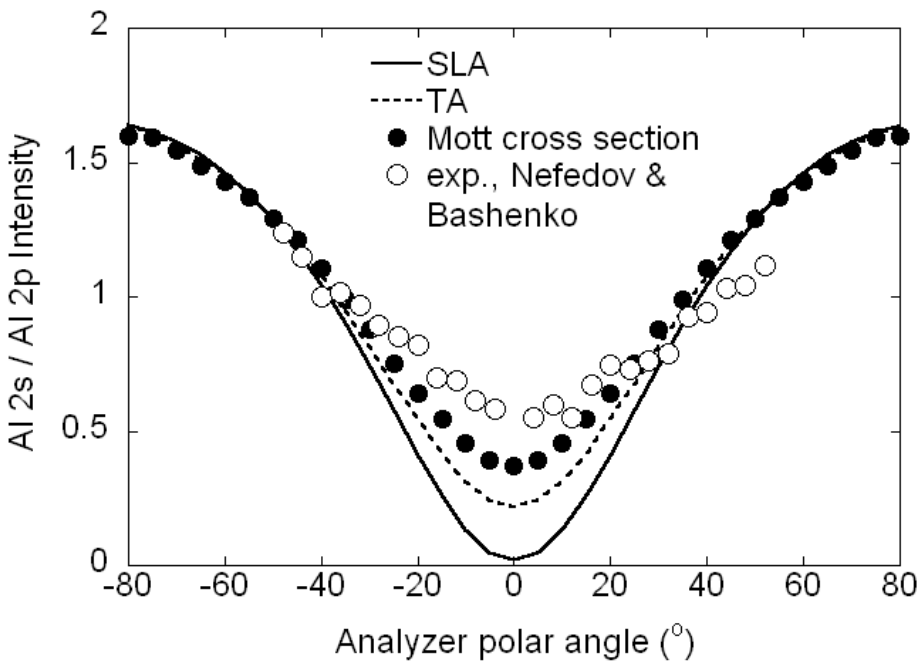


Figure 7.2: Ratio of the Al 2s and Al 2p photoelectron intensities as a function of the emission angle. Open circles: experimental results of Baschenko *et al.* [86]. Filled circles: SESSA simulation based on Mott elastic-scattering cross sections. Dashed line: SESSA simulation based on an isotropic transport cross section. Solid line: SESSA simulation based on the rectilinear motion model (straight-line approximation). In the experiment, the excitation was by Al K α x-rays that illuminate the back side of a thin Al specimen. In the present simulations, a semi-infinite Al specimen was assumed to be irradiated with AlK α x-rays at normal incidence. The half-polar opening angle of the analyzer was taken to be 6°. The fact that the polar analyzer opening angle is finite is responsible for a finite value of the plotted ratio at normal emission in the straight-line approximation.

7.1.3 Angle-resolved XPS for an oxidized silicon wafer with a carbon contamination layer

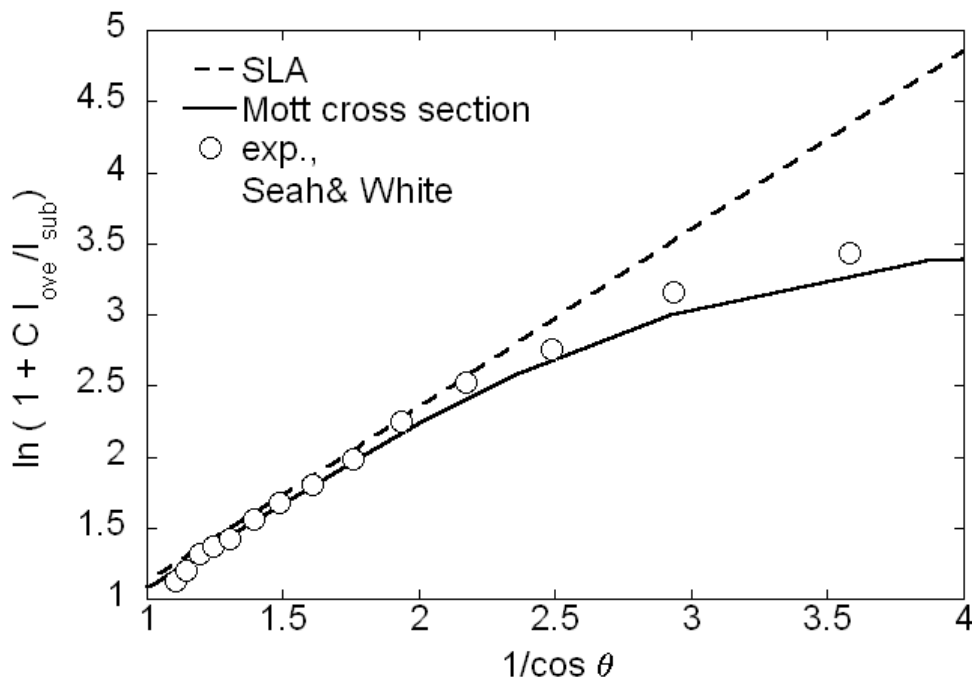


Figure 7.3: A plot of $Y = \ln(1 + CI_{SiO_2} / I_{Si})$ as a function of $1/\cos \theta$, where θ is the electron emission angle with respect to the surface normal, for angle-resolved XPS experiments with Si 2p photoelectrons from a thin SiO_2 film on a Si substrate. Open symbols: experimental data of Seah and White [87]; dashed line: straight-line approximation (SLA); solid line: results of SESSA simulations based on Mott cross sections for elastic scattering.

- **Purpose:** Illustrate the concept of chemical-state labeling using an important practical example. Demonstrate that consistency and accuracy of analysis can be considerably enhanced when different factors affecting the measured intensity are all accounted for simultaneously.
- **Time required for simulation:** ~ 30 s.
- **Directory:** tutorials\sio2-c-arxps
- **CLI-files (*.ses)** : ini.ses, sample.ses, peak.ses, geo.ses, sim.ses, sio2-c-arxps.ses

- **GNUPLOT-files (*.g)** : compare.g
- **Output-files (output*.*)** : sla_all.adf,es_adf.all
- **Other files:** seah.dat

- **Procedure:**

1. Load the file sample.ses and open the “Sample/layer” menu (CTRL-1). The compositional depth-profile is shown in the figure in the bottom-right corner. It is seen to consist of three layers: a Si substrate, a layer consisting of Si and O, and a top layer consisting of C. Select the middle layer by clicking on it. This is equivalent to selecting layer 2 in the “choose layer” box in the top left corner of this menu. It is seen that the Si component of the material constituting this layer is designated as ‘[oxide]’. The Si in the substrate has no chemical state attribute (as verified by clicking on the bottom layer). The chemical state attribute is a string of characters that can be freely chosen by the user and is not in any way interpreted by SESSA; it is only used to label the corresponding peaks. Press CTRL-2 to enter the "Sample/Peaks" menu to see the effect. Here, the silicon peaks appear double: as plain (elemental) silicon and one labelled as ‘[oxide]’. The important point is that these peaks are treated separately in the simulation.
2. Note, furthermore, that the density of the oxide was explicitly set with a corresponding command in the file sample.ses. This is necessary because SESSA can only estimate the density of compounds and such an estimate may be in error by more than 100%.
3. Load the file peak.ses and open the “Sample/Peaks” menu (CTRL-2). It can be seen here that different peak energies have been assigned to the two chemical states of Si: the separation of the peaks facilitates their differentiation in the simulated spectra (but this has no effect whatsoever on the simulated *intensities*).
4. Load the file geo.ses
5. Open the “Model Calculation” menu (CTRL-7) and load the file sim.ses. Go back to the “Sample/Peaks” menu, choose “partial intensities” in the graphical display and inspect the result for the ‘Si2p’ and ‘Si2p[oxide]’ peaks. It is seen that the ratio of the partial intensities for the two peaks vary differently with the polar emission angle: while the partial intensities increase with the number of times the signal-electrons experience an inelastic collision for elemental Si, these quantities decrease for the oxide.
6. Start gnuplot and load the file compare.g. The result should resemble Fig. 7.3

- **Discussion:**

Angle-resolved XPS is an important technique in semiconductor technology for measuring oxide thickness and composition. In principle, the angular distribution of photoelectrons emitted from layered samples carries information on the compositional depth profile. However, there are limits to the amount of information that can be extracted from such data [88].

Experimental data are often analyzed on the basis of an approach in which elastic scattering of the signal electrons is ignored. Within this model, it is found that the intensity ratio of

elemental (substrate) silicon and silicon bound to oxygen in a carbon-contaminated Si/SiO₂ sample is related to the oxide thickness d_{ox} as:

$$\frac{d_{ox}}{L \cos \theta} = \ln(1 + C \frac{I_{ox}}{I_{sub}}(\theta)) \quad (7.2)$$

where L is the attenuation length for Si 2p photoelectrons in the SiO₂ film, θ is the polar emission angle (with respect to the sample normal), I_{ox} is the Si 2p intensity from the SiO₂ overlayer, I_{sub} is the Si 2p intensity from the Si substrate, I_{ox}^∞ and I_{sub}^∞ are the corresponding quantities for bulk samples of SiO₂ and Si, respectively, and $C = I_{sub}^\infty / I_{ox}^\infty$. Elastic-scattering effects and other phenomena that are not intrinsically accounted for in the approach of Eq. (7.2) are sometimes incorporated in the characteristic length L and the value of C . It is clear from Eq. (7.2) that a plot of Y (based on determinations of the four intensities in the logarithmic term) versus $1/\cos \theta$ will give the oxide thickness in units of L (if the plot is linear). It can be seen that the open circles in Fig. 7.3 based on the experimental measurements of Seah and White [87] lie close to a straight line through the origin for $(1/\cos \theta) < 2$ (i.e., $\theta < 60^\circ$).

One reason why the analysis based on Eq. (7.2) is so attractive is that the thickness of the carbonaceous contamination layer does not appear in it. In other words, the derived oxide-layer thickness for an arbitrary thickness of any carbonaceous-contamination layer is independent of the thickness of this layer. On the other hand, for emission angles exceeding 60°, the effects of elastic scattering become quite significant, and the experimental points in Fig. 7.3 then deviate from the straight line expected from Eq. (7.2).

The data of Seah and White in Fig. 7.3 were acquired from experiments with a Si wafer. The results for $\theta < 60^\circ$ were analyzed with Eq. (7.2) to give a mean SiO₂ thickness of 39 Å.

Figure 7.3 shows SESSA results based on the Mott elastic-scattering cross section (solid line) and on the straight-line approximation (SLA) (dashed line). These results were obtained for a 36 Å oxide layer that gave the best consistency between the solid line and the experimental results. There is also reasonable agreement between the derived and reported oxide thicknesses. For emission angles exceeding 60°, the SESSA results with the Mott cross sections show the expected deviation from the dashed line from the SLA due to the effects of elastic scattering.

7.1.4 Angular distribution of photoelectrons emitted from a stratified overlayer-substrate sample

- **Purpose:** Simulation of the peak intensities of a stratified two-layer system (overlayer on an infinite substrate).
- **Time required for simulation:** Seconds
- **Directories and files:**
 - tutorials/V2-1/Layers
 - tutorials/V2-1/Layers/output
- **CLI-files (*.ses):**
 - layers.ses

The peak intensities of a stratified two-layer system (overlayer on an infinite substrate) are calculated and simulated under the following assumptions:

- **Straight line approximation**
- **Infinitely small acceptance solid angle of the analyzer,**

which simplify the following equations and reduce the computation time, but are purely optional for the simulations.

Since we assume that no elastic scattering occurs and that the inelastic mean free paths (IMFPs) of the overlayer and the substrate are identical (which can be done in SESSA easily as all simulation-relevant parameters can be adjusted at will), the integrals describing the intensities of the overlayer and substrate peaks reduce to a very simple form.

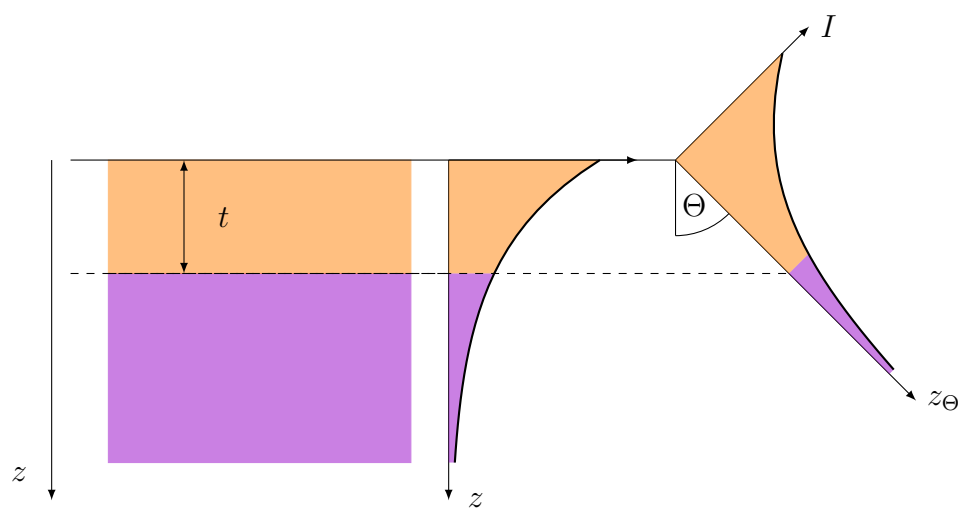


Figure 7.4: Visualization of the established model for layered specimens for two different emission angles Θ . From the detector's point of view, the overlayer thickness t increases with the emission angle Θ , which results in a higher fraction of detected overlayer electrons in direction z_Θ than z .

Overlayer

The angle-dependent signal from an overlayer (OL) with thickness t and IMFP λ is calculated as shown in equations 7.3 and 7.4.

$$I_{OL} = \int_0^t e^{\left(-\frac{z}{\lambda \cdot \cos \theta}\right)} dz = -\lambda \cdot \cos \theta \cdot e^{\left(-\frac{z}{\lambda \cdot \cos \theta}\right)} \Big|_0^t \quad (7.3)$$

$$I_{OL} = \lambda \cdot \cos \theta \left(1 - e^{\left(-\frac{t}{\lambda \cdot \cos \theta}\right)} \right) = \lambda \cdot \mu \left(1 - e^{-\frac{t}{\lambda \cdot \mu}} \right), \quad (7.4)$$

with $\mu = \cos \theta$. According to Lambert's cosine law, the radiance of a surface is reduced by the cosine of the emission angle, therefore μ in equation 7.4 is canceled out and the final expression for the intensity of the overlayer reads as

$$I_{OL} = \lambda \cdot \left(1 - e^{-\frac{t}{\lambda \cdot \mu}} \right) \quad (7.5)$$

Substrate

The substrate signal is calculated similarly but with different integration limits.

$$I_{Sub} = \int_t^\infty e^{\left(-\frac{z}{\lambda \cdot \mu}\right)} dz = -\lambda \cdot \mu \cdot e^{\left(-\frac{z}{\lambda \cdot \mu}\right)} \Big|_t^\infty \quad (7.6)$$

$$I_{Sub} = \lambda \cdot \mu \cdot e^{-\frac{t}{\lambda \cdot \mu}} \quad (7.7)$$

Again, in equation 7.7, μ cancels out due to the Lambert cosine law.

$$I_{Sub} = \lambda \cdot e^{-\frac{t}{\lambda \cdot \mu}} \quad (7.8)$$

Procedure

1. Start SESSA
2. Load the session file `layers.ses`. SESSA will perform a number of simulations of differently tilted planar geometries of Palladium deposited on Gold. The results are automatically saved in the `output/-folder`
3. Navigate to the `output/-folder` and call `plot.gp` from gnuplot. The generated file `OL_Sub.ps` can now be viewed.

Results

The results shown in figure 7.5 were obtained by simulating a Pd/Au overlayer-substrate system with an overlayer thickness of 10 Å. According to equations 7.5 and 7.8, all IMFPs were set to 10 Å so that the expressions for the substrate and overlayer signals acquire a simple form as t/λ cancels to 1.

It can be seen that the calculated and simulated datasets match perfectly, indicating that SESSA yields the expected results.

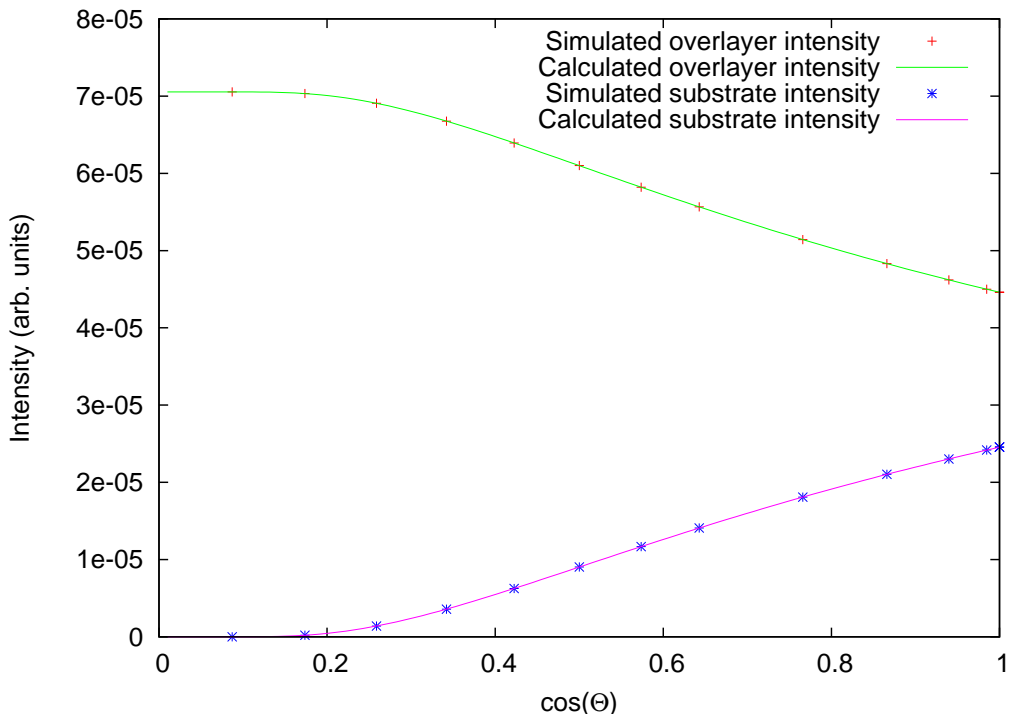


Figure 7.5: Comparison of simulated (dotted) and calculated (solid) intensities for a Pd/Au overlayer-substrate system depending as a function of the cosine of the emission angle $\cos \Theta$

7.1.5 Depth distribution function (DDF) in XPS: comparison with experiment

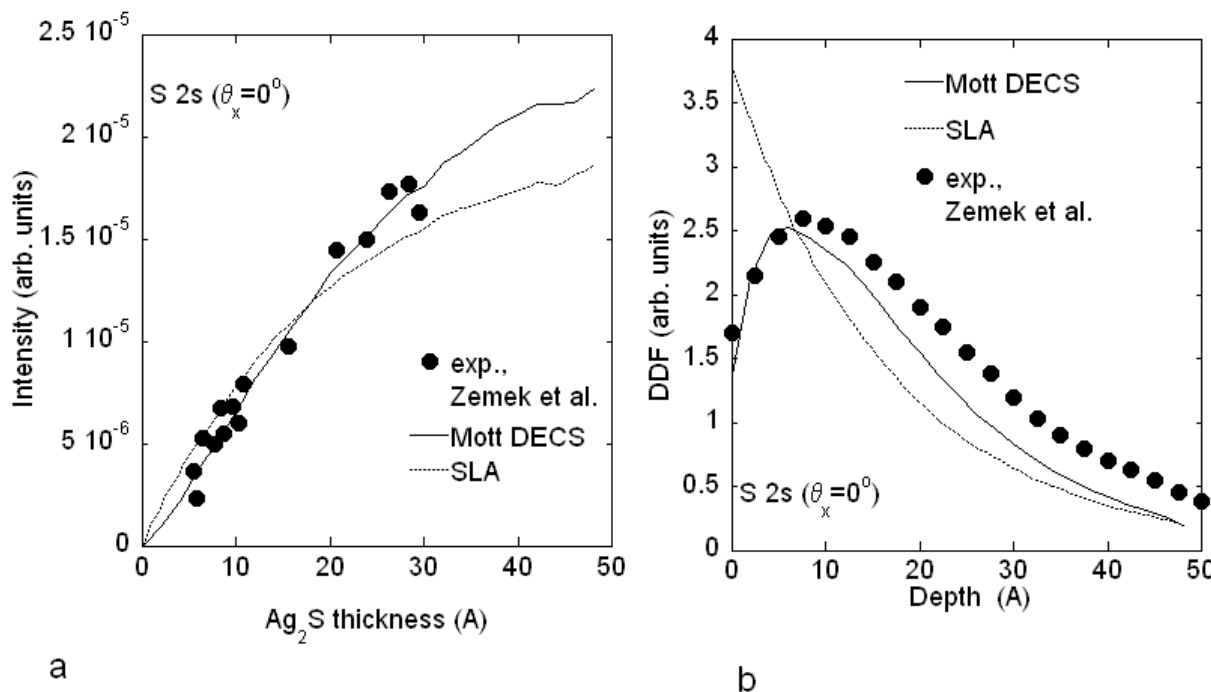


Figure 7.6: (a) Intensity of the S 2s XPS line as a function of the thickness of an Ag_2S overlayer on a Ag substrate that is irradiated with $\text{Al K}\alpha$ x-rays. The photoelectrons are detected along the surface normal with an analyzer polar acceptance angle of 4.1° . Filled symbols: experimental data of Zemek *et al.* [89]; solid line: SESSA with Mott differential elastic-scattering cross sections; dotted line: SESSA using the straight-line approximation (SLA). (b). Depth distribution function (DDF) for the experimental conditions in (a). Dotted line: evaluation of the experimental results in (a); Filled symbols: SESSA with Mott differential elastic-scattering cross sections; solid line: SESSA, straight-line approximation.

- **Purpose:** Demonstrate that a quantitative model for the surface sensitivity in AES and XPS is implicitly contained in SESSA by comparing results for the Depth Distribution Function (DDF) with experiment. We note that this DDF is the emission depth distribution function defined by ISO [90].
- **Time required for simulation:** ~ 5 minutes.
- **Directory:** tutorials\ag2s-ddf

- **CLI-files (*.ses)** : ini.ses, int.ses, mod.ses, mod_sla.ses, ddfini.ses, ddf.ses,
- **Output files:** es, sla, esddf, sladdf
- **Other files:** cleanup.bat, ddfcleanup.bat, zemek.txt
- **Procedure:**
 1. Load the file `ini.ses` and open the “Sample/layer” menu (CTRL-1). If SESSA was started just before loading this file, a warning is displayed which explains that the density of the compound layer (Ag_2S) was only estimated. An appropriate command in the file `sample.ses` sets the density to a realistic value.
 2. Leave the “Sample/layer” menu open and load the file `int.ses`. SESSA will perform a simulation of the intensity of the S 2s line as a function of the thickness of the Ag_2S layer. The change of the profile can be watched in the “Sample/layer” menu during the simulation.
 3. Click on the file `cleanup.bat` (specific to this tutorial) in the `ag2s-ddf` directory. This deletes some unnecessary files in the output directory and merges the results of the simulation for the zero-order partial intensities into the files `es` and `sla`. These files contain the peak intensities calculated with SESSA that are displayed in Fig. 7.6a.
 4. Load the file `ddfini.ses` and open the “Sample/layer” menu (CTRL-2). The sample now consists of a 1 Å buried layer of Ag_2S between an Ag substrate and an Ag overlayer (1 Å = 0.1nm).
 5. Leave the "Sample/layer" menu open and load the file `ddf.ses`. SESSA will perform a simulation of the intensity of the S 2s line as a function of the thickness of the Ag overlayer covering the 1 Å buried Ag_2S layer. The corresponding S 2s intensities as a function of the depth closely match the depth distribution function.
 6. Click on the file `ddfcleanup.bat` in the `ag2s-ddf` directory. This deletes some unnecessary files in the output directory and merges the results of the simulation for the zero-order partial intensities into the files `esddf` and `sladdf`. These files contain the SESSA data for the depth distribution function displayed in Fig. 7.6b.

- **Discussion:**

Specification of the depth distribution function for a given surface electron-spectroscopy experiment represents the most general and comprehensive way to describe the surface sensitivity [91]. The zero-order emission depth distribution function, pertaining to the peak intensity of Auger electrons or photoelectrons that escape without inelastic scattering is defined as the “probability that the particle or radiation leaving the surface in a specified state and given direction originated from a specified depth measured normally from the surface into the material [90]”.

Since the DDF can exhibit a quite complex behaviour, it is not always possible to specify it in detail. Therefore, a number of quantities have been introduced that describe the major effect of the DDF on the surface sensitivity in a simple way. These quantities include the “Attenuation Length”, “Effective Attenuation Length”, “Local Effective Attenuation Length”,

“Practical Effective Attenuation Length”, “Information Depth”, and “Mean Escape Depth”, and have recently been reviewed by Jablonski and Powell [92–94].

In Fig. 7.6(a), the experimental data of Zemek *et al.* [89] for growth of Ag_2S on a Ag substrate are compared with results of a SESSA simulation. In the experiment, a thin Ag foil on which the Ag_2S layers were grown was irradiated on the back side with Al $K\alpha$ x-rays. The solid line is the simulated intensity as a function of the thickness when elastic scattering is accounted for: this line agrees quite well with the experimental results. The dashed line is the result from the straight-line approximation. In Fig. 7.6(b) the DDF derived from the experimental data is compared with the SESSA simulation results for the DDF. Again, a reasonable agreement between experiment and the simulation is seen.

The favorable comparison of the SESSA simulation data with experimental results demonstrates that SESSA is based on a realistic model for the surface sensitivity in electron spectroscopy.

7.1.6 Surface morphology: influence of surface roughness.

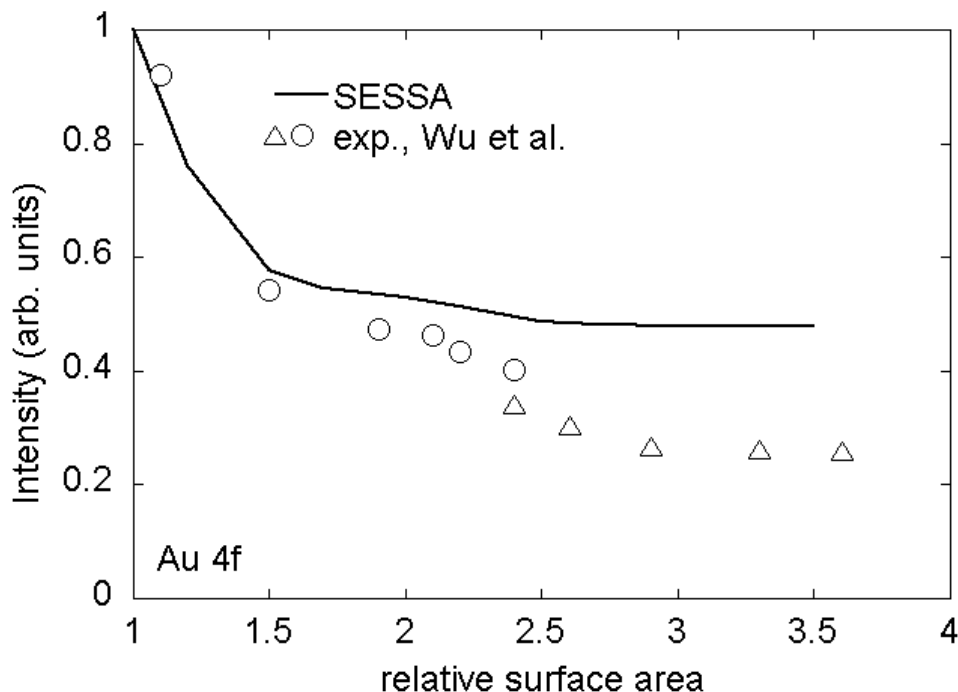


Figure 7.7: Au 4f intensity as a function of the relative surface area. Data points: experimental results from Wu *et al* [95, 96]; solid line: SESSA

- **Purpose:** To demonstrate that the intensity for rough samples decreases with increasing relative surface area.
- **Time required for simulation:** ~30 s.
- **Directory:** tutorials\roughness
- **CLI-files (*.ses):** ini.ses, sample.ses, mod.ses
- **GNUPLOT-files (*.g):** compare.g
- **Output-files (output*.*):** rgh
- **Other files:** wu.txt, rgh.txt, cleanup.bat

- **Procedure:**

1. Load the file `ini.ses` and open the “Sample/layer” menu (CTRL-1).
2. Load the file `mod.ses` and watch the ordinate axis of the plotwindow change when simulations are performed for different values of the relative surface area, indicating that the total measured intensity drops with increasing surface roughness.
3. Click on the file `cleanup.bat` thereby deleting unnecessary files in the output directory and creating the file `rgh` that may be edited to yield the file `rgh.txt`.
4. Load `compare.g` in GNUPlot to view the result (see Fig. 7.7).

- **Discussion:**

The comparison in Fig. 7.7 between SESSA simulation results and the experimental data of Wu *et al.* [95, 96] shows that the simple model for surface roughness implemented in SESSA provides a rough estimate for the effects of surface roughness on the signal-electron intensity. Note that for a realistically rough surface, the relative surface area assumes values between 1 and 1.2 (see Ref. [15]). Larger values of the relative surface area, such as those measured by Wu and co-workers for their samples correspond to porous samples (so called high Brunauer-Emmet-Teller (BET) surfaces [97]).

7.2 Spectral Shape

7.2.1 Au overayers on a Pb substrate: spectral shape as a function of overlayer thickness and emission angle

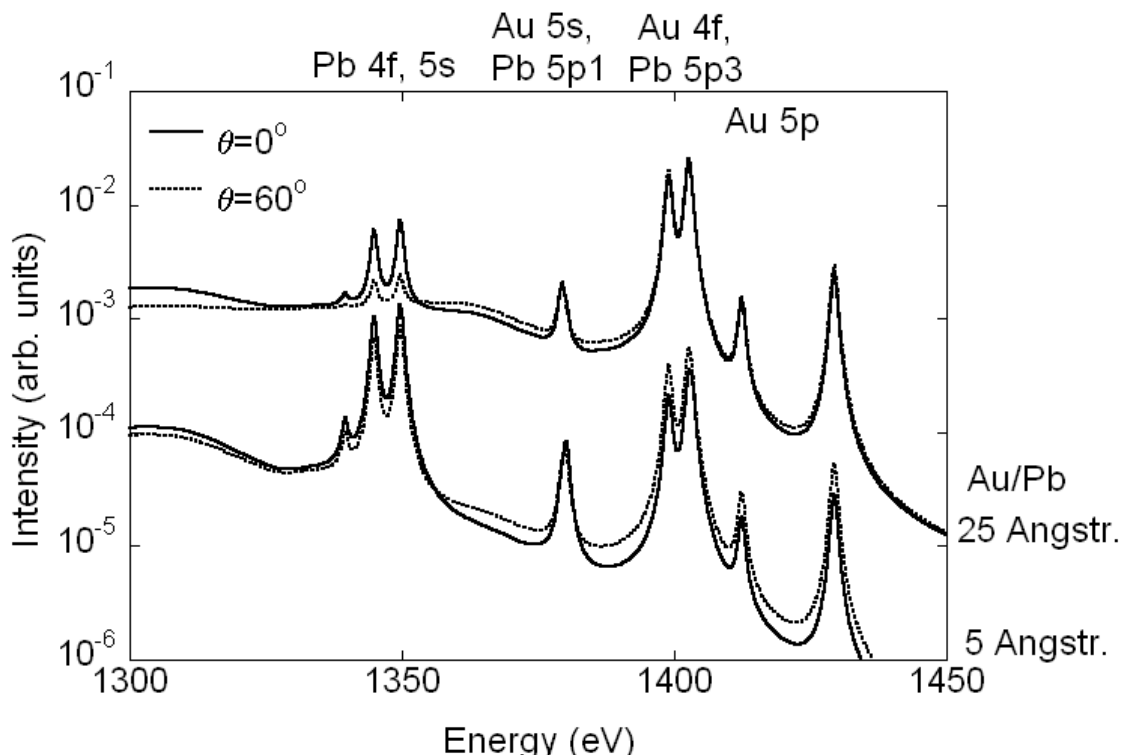


Figure 7.8: SESSA simulation results for the Au and Pb 4f, 5p and 5s spectral regions of two samples of Au overayers on a Pb substrate and excitation by Al K α x-ray radiation. Upper curves: 25 Å Au/Pb; lower curves: 5 Å Au/Pb; Dotted lines: 60° emission angle; solid lines: emission along the surface normal.

- **Purpose:** Demonstrate the change of spectral shape with emission angle and as a function of the compositional depth profile.
- **Time required for simulation:** ~ 30 s.
- **Directory:** tutorials\spc
- **CLI-files (*.ses):** ini.ses, mod5.ses, mod25.ses
- **GNUPLOT-files (*.g):** compare.g

- **Output files** (`output*.*`) : *.spc

- **Other files:** cleanup.bat

- **Procedure:**

1. Load the file `ini.ses`.
2. Load the file `mod5.ses` that performs a simulation for a 5 Å thick Au overlayer on a Pb substrate for normal emission and for an emission angle of 60°. Subsequently, load the file `mod25.ses` that repeats the simulation for a 25 Å thick overlayer.
3. load the file `compare.g` in gnuplot to view the results as displayed in Fig. 7.8.

- **Discussion:**

The results in Fig. 7.8 clearly show that the shape of the spectrum depends on the compositional depth profile of the sample. The same is seen to be true for the relative intensities of the no-loss peaks. Furthermore, the variation of the spectral shape and the relative intensities with emission angle are different for the two depth profiles considered here. This result is in agreement with the expectation that the combined energy and angular distribution of the signal electron flux emitted from a sample carries information on the chemical composition of a specimen near the surface [25, 88].

7.2.2 Need for empirical data to realistically describe spectral shapes.

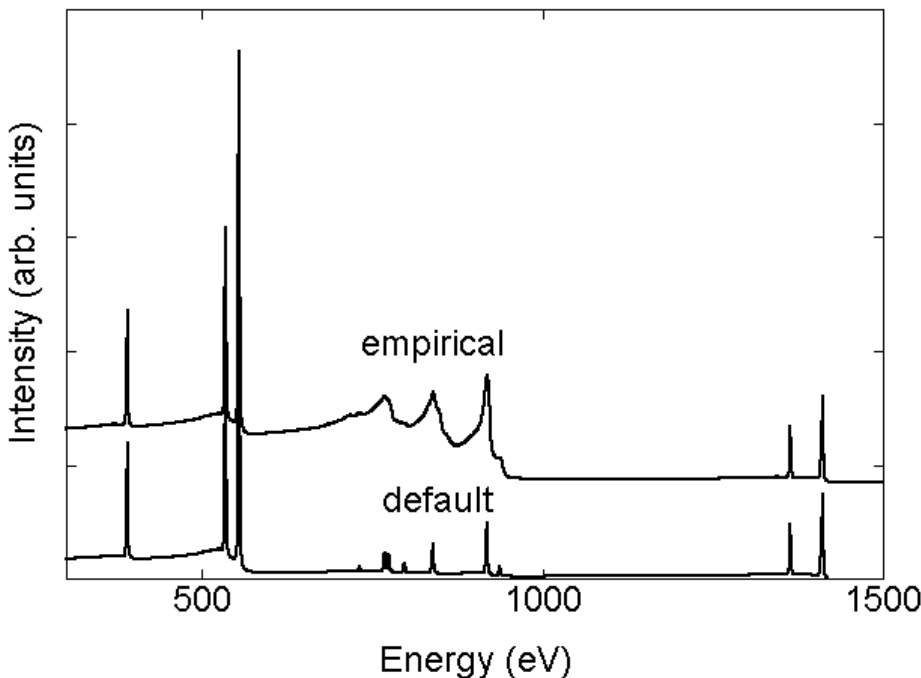


Figure 7.9: XPS spectrum of a Cu sample excited by Al $K\alpha$ x-rays. Upper curve: simulation result from SESSA, using empirical data for the Cu LMM Auger transition; Lower curve: the same simulation based on the default peak shapes contained in SESSA.

- **Purpose:** To show that incorporation of empirical data in SESSA provides a convenient tool for quantitative simulation not only of spectral intensities but also of spectral shapes.
- **Time required for simulation:** ~ 30 s.
- **Directory:** tutorials\aes-empirical
- **CLI-files (*.ses):** cu.ses, cu-emp.ses
- **GNUPLOT-files (*.g):** compare.g
- **Output-files (output*.*):**

- **Procedure:**

1. Load the file cu.ses and open the “Model calculation” menu (CTRL-7). The Al K α Cu XPS spectrum is seen in this menu. Note that the LMM Auger region that is located in the range of kinetic energies between 700 eV and 1000 eV does not look very realistic. Go to the “Sample/peak” menu (CTRL-2) and click on any of the Auger peaks in the peak selection list. The graphical display of the intrinsic peak shape shows that the standard functional forms (Gaussian, Lorentzian, Doniach-Sunjic) do not resemble a realistic Auger peak.
2. Load the file cu-emp.ses and open the “Model calculation” menu (CTRL-7). Open the “Sample/peak” menu (CTRL-2) to see that all Auger peaks except one were removed. The remaining empirical Auger peak comprises a broad spectral range. In the “Model calculation” menu graphical display, a spectrum similar to the previous one is shown, but the Auger part now looks much more realistic.

- **Discussion:**

A drastic difference is seen between the two spectra created by the above procedure (Fig. 7.9). However, comparison of the partial intensities of the Cu LMM peaks reveals that the spectral shape of the signal-electron sources is the only difference; the partial intensities are identical! To appreciate this, note that a simulation of a spectrum in SESSA proceeds in two steps: first, the partial intensities are calculated for a given sample, experimental conditions, etc. The partial intensities represent the number of electrons emitted from a given atomic subshell in a given atom that eventually reach the detector after experiencing a certain number of inelastic collisions. The parameters in the SESSA databases for this purpose are believed to be realistic. In the next step, the partial energy distributions are derived from the energy distribution at the source and the probability for an energy loss in an individual excitation (that is the differential inelastic inverse mean free path, DIIMFP). Although realistic data for the DIIMFP are available within SESSA for a limited number of materials for which detailed optical measurements are found in the literature, realistic data for the spectral shapes of an Auger-electron transition and photoelectron transition are not presently part of the SESSA databases. This situation is particularly problematic for Auger-electron transitions, and emphasizes the necessity for empirical data when simulating the spectral shape.

7.2.3 Transfer of spectral data between different spectrometers

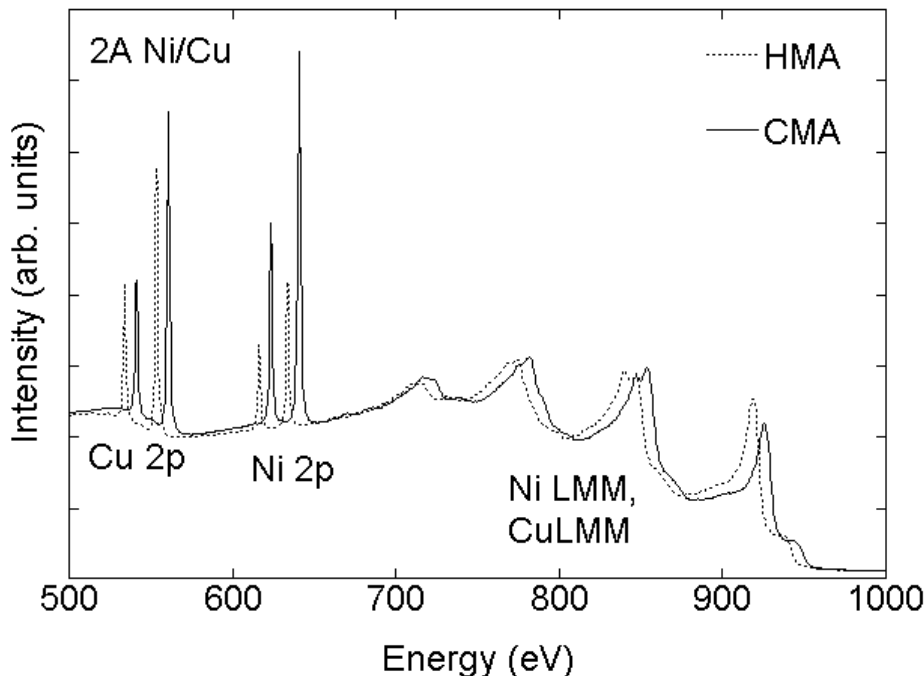


Figure 7.10: XPS spectra of a 2\AA thick Ni layer on a Cu substrate excited by Al $\text{K}\alpha$ x-rays. Dotted line: simulation results from SESSA using a hemispherical analyzer (HMA) for energy selection; solid line: SESSA simulation using a cylindrical mirror analyzer (CMA). To facilitate comparison, the two curves have been slightly shifted in energy relative to each other.

- **Purpose:** Demonstrate that intercomparison of spectra acquired on different instruments can be significantly facilitated when a flexible simulation tool is available that accounts for instrumental effects. In the present case, an effect of solid angle is studied.
- **Time required for simulation:** ~ 30 s.
- **Directory:** tutorials\transfer
- **CLI-files (*.ses):** ini.ses
- **GNUPLOT-files (*.g):** compare.g

- **Output-files** (`output*.*`): reg1.spc

- **Procedure:**

1. Load the file `ini.ses` and open the “Model calculation” menu (CTRL-7). The graphical display in this menu is essentially the same as the results shown in Fig. 7.10.

- **Discussion:**

The results in Fig. 7.10 show that complex differences in spectral shapes can occur for instruments that differ in certain properties. In the present example, this concerns the solid angle of acceptance of the analyzer. This makes it very difficult to compare quantitative information on published spectra from different types of instruments. A simulation such as SESSA can help avoid such problems if instrumental effects on the spectral shape are realistically simulated.

7.2.4 Handbook of simulated XPS spectra.

- **Purpose:** Using the extensive databases in SESSA and the flexibility offered by the CLI, it is possible to produce large customized reference data sets.
- **Time required for simulation:** several minutes.
- **Directory:** tutorials\handbook
- **CLI-files (*.ses):** ini.ses, handbook.ses, handbook-brief.ses, dosim.ses
- **Output-files (output*.*):** XPS spectra of elemental solids throughout the periodic system, with and without a 5 Å thick carbon contamination layer.
- **Procedure:**
 1. Load the file ini.ses
 2. Load the file handbook_brief.ses to get a quicker impression of what handbook.ses does when you start it.
 3. Edit the file dosim.ses and uncomment the indicated line.
 4. Run the file handbook_brief.ses again, now producing a handbook of XPS spectra recorded on samples with a 5 Å carbon contamination layer.
- **Discussion:**

The above CLI files produce two extensive reference data sets for a collection of elemental solids throughout the periodic table. In the second run, a systematic change in the experimental conditions is simulated by adding a 5 Å thick carbon-contamination layer to each sample.

7.3 Techniques other than conventional AES/XPS

7.3.1 Total Reflection XPS (TRXPS)

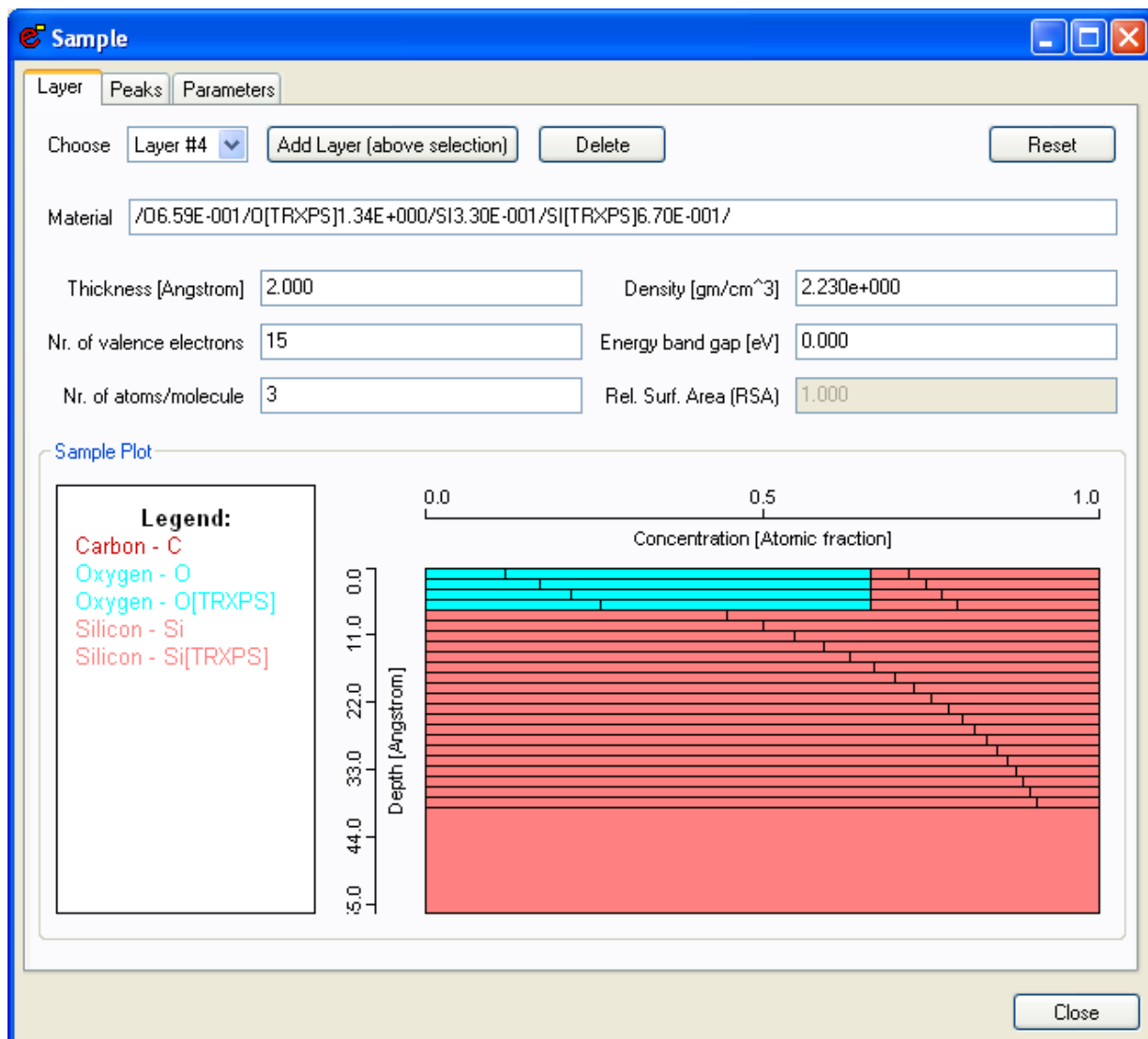


Figure 7.11: The Sample/Layer menu in the GUI showing the excitation depth distribution for TRXPS after loading the file sample.ses

- **Purpose:** Illustrate the fact that the surface sensitivity is generally determined by both the excitation depth distribution function as well as the emission depth distribution function.
- **Time required for simulation:** ~ 30 s.
- **Directory:** tutorials\trxps

- **CLI-files (*.ses)** : sample.ses xps_sim.ses, trxps_sim.ses, trxps.ses

- **GNUPLOT-files (*.g)** :

- **Output-files (output*.*)** : xpsreg1.spc, trxpsreg1.spc

- **Procedure:**

1. Open the Sample window in the GUI and press CTRL-I to load the session file sample.ses. After a while, the structure of the sample is updated on the screen and is seen to consist of a very thin C-contamination layer (layer 1, 0.5 Å) on top of 8 Å of SiO₂ on an Si-substrate (see Fig. (7.11)). The upper 24 layers are seen to consist of a contribution labelled '[trxps]' and a normal unlabelled contribution. The concentration of the species labelled '[trxps]' decreases exponentially with the depth. In the "Sample/Peak" menu, it can also be seen that each peak appears in duplicate, unlabelled as well as labelled. These settings were chosen to mimic a total reflection XPS experiment, where the incidence angle of the exciting x-radiation is chosen to be close to the critical angle for total reflection, leading to a dramatic decrease of the characteristic length (or depth) for creation of photoelectrons. In the present example this characteristic length was arbitrarily chosen to be 20 Å, a typical value in TRXPS.
2. Next, load the file xps_sim.ses. This file performs a simulation for *all* peaks (labelled as well as unlabelled), and writes the corresponding output into the directory output. Since the labelled and unlabelled peaks have the same peak shape and energy, they are added in the resulting spectrum output\xpsreg1.spc. Thus the simulated spectrum should resemble a conventional XPS spectrum, as indeed it does (see the top panel of Fig. 7.12).
3. When the file trxps_sim.ses is loaded next, the same simulation is repeated again but the unlabelled peaks are deleted from the spectra prior to the simulation. In consequence, the resulting spectrum output\xpsreg1.spc now corresponds to a depth distribution of excitation for the species labelled '[trxps]' only. The result is displayed in the bottom panel of Fig. 7.12 on the right hand side. The inelastic background is seen to be significantly decreased, indicating that the surface sensitivity of this spectrum is higher than for an ordinary XPS measurement.
4. It should be noted here that in these simulations, the incidence direction of the x-rays was chosen along the surface normal, as was the detection direction. In other words, the change in the surface sensitivity due to the grazing incidence of the x-rays was simulated only by taking into account the depth distribution of the excitation. For a more realistic simulation of TRXPS with the present version of SESSA, it is imperative to properly account for the experimental geometry, since the relative peak intensities for photoelectrons with different asymmetry parameters depend sensitively on the values of this asymmetry parameter, in particular for typical TRXPS geometrical configurations. It is easy to perform realistic simulations with SESSA; one merely has to specify the correct geometrical configuration in the geometry menu. Since the example studied here merely serves illustrative purposes and is not compared with actual experimental data, the simulations were performed for the default geometrical configuration.

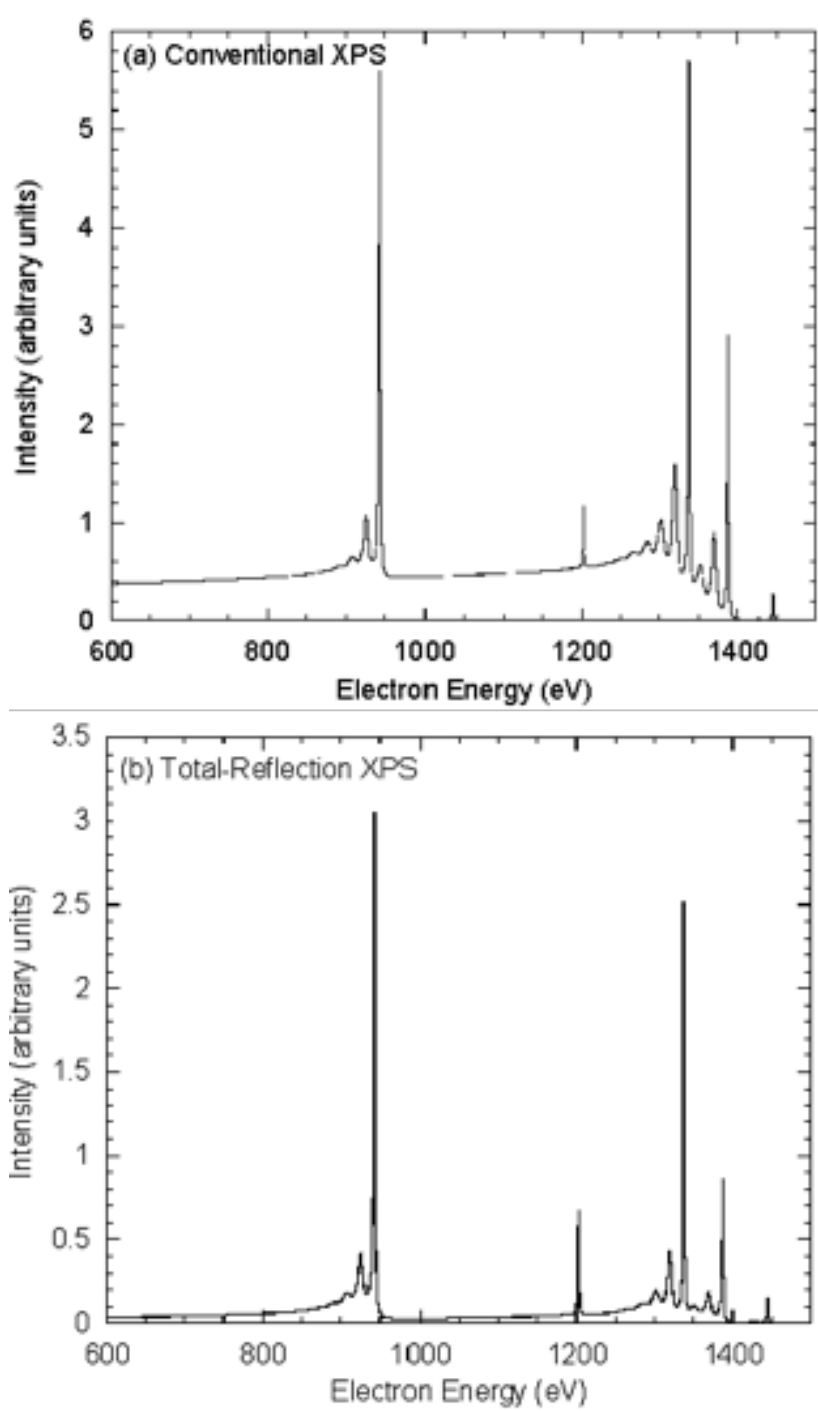


Figure 7.12: Simulated spectra of a sample consisting of a 0.5 \AA thick C-contamination layer on top of a 10 \AA thick SiO_2 layer on a Si substrate. The top panel shows the simulated conventional XPS spectrum, the bottom panel shows the simulated Total Reflection XPS spectrum, where the angle of incidence of the X-rays is close to the angle of total reflection. These spectra were simulated as described in the text.

- **Discussion:**

In surface analysis techniques employing particle beams, the analyzed depth range is generally determined by the penetration of the exciting radiation into the surface, described by the so-called excitation depth distribution function $\phi_x(z, \theta_x)$, the depth distribution of species leading to the generation of the detected signal $c(z)$, and the probability for escape as a function of the depth. In electron spectroscopy it is convenient in this connection to introduce the partial intensities of electrons that reach the detector after participating in a given number of scattering events C_n . The escape probability for n -fold inelastically scattered electrons is described by the partial escape distributions, or emission depth distribution functions $\phi_{e,n}(z, \theta_e)$. Then the partial intensities are given by:

$$C_n(\theta_x, \theta_e) = \int_0^{\infty} \phi_x(z, \theta_x) c(z) \phi_{e,n}(z, \theta_e) dz \quad (7.9)$$

where the subscript "x" represents the "excitation", while "e" denotes the "emission" process. The excitation depth distribution function can be described in terms of a Beer-Lambert attenuation law:

$$\phi_x(z, \theta_x) = \exp(-\mu_x \varrho z / \cos \theta_x) \quad (7.10)$$

where μ_x is the mass absorption coefficient determining the relevant excitation range (measured along the photon trajectory) and ϱ is the mass density of the material. The characteristic length for the emission depth distribution function is approximately given by the inelastic mean free path that is orders of magnitude smaller than the x-ray absorption length ($\lambda \ll 1/\mu_x \varrho$) for conventional XPS. In this case the variation of the excitation depth distribution with depth in the integral (7.9) can be neglected and the surface sensitivity of XPS is entirely determined by the escape process.

When the angle of incidence of the x-rays is close to the critical angle for total reflection $\theta_{x,c}$, the characteristic length for the excitation process becomes comparable to the inelastic mean free path [98], and a variation of the (glancing) incidence angle according to Eq. (7.9) allows the probing of different depth regions by effectively changing the excitation depth distribution experimentally.

In this case, the detected photoelectrons mainly escape from shallow depths (as indicated by the depth distribution of the species labelled '[trxps]' in the Sample/Layer menu), and consequently the higher-order partial intensities that make up the inelastic background are suppressed, since the emission depth distribution function for increasing order of scattering samples increasingly larger depths (approximately $n\lambda_i / \cos \theta_e$ for n -th order scattering [25]). This explains the reduced inelastic background seen in the TRXPS spectra in Fig. 7.12.

7.3.2 Ion-induced Auger-electron emission.

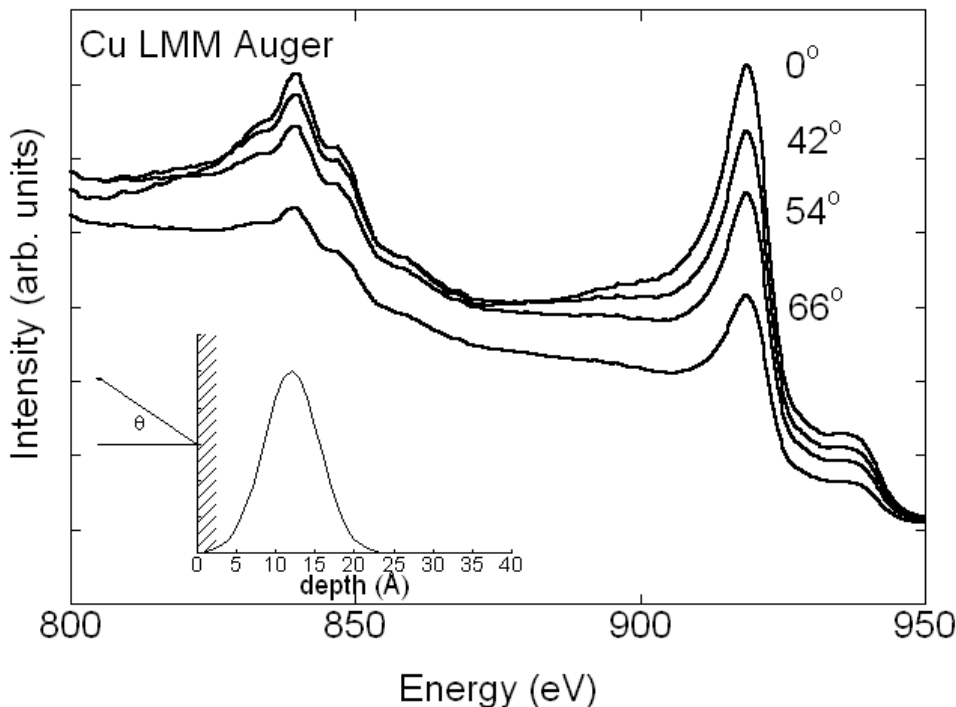


Figure 7.13: Cu LMM Auger spectra for different emission angles (with respect to the surface normal) and for the source depth distribution shown in the inset. These results simulate ion-induced Auger electron spectra.

- **Purpose:** Demonstrate that the source depth distribution can be specified in a flexible way using a technique involving chemical-state labelling.
- **Time required for simulation:** ~5 min.
- **Directory:** tutorials\ion-induced
- **CLI-files (*.ses):** sim.ses, geo.ses, cu.ses
- **GNUPLOT-files (*.g):** pi.g, spc.g
- **Output-files (output*.*):** cucuLM9_emitting.*

- **Other files:** CULMM.REG

- **Procedure:**

1. Start SESSA.
2. Open the sample menu (CTRL-5). Load the file cu.ses and wait a moment. The commands in this file set up a depth profile of emitters distributed with a Gaussian profile at 12 Å mean depth and a full width at half maximum intensity of 5 Å. This profile is assumed to be caused by energy deposited in the solid by some kind of incident particle (e.g., ions) and the energy deposition profile is assumed to be related to the depth profile for Auger electron emission. The profile is seen in the sample menu after SESSA has processed the commands in this file. By clicking on the various layers in the depth profile and observing the material box in the sample GUI menu, it is seen how the chemical-state labelling can be used to specify a depth profile of emitters in a flexible way.
3. Load the file geo.ses. This sets up the geometry: the analyzer is rotated around the sample surface normal in the range between 0 and 60 °.
4. Load the file sim.ses. SESSA performs a simulation of the spectrum for the specified geometries. Open the simulation menu (CTRL-7) before or after loading sim.ses to see the simulation results.
5. Open the “Sample/Peak” menu and choose “partial intensities” in the display selection box to view the partial intensities. You may wish to double click on this window to transfer its contents to the separate plot window that can be enlarged to fit the screen, improving clarity.

- **Discussion:**

Figure 7.13 shows the result of the simulation. It is seen that both the peak height and peak shape depend on emission angle. Inspection of the partial intensities reveals the reason for the dependence of the peak shape on the emission angle: for more oblique emission, the signal electrons have to travel a longer distance through the solid thereby increasing the probability for an energy loss. In principle, measurements of the angular distribution of the peak shape contain information on the emission depth distribution. However, it is difficult to rigorously retrieve such information from such measurements. Simulations that optimize the consistency between experiment and theory by varying the depth distribution of the emitters provide a straightforward means of obtaining at least a rough impression of the emission depth distribution.

8 Tutorials for simulating advanced geometries using PENGEO

During the simulation of electron trajectories, SESSA needs to monitor the material through which an electron is traveling and at what point it crosses an interface. For this purpose, the PENGEO package [48] (part of the PENELOPE code) was included in SESSA. When a sample morphology has been defined, a PENGEO file (*.geo) is generated detailing geometrical features and material distribution for the simulation. During the simulation, the geometry file is read into PENGEO which then provides two essential pieces of information: 1) The present material at a given location and 2) for a given linear path whether an interface is crossed and if so where this happens.

SESSA offers many possibilities to simulate electron spectra of nanostructures with different morphologies that are highly customizable. Some morphologies are preimplemented (see section 4.4) and SESSA automatically generates the necessary PENGEO files. For geometries beyond these, SESSA V2.1 allows the user to specify morphology by providing a custom PENGEO file.

The present chapter serves to explain and provide examples on how SESSA V2.1 and PENGEO can be utilised to simulate almost arbitrary nanomorphologies. Several simple analytical models are presented together with the corresponding results obtained with SESSA V2.1. These results shall facilitate the understanding of how SESSA performs calculations and, by replicating them, a deeper understanding of the program's internal functionality shall be acquired.

It is absolutely necessary for a successful SESSA simulation to provide a correct PENGEO file. This is by no means trivial and neither SESSA nor PENGEO provide an automatic error detection. The introduction provided herein is not a complete instruction on the use of PENGEO for which the user is referred to the original publication [48].

The following tutorials are described for use on Linux or Mac systems, but should also work on Windows systems with analogous procedures.

8.1 Simulations with external PENGEO geometry files

SESSA V2.1 is capable of loading and simulating external PENGEO geometry files. A geometry file can be loaded by selecting "PENGEO" in the Sample menu from the Morphology List or by invoking the following command in the command line interface (CTRL+9):

```
sample morphology set penelope "path/file.geo"
```

This functionality enables SESSA to perform simulations with nanostructure morphologies specified by a user in the form of PENGEO instructions in a *.geo file.

After selecting the geometry file in the file dialog, it is checked for validity. If no error warning is displayed, the file is syntactically correct.

Adapt the following settings to ensure a successful simulation:

- After loading the simulation, the number of layers should be equal to the number of materials used within the PENGEOOM geometry file.
- The material numbers assigned to each body or module within the PENGEOOM geometry file must be equivalent to the material numbering in SESSA
 - In the sample preview, the top layer (the island) corresponds to material 1, while the substrate layer stands for the material with the highest number. Add layers in the layer pane in the sample menu (CTRL+1) according to the number of materials present in the geometry file.
- Within the morphology-field
 - Adapt the x and y periodicities according to the desired dimensions of the nanostructures. These have to match the dimensions of the limiting body defined in the .geo file (see section 8.4).
 - Set the height of the sample to the maximum height of the nanostructure.

8.2 Example: Simulation for infinite core-shell cylinders

- **Purpose:** Demonstration of the use of PENGEOm geometry files for simulation of non-standard nanostructures. Simulation of a photoelectron spectrum for an infinite core-shell cylinder with varying core radii.
- **Time required for simulation:** Seconds to few minutes
- **Directories:**
 - tutorials/V2-1/Cylinder
 - tutorials/V2-1/Cylinder/geometry_files
 - tutorials/V2-1/Cylinder/sessa_files
 - tutorials/V2-1/Cylinder/gnuplot_files
 - tutorials/V2-1/Cylinder/mathematica_files
- **CLI-files (*.ses):**
 - simu.ses (main CLI session file)
 - conf.ses
 - geo_reset.ses

8.2.1 Analytical model

The photoelectron spectrum and peak intensities of an infinitely long core-shell cylinder are calculated for varying core radii. Since such a morphology is not pre-implemented in the SESSA morphology menu (see section 4.4), customised PENGEOm geometry files are loaded into SESSA. A separate file is necessary for each pair of core radius and shell thickness.

The analytical model is based on the following assumptions:

- **Straight line approximation**
- **Identical IMFPs of core and shell materials**
- **Infinitely small solid angle of acceptance of the analyzer,**

which were chosen to simplify the following equations and reduce the computation time but are purely optional for the simulations.

To calculate the core and shell photoelectron signals arising from a cylinder, all contributions throughout the depth need to be taken into account. Since the IMFPs of the core and shell materials are assumed to be equal in the present case and the cylinder's diameter does not change along its length, the signals can be easily obtained by integrating the exponential function across the cross section of the cylinder in two dimensions. Figure 8.1 shows the integral over a cylindrical cross section with the core and shell contributions highlighted in different colors. To get the core or shell signals, the integration needs to be performed over every part of the cylinder that contributes to the particular signal.

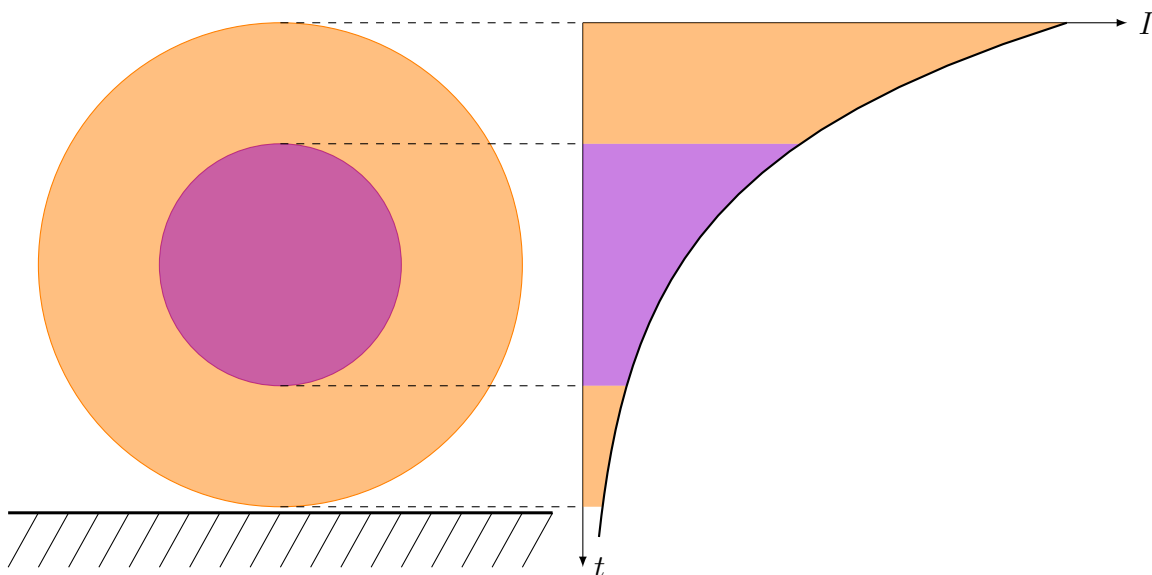


Figure 8.1: Cross-sectional visualization of the selected model for core-shell cylinders. Depending on the lateral position, the shell and the core or only the shell contribute to the signal I . The graph on the right schematically illustrates the contributions of the core and shell signals as a function of the depth t for vertical photoemission on a line through the center of the cylinder.

Core signal for an infinite core-shell cylinder

According to Fig. 8.2, to calculate the core intensity the exponential function first has to be integrated from $d_o - d_i$ to $d_o + d_i$ as a function of h . In Figure 8.2 this corresponds to an integration along a vertical line within the purple core. Then, the resulting expression is integrated from $r_o - r_i$ to $r_o + r_i$, which corresponds to an integration along the horizontal direction. The full integrand is shown in equation 8.1, in which I_C stands for the core intensity.

$$I_C = \int_{r_o - r_i}^{r_o + r_i} \int_{d_o - d_i}^{d_o + d_i} e^{-t/\lambda} dt dh \quad (8.1)$$

Solving equation 8.1 analytically is impossible; therefore numerical integration methods have to be applied.

d_i and d_o can be expressed as functions of h by applying simple geometrical relationships, since d_i , r_i and $r_o - h$ as well as d_o , r_o and $r_o - h$ form right-handed triangles. Expressions for d_i and d_o are shown in equations 8.2 and 8.3.

$$d_i = \sqrt{2r_i(h - (r_o - r_i)) - (h - (r_o - r_i))^2} \quad (8.2)$$

$$d_o = \sqrt{2r_o h - h^2} \quad (8.3)$$

Shell signal for an infinite core-shell cylinder

The shell signal is calculated similarly. The integral is taken over the whole cylinder with subtraction of the core region.

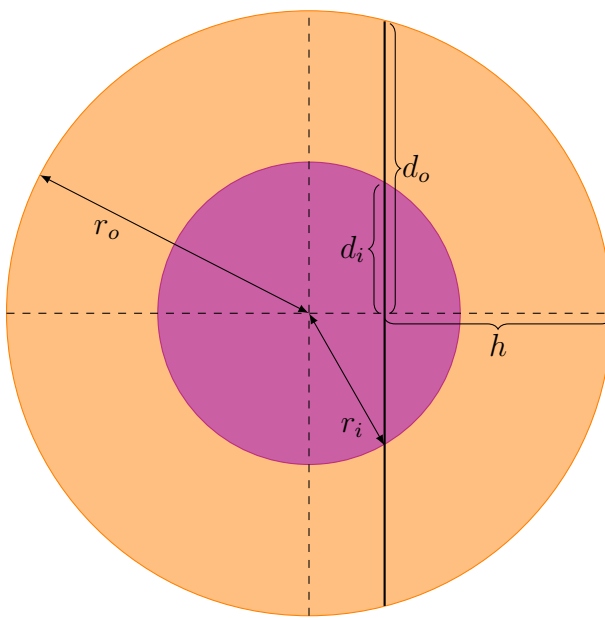


Figure 8.2: Illustration of the variables used to calculate the core and shell intensities for an infinite cylinder. r_i is the inner radius (core radius), r_o is the outer radius (total radius), h is the distance from the outer edge from the cylinder and is used as the integration variable and d_i and d_o are the local core and shell thicknesses along the source-analyzer-axis, respectively, as functions of h .

$$I_S = \int_0^{2r_o} \int_0^{2d_o} e^{-t/\lambda} dt dh - I_C \quad (8.4)$$

8.2.2 SESSA simulation

1. Start SESSA
2. Load the session file simu.ses. SESSA will perform 34 simulations for a cylinder with an outer radius of 35 Å and varying inner radii from 1 Å to 34 Å (1 Å = 0.1 nm).
3. For every geometry, a result file is saved under output/ containing the intensities for the core and shell.
4. Make `extract_data.sh` executable and run it or use the command `sh extract_data.sh`. The short script extracts the data from the output files and saves it in `all_data.dat`.
5. Navigate to the gnuplot/-subfolder and call `plot.gp` from gnuplot. The generated file `comp_cylinder.ps` can now be viewed.

8.2.3 Results

Figure 8.3 shows the core-shell intensity ratio as a function of a core radius for simulated and calculated data, which match very well. The simulation was formally performed for the Au4f_{7/2} and Pd3d_{5/2} peaks of a palladium/gold core-shell system. The IMFPs were set to 10 Å so that the expressions become easier to handle.

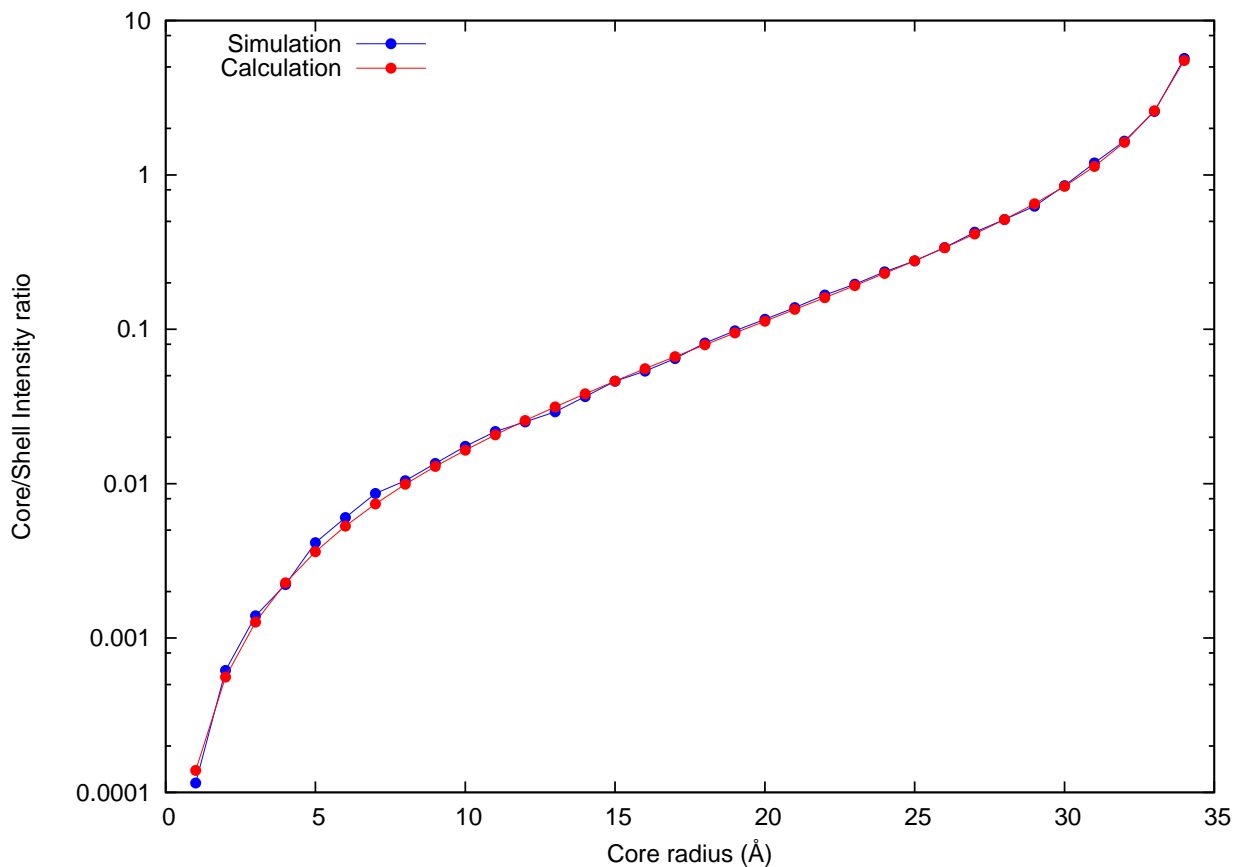


Figure 8.3: Comparison of simulated and calculated core-shell intensity ratios for an infinite cylinder with constant outer radius and core radii varying from 1 Å to 34 Å. The shell material was gold and the core palladium, with the Au4f_{7/2} and Pd3d_{5/2} peaks used to calculate the intensity ratio. To obtain simpler expressions, the IMFPs of both peaks were set to 10 Å.

8.3 Example: Simulation for dispersed powder of core-shell particles including the angular distribution of photoelectrons

- **Purpose:** Simulation of a random (disordered) arrangement of core-shell particles
- **Time required for simulation:** Minutes
- **Directories and files:**
 - tutorials/V2-1/Disperse/
 - * simu_disperse_template_minimal.ses
 - tutorials/V2-1/Disperse/crea_geo
 - * disperse_const_R.cpp
 - * disperse_var_R.cpp
 - tutorials/V2-1/Disperse/crea_geo (automatically generated files)
 - * vspheres.tex
 - * vsp_inc.tex
 - * various *.geo-files
 - tutorials/V2-1/Disperse/angular_distribution
 - * simu_PdAu.ses
 - * conf.ses

The PENGEO geometry package implemented in SESSA allows a user to simulate arbitrary geometries, as long as a geometry file can be created that adequately reproduces the morphology in question. In this section, a simple program for creation of powder-like geometries will be presented which can be used as input for simulations. The algorithm described in the following is implemented in C++ in the files `disperse_const_R.cpp` and `disperse_var_R.cpp`.

A powder can be viewed as a pile of randomly arranged particles. Therefore, a simple algorithm to create such a geometry would randomly place a particle within some area and check if the particle intersects any other particle within an area of $\pm R$. If so, the particle's z-position would be adjusted to permit contact but not intersection with other particles. The algorithm implemented for creating the geometry files is described in the following sections works as follows:

1. Generate a random position within the limits of a pre-defined, square plane.
2. Place a core-shell particle at that position.
3. Check if the particle intersects any other particle that already exists
 - a) Intersection occurs if $d_{tot} < 2R$ with R being the radius of the spheres and d_{tot} the distance between the centers of the spheres. d_{tot} is computed using the Pythagorean theorem in 3D space:

$$d_{tot} = \sqrt{d_x^2 + d_y^2 + d_z^2}$$

where d_x , d_y and d_z are the distances between the sphere centers along the x, y and z-axes, respectively.

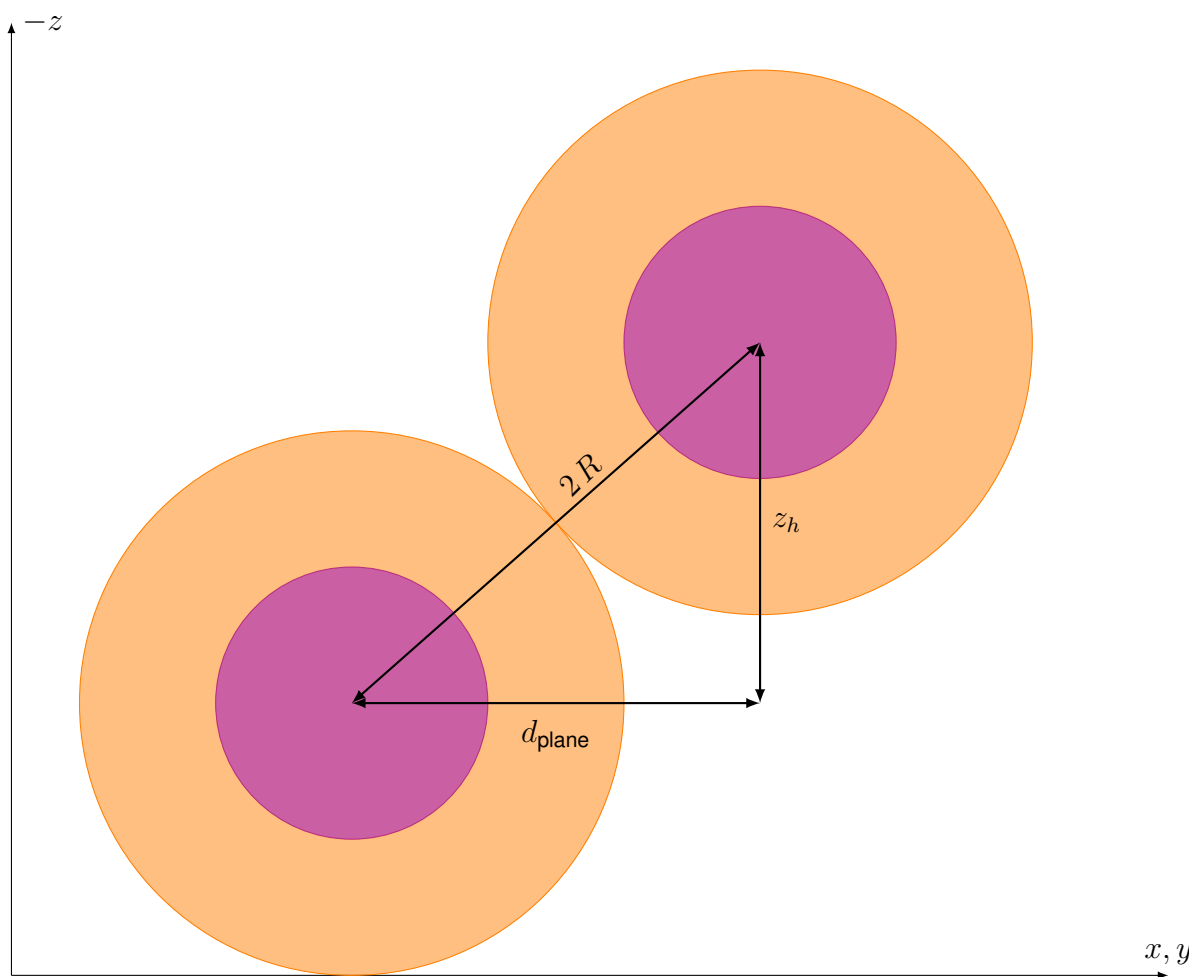


Figure 8.4: Visual representation of the lengths d_{plane} , $2R$ and z_h , which are calculated for creating PENGEOm geometry files of dispersed powders consisting of core-shell particles.

- b) If a particle intersects an existing particle, it is raised by $z_h = \sqrt{(2R)^2 - d_{\text{plane}}^2}$, as shown in figure 8.4. d_{plane} denotes the distance between the particles in the xy plane.
- c) Return to step 2 and check if the newly positioned particle intersects any other particle.

The task of generating a PENGEOm file for a significant number of nanoparticles in the dispersed powder including the generation and checking of the random positions is hardly practical to be done by hand, especially if different cases are to be compared. In this example, therefore, the PENGEOm file will be generated automatically by a C++ program according to the user's input of necessary parameters.

A schematic representation of an exemplary nanostructure of dispersed core-shell particles is displayed in Fig. 8.5.

8.3.1 Creation of dispersed powder geometries of identical core-shell particles

- Directory: Disperse/crea_geo
- Files: disperse_const_R.cpp

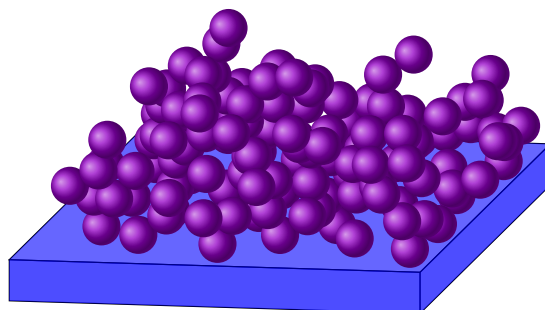


Figure 8.5: Schematic representation of a dispersed powder of core-shell particles. Nanostructures such as these can be generated by the scripts explained within this chapter

Compile the file `disperse_const_R.cpp` with a standard C++ compiler (`g++ disperse_const_R.cpp -o disperse_const_R`). The compiled executable can be run with the following parameters in order to create PENGEOOM geometry files representing a dispersed powder of core-shell particles:

- **Number of core-shell particles to placed**
- **Core radius**
- **Shell thickness**
- **x periodicity**
- **y periodicity.**

All size parameters are specified in units of Å. The two periodicity parameters correspond to the bounding box into which the nanoparticles are randomly placed.

In order to create a powder of 100 core-shell particles consisting of a core with a radius of 60 Å and a shell with a thickness of 30 Å (total particle diameter 180 Å) within a 1500 Å × 1500 Å area, the following command should be run: `./disperse_const_R 100 60 30 1500 1500`. For a visualization of the geometry resulting from this example see figure 8.6a.

Three different PENGEOOM geometry files are written by the executable for the different purposes:

- `disperse_constR_periodic.geo` with borders suitable for simulation of a periodically recurring, dispersed structure
- `disperse_constR_single.geo` without borders for simulation of a single structure
- `disperse_constR_view.geo` without the substrate layer which allows viewing the structure using the PENGEOOM viewer.

The electron starting position and the periodicities in the x and y directions are written to the very ends of these geometry files, underneath the PENGEOOM code. This information is crucial for the simulation and needs to be supplied manually by the user through the respective fields in the sample window after choosing PENGEOOM as the morphology in the Sample menu. The starting positions of the electrons are needed since simulations in SESSA are carried out in the trajectory reversal mode.

The created geometry files can be used as input for SESSA simulations, as described in section 8.1.

8.3.2 Creation of dispersed powder geometries of core-shell particles with variable structural parameters

- Directory: Disperse/crea_geo
- Files: disperse_var_R.cpp

Real core-shell nanoparticle samples often exhibit significantly broad distributions of core radii and shell thicknesses as well as eccentric cores. These three variabilities can be incorporated in the automatically generated PENGEO files and their influence included in SESSA simulations.

The source code for the simulation of a powder with varying structural parameters is an extension of the algorithm used in section 8.3.1. Instead of identical particles, the core radii and shell thicknesses as well as eccentric core displacements (eccentricity) follow a normal distribution. The C++ file used in this example should be compiled analogously, but with C++11-support (e.g. g++ -std=c++11 disperse_var_R.cpp -o disperse_var_R).

The widths of the distributions can be adapted separately through three extra parameters:

- **Number of core-shell particles to place**
- **Core radius**
- **Core radius standard deviation**
- **Shell thickness**
- **Shell thickness standard deviation**
- **x periodicity**
- **y periodicity**
- **RMS eccentricity (in % of the particle's shell thickness).**

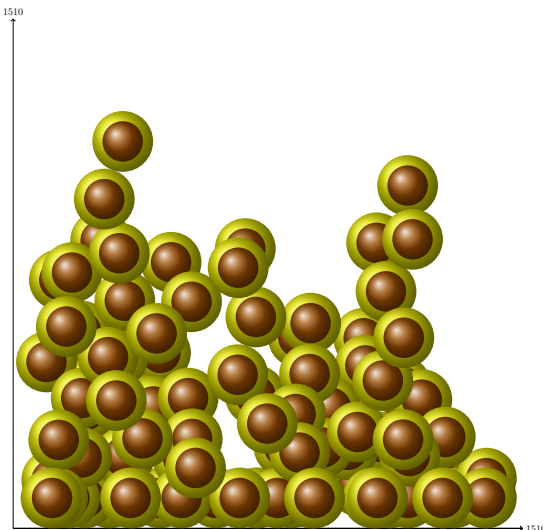
The C++-program automatically makes sure that no core can extend beyond the shell due to the eccentric core displacement.

Assuming the same values as in the preceding case, for a core-shell particle with core radius of 60 Å with a standard deviation of 10 Å, a shell with thickness 30 Å with a standard deviation of 10 Å and an RMS eccentricity of 40 %, the following command should be run: ./disperse_var_R 100 60 10 30 10 1500 1500 40 . These parameters were chosen to demonstrate the influence of such variations. Please use values that are realistic for any specific sample to be analyzed. For a visualization of the geometry resulting from this example, see figure 8.6b.

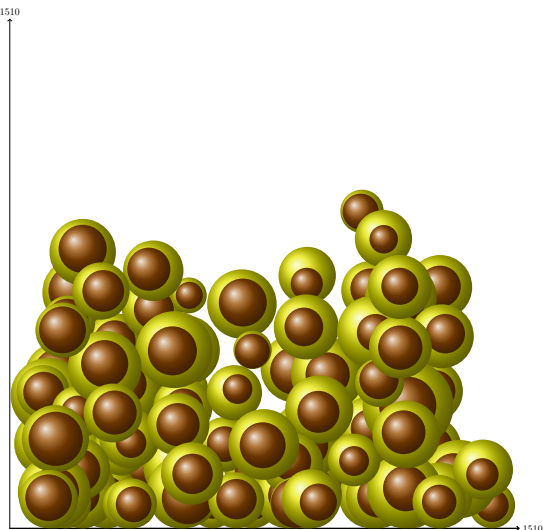
The created files are named as follows:

- disperse_varR_periodic.geo with borders suitable for simulation of a periodically recurring, dispersed structure
- disperse_varR_single.geo without borders for simulation of a single structure
- disperse_vartR_view.geo without the substrate layer which allows viewing the structure using the PENGEO viewer.

To reproduce the powder geometry of identical particles as described in section 8.3.1, set the parameters for the two standard deviations as well as the eccentricity to 0 when executing the C++ program.



(a) Identical particles.



(b) Variable structural parameters.

Figure 8.6: Visualisation of core-shell nanoparticles using LaTeX and TikZ. The geometries were generated according to the examples given in sections 8.3.1 (a) and 8.3.2 (b). The commands used to generate these geometries are: `./disperse_const_R 100 60 30 1500 1500` and `./disperse_var_R 100 60 10 30 10 1500 1500 40`, respectively.

8.3.3 Visualization of dispersed powder geometries using LaTeX and PGF/TikZ

After the creation of a core-shell nanoparticle powder geometry as described above, it is very useful to visualize them. One way to do this uses LaTeX and the packages PGF and TikZ. The C++ program used to generate the PENGEO file described in section 8.3.2 generates two .tex-files:

- `vspheres.tex` (main file)
- `vsp_inc.tex` (containing the particle coordinates)

Please compile the main file, `vspheres.tex`, to obtain a side view representation of the generated powder geometry. Figure 8.6 shows two exemplary visualizations obtained in this way that correspond to the examples provided in sections 8.3.1 (a) and 8.3.2 (b).

The package TikZ is not included by default in standard TeX distributions, but will be found by automatic package installation functions. For further instructions on the use of TikZ, please refer to the PGF/TikZ documentation [99].

8.3.4 Simulation template for dispersed core-shell nanoparticle geometries

For simulation of dispersed geometries, the following procedure should be adopted:

- Create a set of geometry files as described in the preceding sections and select the periodic or single file depending on the simulation.

- Create a session file as shown below. A minimal template is located within the `Disperse/` folder, named `simu_dipsperse_template_minimal.ses`. Refer to the comments in this template for further advice. Lines starting with `-` are comments and will not be parsed by SESSA.
- Reading a `*.geo` file into SESSA also invokes the command `\model set single false`.
 - If the `.geo` file for a periodic geometry is used, no further action needs to be taken, but the user must make sure that the `single` option remains set to `false`.
 - If the `.geo` file for a single geometry is used, the `single` option must be set to `true` via the command line interface. It is also highly recommended to use the command `\model set nosub true` to exclude the substrate from the simulation when using the `single` option.
 - Doing otherwise in either case causes SESSA to freeze or crash.

The following template contains a minimal example for simulating a dispersed powder of core-shell nanoparticles using a PENGEO file generated by the C++ program as explained above. The template file can be found under `Disperse/simu_dipsperse_template_minimal.ses`

The command `\SAMPLE SET THICKNESS 1.236505233060627e+03 LAYER 1` passes on the height of the geometry to SESSA. This very critical parameter is generally not known before the automatic generation of the powder geometry. However, it must be set correctly for a successful SESSA simulation. It is therefore recommended to copy the exact value from the end of the automatically generated `.geo` file. The value set in the template corresponds to the geometry for the example presented in section 8.3.1.

```
-- Start with an empty project according to the
-- initialization file (bin/SESSA_ini.ses)
\PROJECT RESET

-----
-- Load the PENGEO file, specify absolute path or relative path from the
-- location of this .ses file
\SAMPLE MORPHOLOGY SET PENELOPE "crea_geo/disperse_varR_periodic.geo"

-- add two layers above the substrate
\SAMPLE ADD LAYER /Si1.0/ THICKNESS 5 ABOVE 0
\SAMPLE ADD LAYER /Si1.0/ THICKNESS 5 ABOVE 0

-- Set materials as needed in the following order:
-- LAYER 1 = Shell material
-- LAYER 2 = Core material
-- LAYER 3 = Substrate material
\SAMPLE SET MATERIAL Ag LAYER 1
\SAMPLE SET MATERIAL Au LAYER 2
\SAMPLE SET MATERIAL Si LAYER 3

-- Specify the dimensions of the defined nanostructure
-- Set the x and y periodicities and the height to
```

```
-- match the periodicity and height of the geometry
\SAMPLE MORPHOLOGY SET X_PERIOD 1500
\SAMPLE MORPHOLOGY SET Y_PERIOD 1500

-- Set the height of the sample as the electron starting height
-- The exact height can be read out from the end of the
-- automatically generated .geo-file and should be copied directly
\SAMPLE SET THICKNESS 1.236505233060627e+03 LAYER 1
```

```
-- Delete all unnecessary peaks in the "peaks" pane, so that
-- only the desired core and shell peaks are simulated
-- In this case, delete all substrate peaks (Si 2s, Si 2p1/2, Si 2p3/2)
\SAMPLE PEAK DELETE PEAK 3
\SAMPLE PEAK DELETE PEAK 2
\SAMPLE PEAK DELETE PEAK 1
```

```
-- Specify parameters for the simulation
-- Convergence factor, default is 1e-2,
-- 1e-4 or lower is recommended for nanoparticle powders
\MODEL SET CONVERGENCE 1.000e-04
```

```
-- Switch straight line approximation on or off, default is off/false
\MODEL SET SLA false
```

```
-- Specify number of collisions that are simulated along the trajectories,
-- default is auto, choose 0 if only main peak intensities are of interest
-- and background can be discarded
--\MODEL SET NCOL 0 REGION 1 (no inelastic background)
--\MODEL AUTO NCOL REGION 1 (auto, default)
```

```
-- Run the simulation automatically (optional)
\MODEL SIMULATE
```

8.3.5 Simulation of the angular distribution of photoelectrons from a dispersed powder of core-shell particles

The directory `angular_distribution` contains a SESSA session file which can be loaded and will run simulations of seven different dispersed powders consisting of identical Pd@Au core-shell

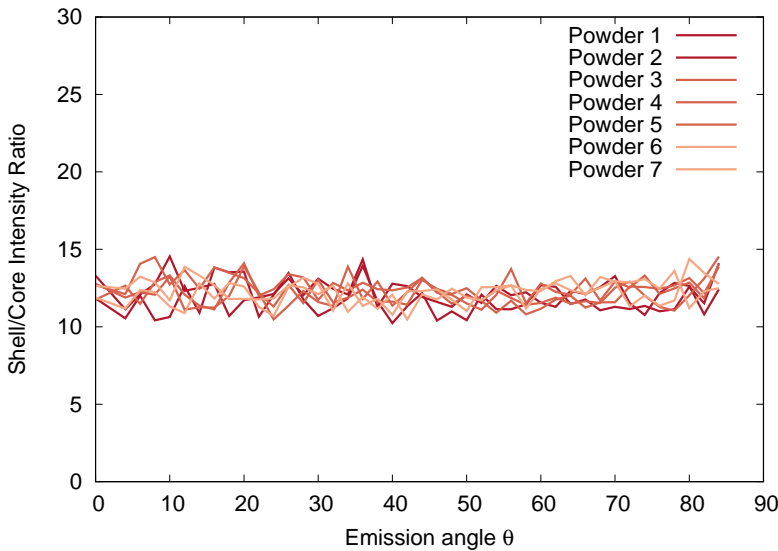
particles with 2 nm radius and a shell thickness of 1.5 nm. With the default settings of the template, the simulations are performed with the straight line approximation. Employing the straight line approximation significantly decreases the simulation time, which can range up to tens of minutes, depending on the predefined convergence criterion.

The subfolder `geometry_files` contains seven geometry files, created by running the program described in section 8.3.1 for creating dispersed powders of core-shell particles with identical geometry. The filenames of the geometry files correspond to the heights of the nanostructures.

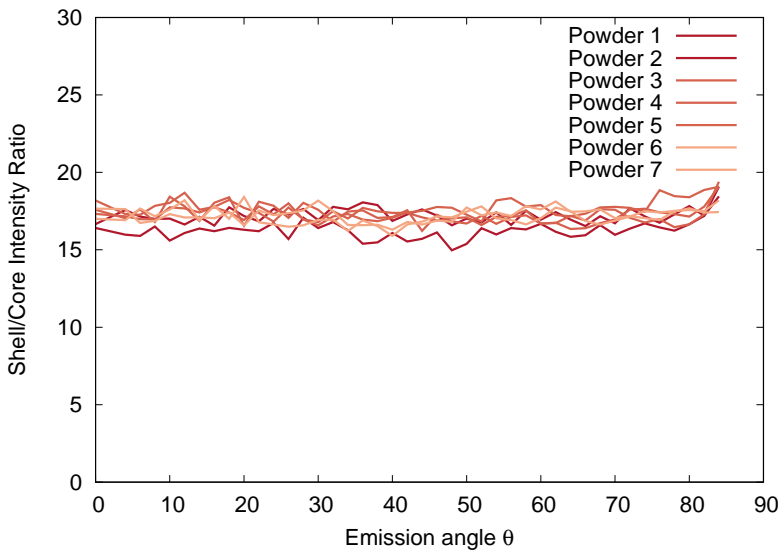
1. Start SESSA
2. Load the session file `simu_PdAu.ses`. SESSA will perform simulations for each geometry file located under `geometry_files`.
3. For every geometry, a result file is saved under `output/` containing the intensities for the core and shell material for each geometry file.
4. Navigate to the folder `gnuplot_files/` and call `plot.gp` from gnuplot or directly via the command `gnuplot plot.gp`. The generated file `pow_const_R.pdf` can now be viewed.

Figure 8.7 shows the peak-intensity ratio for the $\text{Au4f}_{7/2}$ and $\text{Pd3d}_{5/2}$ peaks, corresponding to the shell-to-core intensity ratio for each geometry file as a function of the electron emission angle relative to the surface normal of the substrate. It can easily be seen that the mean peak-intensity ratio emerging from dispersed powders of core-shell particles is equivalent to the peak-intensity ratio of a single sphere [100]. Figure 8.7a shows the results of the simulations as defined in the template, using the straight line approximation and a convergence factor of 10^{-3} . Figure 8.7b shows the simulation results without the straight line approximation and using a stricter convergence factor of 10^{-4} , leading to a computation time that is more than 10x longer. It should be noted that the main difference between the results in Figs. 8.7(a) and 8.7(b) is due to the effects of elastic scattering that were considered in the results of Fig. 8.7(b) and ignored in Fig. 8.7(a).

As can be seen by comparing both graphs, the use of the straight line approximation has a significant influence on the shell/core ratio. The noise is reduced by using a stricter convergence criterion. Some residual noise and the slight difference of the average intensity ratios between the powders is likely a result of slight anisotropies in the powder geometries resulting from the periodic repetition of a comparatively small nanostructure. This can be further reduced at the further cost of computation time by creating powder geometries with larger repetition units. However, in both cases, the lack of a systematic angular dependence is demonstrated.



(a) With straight line approximation, convergence 10^{-3} .



(b) Without straight line approximation, convergence 10^{-4}

Figure 8.7: Shell/core intensity ratio of a dispersed powder consisting of Pd/Au core-shell particles with 2 nm core radius and a shell thickness of 1.5 nm as a function of the electron emission angle relative to the surface normal of the substrate. The Au4f_{7/2} and Pd3d_{5/2} peaks were used to calculate the intensity ratio. The average intensity ratio is equivalent to the intensity ratio obtained from a single core-shell particle of the same dimensions and material composition, as shown in [100].

(a): Results according to the template, straight line approximation, convergence 10^{-3} .

(b): Results without straight line approximation, convergence 10^{-4} , computation time more than 10x longer.

8.4 Guidelines for creating PENGEOm geometries

- **Purpose:** Acquaintance with the limiting body templates defining the simulation volume
- **Directory:**
 - tutorials/V2-1/Various/limiting_bodies
- **Files:**
 - 500.geo
 - 600.geo

For an extensive description on how to create PENGEOm geometries, please refer to the PENGEOm documentation [48]. The following guidelines should be followed to assure that the geometry file meets all requirements for a successful simulation. The morphologies defined by PENGEOm geometry files consist of two essentially separate parts, i.e., the actual representation of the nanostructure and a limiting body.

SESSA enables the user to simulate single and periodic nanostructures that can be loaded into SESSA with the command \SAMPLE MORPHOLOGY SET PENELOPE <string>. By default, a periodic nanostructure is assumed and the command \model set single false is executed automatically. This must not be changed when a periodic geometry is loaded into SESSA, but \model set single true must be used if a single geometry is loaded. The single option disables the periodic boundary conditions, so that a single nanostructure located on a semi-infinite substrate is simulated instead of a periodic arrangement of the nanostructure. This distinction must also be made in the PENGEOm file as will be described in the following.

For periodic morphologies, the limiting body surrounds an area having the dimensions of the x and y period, whereas in the case of a non-periodic single structure the limiting body encloses an area ranging from $-7 \times 10^6 \text{ \AA}$ to $+7 \times 10^6 \text{ \AA}$ in the x and y directions.

For simulations employing the single option or the standard setting of a periodically repeating structure, different limiting bodies have to be defined. The limiting body materials for the single and periodic cases have to be specified by assigning the numbers 600 and 500 to the material of the body, respectively.

- Orientation and positioning of the geometry
 - **The substrate surface normal must point towards the negative z-axis**
 - The outward substrate is to be positioned at $x = y = z = 0$ with the x and y dimensions extending in the respective positive directions and z pointing towards the negative z axis. Thus, the main volume of the substrate is located in the (+, +, +)-octant in Euclidean 3D space with the surface normal pointing towards the negative z-axis.

The following two sections can be used as templates to define arbitrary nanostructures with correctly defined limiting bodies. They can both be easily obtained by running a simulation of a planar substrate and inspecting the file bin/geometry.geo in the SESSA installation directory. Also, the files 600.geo and 500.geo discussed below can be found in the folder geometry_files.

In order to gain a deeper understanding of how to correctly define nanostructures in SESSA, the user is advised to run simulations of the different preimplemented morphologies using the GUI and inspect the resulting geometry files bin/geometry.geo.

It is important to note that the PENGEOm syntax requires lengths of numbers and other parts of the code to be constant by adding spaces and zeros. This is necessary for the correct parsing of the .geo files by PENGEOm and should not be changed by the user.

Limiting bodies for a single nanostructure on a semi-infinite substrate

To simulate a single nanostructure the following command has to be issued before the simulation, which deactivates the periodic boundary conditions: \SAMPLE MORPHOLOGY SET PENELOPE (see chapter 4.4.3). By means of this command, the simulation is performed on a single nanostructure located on a semi-infinite substrate.

The beginning of a valid geometry file defining an infinite substrate upon which any structure can be placed should look as follows and can be found in the template file 600.geo

The top view of the nanostructure defined by the above file is shown in Figure 8.8. The limiting body in this visualization is given by the circular, purple area surrounding the blue substrate. Correspondingly, the limiting body is defined by MODULE (N), with $N = 1\dots 5$. The last module, with the specified material “3” corresponds to the substrate, shown in blue in Figure 8.8. Modules 1-4 limit the substrate area in the xy plane while module 5 limits the vacuum above the substrate area in the negative z direction.

As pointed out in the above file, the z-shift of surface 6 can be set to a user-defined value. This surface comprises the “capstone” of the morphology and thus needs to be set to a value larger than the maximum z value of the nanostructure.

The substrate, module 6, spans x, y and z directions up to the numerical limits of PENGEO. Figure 8.8 shows the top view of the geometry within the limiting sphere which constitutes the numerical limit of the geometry as imposed by PENGEO.

Limiting bodies for periodic nanostructures on semi-infinite substrates

If a standard, periodic structure is to be simulated, the limiting bodies need to be placed in a way that they limit the unit cell at $x = -\epsilon$, $y = -\epsilon$, $x = x_{\text{period}} + \epsilon$ and $y = y_{\text{period}} + \epsilon$ with $\epsilon \approx 10^{-4}$ Å.

The reason for adding ϵ stems from the fact, that during the simulation, SESSA will randomly position electrons within a range from 0 to x_{period} . To avoid ambiguities in the border region of the geometry, the unit cell has to be expanded. However, within SESSA, the original values of x_{period} and y_{period} should be used as input for the respective x and y period parameters.

A template for the simulation of a periodic nanostructure on a semi-infinite planar substrate with correctly defined limiting bodies is provided below and can be found in the template file 500.geo.

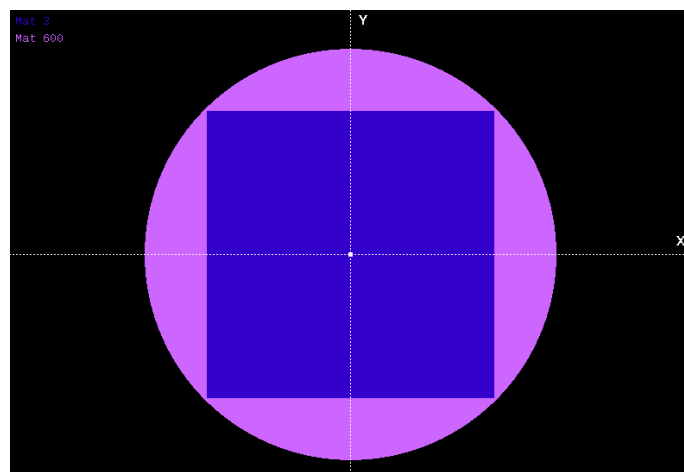


Figure 8.8: View of the xy plane at height $z = 0$ of the limiting body 600 for geometries with the single option. The substrate ranges from $-7 \times 10^6 \text{ \AA}$ to $+7 \times 10^6 \text{ \AA}$ in the x and y directions. The limiting body with the material specifier 600 is depicted in purple, while the substrate is depicted in blue. The circular shape of the circumference of the limiting body is given due to the nature of the PENGEO implementation.

Again, the height of the nanostructure is to be set within the definition of surface 6, which for the given example can be set to -0.1.

Figure 8.9 shows the profile of the defined nanostructure along the xz plane at $y = 0$. The limiting body (yellow), surrounds the vacuum (black) as well as the substrate (blue). The substrate is located at $z = 0$ and extends towards the positive z axis. The "height" of the nanostructure, that could be placed in the vacuum between the substrate and the limiting body, can be adapted by setting the z-shift parameter of surface 6 in the above geometry file.

As stated in section 8.1, the number for each material used in the external geometry file has to be set manually within the sample menu in SESSA by adding or removing layers. The numbering of each of the materials has to be in accord with the numbering system in SESSA.

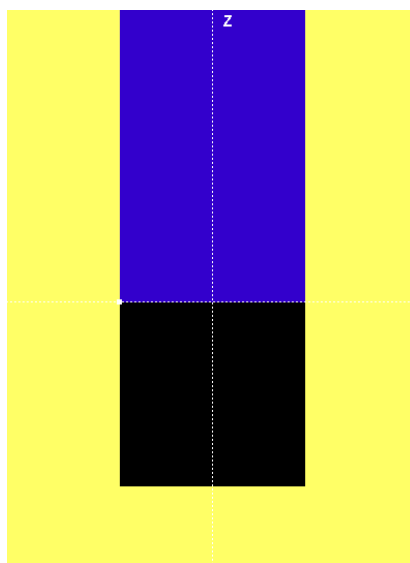


Figure 8.9: View of the xz plane at $y = 0$ of the limiting body 500 for simulation of periodic structures. The yellow area depicts the limiting body, which surrounds the substrate material (blue area) and vacuum (black). As shown, the substrate spans from $z = 0$ along the positive z axis. If in the course of a simulation of a periodic structure, an electron crosses the substrate-limiting body interface, it is repositioned at the opposite interface and the trajectory is continued.

9 Calling SESSA from an external application

A special and important feature of SESSA is that it can not only be operated interactively as a stand-alone program, but that it can also be run from within an external application. This external application could be a simple program, written by a SESSA user in which a certain parameter such as the thickness of a given layer in a specimen is varied over a certain range in order to compare measured and simulated spectra as a function of layer thickness. The external software could also be more complex software such as a non-linear least-squares fitting program that automatically optimizes the structural parameters of a specimen so that the final result of a series of SESSA simulations optimally matches experimental data. That is, a user could retrieve the optimal specimen structure by means of an inverse modeling approach in which SESSA provides the simulation core. An external application can thus harness the full potential of SESSA, for an arbitrary application, in a simple way, as explained below. This feature of SESSA was introduced in Version 1.3.

The communication of an external program with the SESSA software is implemented via the so-called piping mechanism. This method implies that the external software actually invokes the SESSA software and subsequently passes commands to SESSA by writing a string of characters to a file-handle that was opened for this purpose. In addition, feedback from SESSA can be read from the same filehandle. This mechanism is what is generally referred to as “piping”. The commands that are passed to SESSA via the piping mechanism are identical to the SESSA CLI-commands that are explained in this Users’ Guide. For the external software to access results of SESSA simulations or database operations, one needs to tell SESSA to write the corresponding information to a file, open the corresponding file, and read the relevant information from within the external software. This procedure is explained in the sample programs SESSA_LINUX.c in listing 9.1 (for the Linux or MacIntosh OSX operating system) and SESSA_WINDOWS.c in listing 9.2 (for the Windows operating system). These programs are also included in digital form with the SESSA software in the folder “External software”. These sample programs are intended to guide a user in applying this special feature of SESSA. They can also be used as a first building block to incorporate the functionality of SESSA in any software for quantification of electron spectra. Note that the names of files and directories that are used in these sample programs will need to be changed according to the user’s installation of SESSA in order for these programs to run.

While the mechanism of calling SESSA from an external application, as explained above, is completely analogous on the Windows and Linux or MacIntosh OSX operating systems, it is simpler on the latter and therefore the various required steps in the file SESSA_LINUX.c in listing 9.1 will be described first.

9.1 The Program SESSA_LINUX.c

In section “//1.”, #include statements and variable declarations for the sample program are given. The filepointer named fp is declared to serve as the pipe through which commands are

relayed to SESSA.

In section “//2.”, the pipe is opened, i.e., the SESSA software is invoked and each string of characters written to the filepointer `fp` at any later time via a call to `fprintf(fp)`, “SESSA CLI-command” will be interpreted by SESSA as if a command had been interactively made on the SESSA CLI console. Note that the first argument of the `popen` command should contain the full directory path and filename of the SESSA executable as it is installed on the user’s computer. The option ‘-c’ must be added to indicate that SESSA is to be run in the console mode. A user may verify the correct value of the path and filename by opening a shell in Linux or MacIntosh OSX, and typing the path and filename of the SESSA-executable with the ‘-c’ option appended, and SESSA should start and run in the console mode and will accept the CLI commands issued by the user in the shell.

Commands for the control of SESSA can be written as appropriate strings of characters to the filepointer `fp` using the `fprintf` statement as exemplified in Section “//3.”. These commands are issued within the external program and passed to SESSA after the `popen` statement of Section “//2.”. Note that the buffer of the filepointer needs to be flushed using a `fflush(fp)` statement after each SESSA CLI command in order for the command to be actually processed. In the sample program, SESSA is reset to its default conditions by the first command, the material is then set to SiO₂, the number of collisions in the simulation is set to 10, and the simulation is performed by the following command. The subsequent three commands make SESSA write the desired output to a file, which is then opened for further processing in Section “//4.” The last CLI command deactivates SESSA.

In Section “//4.”, one of the files produced by the software, as discussed above, is opened and the partial intensities of the Si 2p peak are read by the external software. In the simple example program, these partial intensities are finally written to the screen, thereby demonstrating the means of bidirectional communication between SESSA and the external application.

Listing 9.1: Illustrative program for calling SESSA from an external application using the Linux or OSX operating systems.

```
1 // Calling SESSA from an external application on LINUX or OSX operating systems
2
3 // 1.) Variable declarations
4 #include <stdio.h>
5 #include <stdlib.h>
6 #include <math.h>
7 main() {
8     double x,y; int k; char c[100];
9     FILE *fp ;
10
11 // 2.) activate SESSA
12     if (( fp=popen( "/Applications/SESSA\\ v1.3.app/Contents/MacOS/SESSA\\ v1.3 -c ", "w"
13 )) == NULL)
14     { perror("popen"); exit(1); }
15
16 // 3.) Now pipe commands to SESSA just as you would in the SESSA CLI
17     fprintf(fp, "PROJECT RESET\n");
18     fflush(fp);
19     fprintf(fp, "SAMPLE SET MATERIAL /Si/O2/ LAYER 1\n");
20     fflush(fp);
21     fprintf(fp, "MODEL SET NCOL 10 REGION 1\n");
22     fflush(fp);
23     fprintf(fp, "MODEL SIMULATE\n");
24     fflush(fp);
25     fprintf(fp, "PROJECT SAVE OUTPUT \"/Users/werner/Desktop/testsessalinux/output/
```

```
25 test\"\\n");
26 fflush(fp);
27 fprintf(fp, "SAMPLE PEAK PLOT PART_INT PEAK 1\\n");
28 fflush(fp);
29 fprintf(fp, "PLOT SAVE DATA \"/Users/werner/Desktop/testsessalinux/output/Si2p.cn
30 \"\\n");
31 fflush(fp);
32 fprintf(fp, "quit\\n");
33 fflush(fp);
34 pclose(fp);

35 // 4.) Now we can open the output SESSA has produced for further analysis
36 fp=fopen("/Users/werner/Desktop/testsessalinux/output/Si2p.cn","r");
37 if(fp==NULL) {
38     printf("Error:can't open file .\\n");
39     else { k=0;
40         printf("First partial intensities:\\n");
41         while(fgets(c,100,fp)!=NULL) {
42             if (c[0]== '#')
43                 continue;
44             fscanf(fp, "%le %le",&x,&y );
45             if (k>1) {printf ("%le %le\\n",x,y)};
46             k++;
47         }
48     }
49 }
```

9.2 The Program SESSA_WINDOWS.c

The mechanism for external calling of SESSA with the Windows operating system is analogous to that described in the previous section. The only essential difference is that SESSA needs to be invoked from the command line within Windows before the external application is launched. After issuing one of the following the commands on a Windows terminal console:

```
> SESSA -p  
or  
> SESSA -c
```

SESSA starts in the pipemode. SESSA then runs in the background without opening windows for the graphical user interface or any other action noticeable by the user. In this mode, SESSA has opened a so-called named pipe identified by “\ \.\pipe\SessaPipe” through which it expects valid SESSA CLI commands at a later time.

In the sample program SESSA_WINDOWS.c in listing 9.2, the Section marked “//1.” provides the include statements and variable declarations used within the sample program. In the Sections “//F1.” and “//F2.”, the functions WriteToPipe and WaitForCommand are declared that are used to relay commands and flush the buffer. These functions are equivalent to the `fprintf` and `fflush` commands shown in Section “//3.” of listing 9.1.

The file-pointer named `hFile` is declared in Section “//2.” with the `CreateFile` command as the pipe through which desired CLI commands are relayed to SESSA from the external program. This is done by opening a channel to the named pipe “\ \.\pipe\SessaPipe” that was established previously when SESSA was started with the ‘-p’ or ‘-c’ option. All further communications from the external program to SESSA can then proceed by writing a string of characters corresponding to one or more valid SESSA CLI commands to this named pipe. The communications in the

opposite direction, i.e., from SESSA to the external program, again proceed via the output files produced by SESSA, as in the case described in the previous section.

Listing 9.2: Illustrative program for calling SESSA from an external application using the Windows operating system.

```
//SESSA_WINDOWS.c / Calling SESSA on the Windows operating system
2
// 1.) Variable Declarations
4 #include <windows.h>
5 #include <stdio.h>
6 #define BUFSIZE 1024
7 HANDLE hFile;
8 char buffer[BUFSIZE];
9
10 //F1.) Function to actually relay a command to SESSA
11 void WriteToPipe(char* message)
12 {
13     DWORD dwWrite;
14     BOOL success;
15     printf("Sending message %s to pipe\n", message);
16     strcpy(buffer, message);
17     strcat(buffer, "\n");
18     success = WriteFile(hFile, buffer, strlen(buffer), &dwWrite, NULL);
19     if(!success) {
20         printf("WriteFile to pipe failed (%s, GLE=%d)\n", message, GetLastError());
21         exit(-1);
22     }
23 }
24
25 //F2.) Clear Buffer and wait
26 void WaitForCommand()
27 {
28     BOOL success, finished;
29     DWORD cbRead;
30     do {
31         success = ReadFile(hFile, // pipe handle
32                             buffer, // buffer to receive reply
33                             BUFSIZE, // size of buffer
34                             &cbRead, // number of bytes read
35                             NULL); // not overlapped
36         if (!success && GetLastError() !=ERROR_MORE_DATA)
37             break;
38         buffer[cbRead] = '\0';
39         printf("Sessa: %s", buffer);
40         finished = strstr(buffer, "Done") !=NULL;
41     } while (!success || !finished); // repeat loop if ERROR_MORE_DATA
42 }
43
44 int main()
45 {
46     FILE* fp;
47
48 // 2.) Open the pipe to SESSA
49     hFile = CreateFile("\\\\.\pipe\\SessaPipe",
50                         GENERIC_WRITE | GENERIC_READ,
51                         0,
52                         NULL,
53                         OPEN_EXISTING,
54                         0,
```

```
54     NULL) ;
55     if (hFile == INVALID_HANDLE_VALUE) {
56         printf("CreateFile failed for Named Pipe client\n" );
57         exit(-1);}
58
59 // 3.) Pass CLI commands to SESSA
60 WriteToPipe("PROJECT RESET");
61 WaitForCommand();
62 WriteToPipe("SAMPLE SET MATERIAL /Si/O2/ LAYER 1"); WaitForCommand();
63 WriteToPipe("MODEL SIMULATE");
64 WaitForCommand();
65 WriteToPipe("SAMPLE PEAK PLOT PART_INT PEAK 1"); WaitForCommand();
66 WriteToPipe("PLOT SAVE DATA \"C:\\Temp\\Si2s.txt\""); WaitForCommand();
67 WriteToPipe("QUIT");
68 WaitForCommand();
69 CloseHandle(hFile);
70
71 // 4.) Open the SESSA output for further analysis
72 fp = fopen("C:\\Temp\\Si2s.txt", "r");
73 if (fp==NULL) {
74     puts("Error: cannot open data file.");
75     exit(-1);
76 } else {
77     puts("Showing partial intensities for the Si2s peak");
78     puts("\n\t\tC_n");
79     while(fgets(buffer, BUFSIZE, fp)!=NULL) {
80         double x, y;
81         if(buffer[0]== '#')
82             continue;
83         fscanf(fp, "%le %le", &x, &y );
84         printf("%le\t%le\n", x, y);
85     }
86     fclose(fp);
87 }
88 }
```

In Section “//3.”, CLI commands are sent to SESSA for processing through the named pipe using the `WriteToPipe` function in conjunction with the `WaitForCommand` function that clears the buffer. As in the example program of listing 9.1, a simulation is setup and run for SiO_2 and, in the present case, the partial intensities for the Si 2s peak are written to a file which is then read in section “//4.”. These partial intensities are again printed on the screen, thereby demonstrating the mechanism for bidirectional communication between SESSA and the external program.

10 Getting Help and additional information

10.1 Getting Help

Online help is provided by SESSA in the GUI and in the CLI. In the GUI, selecting "Help" in the main menu and then selecting "SESSA help" invokes Adobe Acrobat (Reader) or other software to display PDF files. The present manual will then be displayed on screen, together with bookmarks and thumbnails that facilitate navigation through this documentation.

In the CLI, typing HELP in any scope produces corresponding help messages. This can also be achieved by opening the command syntax tree in the CLI console by clicking on the button "Command List" and clicking on the command in the list for which information is desired.

10.2 General Information

The second option in the "Help menu" is the "About Box" and the "disclaimer box". The disclaimer box displays the message that can also be found on page ii of this manual. The About box provides some general information on the history of SESSA and acknowledges software resources that were helpful in its development. The latter comprise:

- NetCDF - <http://www.unidata.ucar.edu/software/netcdf/>
- wxWidgets - <http://www.wxwidgets.org/>
- Inno Setup <http://www.jrsoftware.org/isinfo.php/>
- SCITE - <http://www.scintilla.org/SciTE.html>
- GIT - <https://git-scm.com/>
- PENELOPE geometry routines (PENGEOM) -
<http://www.oecd-nea.org/tools/abstract/detail/nea-1525/>
- MinGW Compiler Toolset 3.4.5 - <http://www.mingw.org/>
- CMake - Cross Platform Make - <https://cmake.org/>
- GNU Compiler Collection (GCC) - <https://gcc.gnu.org/>

The authors gratefully acknowledge the use of these resources for the development of SESSA.

10.3 Known issues

10.3.1 Porting session files between operating systems

A common compatibility issue between operating systems is the format of text files. Particularly, the different newline characters between Windows and Unix (e.g. Linux or Mac) often have to be taken care of when using SESSA session files both on Windows and Unix systems. Otherwise, errors and unpredictable responses of the Software may occur when executing commands from a session file.

Loading a session file into SESSA on a Unix system that was created with Windows newline characters will fail. Loading a Unix-encoded session file into SESSA on a Windows system works, but depending on the text editor in use, the file may be displayed without any line breaks. Under Linux, this can be fixed easily using the commands `dos2unix <path/filename>` (to convert from Windows to Unix format) and `unix2dos <path/filename>` (to convert from Unix to Windows format).

11 Survey of applications of SESSA in the scientific literature

List of Publications illustrating the application of SESSA in various applications. The list below contains a number of publications in the scientific literature where SESSA has been used to aid in the quantitative interpretation of XPS data. The list contains those publications the present authors are aware of at the time of writing and is by no means extensive or complete.

1. **Practical Guides for X-Ray Photoelectron Spectroscopy (XPS): Initial Questions,**
D. R. Baer, K. Artyushkova, C. R. Brundle, J. E. Castle, M. H. Engelhard, K. J. Gaskell, J. T. Grant, R. T. Haasch, M. R. Linford, C. J. Powell, P. M. A. Sherwood, and V. S. Smentkowski, J. Vac. Sci. Technol. A 37, 031401 (2019)
2. **Effective Attenuation Length Dependence on Photoelectron Kinetic Energy for Gold from 1 keV to 10 keV: Role of Island Growth in Overlayer Experiments,**
C. J. Powell and A. Jablonski, J. Electron Spectrosc. Relat. Phenom. 236, 27 (2019)
3. **Determining the Thickness and Completeness of the Shell of Polymer Core-Shell Nanoparticles by X-ray Photoelectron Spectroscopy, Secondary Ion Mass Spectrometry, and Transmission Scanning Electron Microscopy,**
Anja Müller, Thomas Heinrich, Sven Tougaard, Wolfgang S. M. Werner, Martin Hronek, Valentin Kunz, Jörg Radnik, Jörg M. Stockmann, Vasile-Dan Hodoroaba, Sigrid Benemann, Nithiya Nirmalanathan-Budau, Daniel Geißler, Katia Sparmacci, and Wolfgang E. S. Unger, J. Phys. Chem. C 123 (2019)29765-29775
4. **The use of ionic liquids for the determination of the spectrometer transmission function in X-ray photoelectron spectroscopy (XPS),**
Markus Holzweber, Andreas Lippitz, Ronald Hesse, Reinhard Denecke, Wolfgang S.M. Werner, Wolfgang E.S. Unger, Journal of Electron Spectroscopy and Related Phenomena 213(2019)51-56
5. **Comparisons of Analytical Approaches for Determining Shell Thicknesses of Core-Shell Nanoparticles by X-ray Photoelectron Spectroscopy,**
C. J. Powell, W. S. M. Werner, H. Kalbe, A. G. Shard, and D. G. Castner, J. Phys. Chem. C 122(2018)4073-4082
6. **Simulated Photoelectron Intensities at the Aqueous Solution-Air Interface for Flat and Cylindrical (Microjet) Geometries,**
G. Olivier, K. M. Parry, C. J. Powell, D. J. Tobias and M. A. Brown, Phys. Chem. Chem. Physics 19, 6330 (2017)
7. **Quantitative Analysis of Trace Levels of Surface Contamination by X-ray Photoelectron Spectroscopy, Part I: Statistical Uncertainty near the Detection Limit,**

S. B. Hill, N. S. Faradzhev, and C. J. Powell,
Surf. Interface Anal. 49, 1187 (2017)

8. **Quantitative Analysis of Trace Levels of Surface Contamination by X-ray Photoelectron Spectroscopy, Part II: Systematic Uncertainties and Absolute Quantification,**
N. S. Faradzhev, S. B. Hill, and C. J. Powell,
Surf. Interface Anal. 49, 1214 (2017)
9. **Quantitative Interpretation of Molecular Dynamics Simulations for X-ray Photoelectron Spectroscopy of Aqueous Solutions,**
G. Olivieri, K. M. Parry, C. J. Powell, D. J. Tobias, and M. A. Brown,
J. Chem. Phys. 144, 154704 (2016)
10. **Evaluation of Two Methods for Determining Shell Thicknesses of Core-Shell Nanoparticles by X-ray Photoelectron Spectroscopy,**
C. J. Powell, W. S. M. Werner, A. G. Shard, and D. G. Castner,
J. Phys. Chem. C 120(2016)22730-22738
11. **Correction to "Evaluating the Internal Structure of Core-shell Nanoparticles Using X-ray Photoelectron Intensities and Simulated Spectra",**
M. Chudzicki, W. S. M. Werner, A. G. Shard, Y.-C. Wang, D. G. Castner, and C. J. Powell,
J. Phys. Chem. C 120(2016)2484
12. **Evaluating the Internal Structure of Core-Shell Nanoparticles Using X-ray Photoelectron Intensities and Simulated Spectra,**
M. Chudzicki, W. S. M. Werner, A. G. Shard, Y.-C. Wang, D. G. Castner, and C. J. Powell,*
J. Phys. Chem. C, 2015, 119 (31), 17687-17696.
13. **Evaluating the Internal Structure of Core-shell Nanoparticles Using X-ray Photoelectron Intensities and Simulated Spectra,**
M. Chudzicki, W. S. M. Werner, A. G. Shard, Y.-C. Wang, D. G. Castner, and C. J. Powell,
J. Phys. Chem. C 2015, 119, 17687
14. **Interpretation of nanoparticle X-ray photoelectron intensities,**
Wolfgang S. M. Werner, Maksymilian Chudzicki, Werner Smekal, and Cedric J. Powell,
Applied Physics Letters 104(2014)243106;
15. **Sample-morphology effects on x-ray photoelectron peak intensities. II. Estimation of detection limits for thin-film materials,**
Cedric J. Powell, Wolfgang S. M. Werner and Werner Smekal,
J. Vac. Sci. Technol. A 32(5),050603 (2014)
16. **Sample-morphology effects on x-ray photoelectron peak intensities,**
Cedric J. Powell, Sven Tougaard, Wolfgang S. M. Werner and Werner Smekal,
J. Vac. Sci. Technol. A 31(2),021402 (2013)
17. **Simulation of Electron Spectra for Surface Analysis (SESSA)for quantitative interpretation of (hard) X-ray photoelectron spectra(HAXPES),**
Wolfgang S.M. Werner, Werner Smekal, Thomas Hisch, Julia Himmelsbach, Cedric J. Powell,
Journal of Electron Spectroscopy and Related Phenomena 190 (2013) 137-143

18. **Photoelectron angular distributions of Cu, Ag, Pt and Au samples: experiments and simulations,**
G. Tasneem, C. Tomastik, S. Gerhold, W. S. M. Werner, W. Smekal and C. J. Powell,
Surf. Interf. Anal. 43(2010)934
19. **Simulation of parallel angle-resolved X-ray photoelectron spectroscopy data,**
G. Tasneem, W. S. M. Werner, W. Smekal and C. J. Powell,
Surf. Interf. Anal. 42(2010)1072
20. **Effective attenuation lengths for photoelectrons in thin films of silicon oxynitride and hafnium oxynitride on silicon,**
C.J. Powell, W.S.M. Werner, W.S. Smekal, W. and G. Tasneem,
Surf. Interf. Anal. 45(2010)628
21. **Interlaboratory study comparing analyses of simulated angle-resolved X-ray photo-electron spectroscopy data,**
G. Tasneem, W.S.M. Werner, W.S. Smekal, W. and C.J. Powell,
Surf. Interf. Anal. 46(2010)321
22. **Electron transport for spectrum analysis and experiment design,**
W.S.M. Werner,
J. Elec. Spec. Rel. Phen. 178-179(2010)154-177
23. **Report on the 47th IUVSTA Workshop "Angle-Resolved XPS: the current status and future prospects for angle-resolved XPS of nano and subnano films",**
A. Herrera-Gomez, J. T. Grant, P. J. Cumpson, M. Jenko, F. S. Aguirre-Tostado, C. R. Brundle, T. Conard, G. Conti, C. S. Fadley, J. Fulghum, K. Kobayashi, L. Köver H. Nohira, R. L. Opila, S. Oswald, R. W. Paynter, R. M. Wallace, W. S. M. Werner and J. Wolstenholme,
Surf. Interf. Anal. 41 (2009)840
24. **Distinguishability of N Composition Profiles In SiON Films On Si By Angle Resolved X-Ray Photoelectron Spectroscopy,**
C. J. Powell, W. S. M. Werner, and W. Smekal,
Proceedings of the NIST nanoelectronics conference 2007, CP931, Frontiers of Characterization and Metrology for Nanoelectronics, edited by D. G. Seiler, A. C. Diebold, R. McDonald, C. M. Gamer, D. Herr, R. P. Khosla, and E. M. Secula, AIP Conference Proceedings 931 (American Institute of Physics, Melville, 2007), p. 303.
25. **Refined calculations of effective attenuation lengths for SiO₂ film thicknesses by x-ray photoelectron spectroscopy,**
C.J. Powell, W.S.M. Werner and W. S. Smekal,
Appl. Phys. Lett., 89, 252116 (2006)
26. **Distinguishability of N composition profiles in SiON films on Si by angle-resolved x-ray photoelectron spectroscopy,**
C.J. Powell, W.S.M. Werner and W. S. Smekal,
Appl. Phys. Lett., 89, 172101 (2006)
27. **Angular-resolved elastic peak electron spectroscopy: experiment and Monte Carlo calculations,**
J. Zemek, P. Jiricek, W. S. M. Werner, B. Lesiak and A. Jablonski,
Surf. Interf. Anal. 38(2006)615

28. **Intrinsic and extrinsic excitations in deep core photoelectron spectra of solid Ge,**
L. Kover, M. Novak, S. Egri, I. Cserny, Z. Berenyi, J. Toth, D. Varga, W. Drube, F. Yubero, S. Tougaard and W. S. M. Werner,
Surf. Interf. Anal. 38(2006)569
29. **A new NIST Database for the Simulation of Electron spectra for Surface Analysis (SESSA): Application to angle resolved Photoelectron Spectroscopy of HfO₂, ZrO₂, HfSiO₄ and ZrSiO₄ Films on Silicon,**
C.J. Powell, W. Smekal and W.S.M. Werner,
Characterization and Metrology for ULSI Technology 2005, edited by D. G. Seiler, A. C. Diebold, R. McDonald, C. R. Ayre, R. P. Khosla, S. Zollner, and E. M. Secular, AIP Conference Proceedings 788 (American Institute of Physics, Melville, 2005), p. 107.
30. **Simulation of electron spectra for surface analysis(SESSA): a novel software tool for quantitative Auger-electron spectroscopy and X-ray photoelectronspectroscopy,**
Werner Smekal, Wolfgang S. M. Werner and Cedric J. Powell,
Surf. Interface Anal. 37(2005)1059
31. **Simulation of electron spectra for surface analysis using the partial-intensity approach (PIA),**
W.S.M. Werner,
Surf. Interface Anal. 37(2005)846

12 Contacts

If you have comments or questions about the database, the NIST Measurement Services Division would like to hear from you. Also, if you have any problems with the disk or installation, please let us know by contacting

- Standard Reference Data Program
National Institute of Standards and Technology
100 Bureau Drive, stop 2310, Gaithersburg. MD 20899-2310
data@nist.gov
Phone:(301)975-2008
FAX:(301)926-0416

If you have technical questions relating to the database, please contact:

- Dr. C.J. Powell
National Institute of Standards and Technology
100 Bureau Drive, stop 8370, Gaithersburg. MD 20899-8370
Cedric.powell@nist.gov
Phone:(301)975-2534
FAX:(301)216-1134
- Prof. Dr. W.S.M. Werner
Institut für Allgemeine Physik
Vienna University of Technology
Wiedner Hauptstr. 8-10, A-1040, Vienna, Austria
werner@iap.tuwien.ac.at
Phone:+43-1-58801-13462
FAX: +43-1-58801-13499

13 Acknowledgments

The authors are grateful for the work of Herbert Beilschmidt, Thomas Cabela, Gerald Richter, Ljubomir Milanović, Fabian Moser, Alexander Gross, Gunther Cronenberg, Stephan Heiss, Lukas Hille, Rudolf Höfler, Wernfried Mayr-Schmölzer, Heinrich Schindler, Thomas Hisch, Martin Hronek, Maksymilian Chudzicki, Alessandra Bellissimo, Henryk Kalbe and Olga Ridzel in programming, further developing SESSA and for producing the database compilation at the Institute of Applied Physics, Vienna University of Technology.

14 Bibliography

- [1] W S M Werner. *Surf. Interface Anal.*, 31:141, 2001.
- [2] W S M Werner. Electron transport in solids. In D Briggs and J. Grant, editors, *Surface Analysis by Auger and X-Ray Photoelectron Spectroscopy*. IM Publications, Chichester, UK, 2003.
- [3] K D Sevier. *Low Energy Electron Spectrometry*. Wiley-Interscience, New York, 1972.
- [4] T A Carlson. *Photoelectron and Auger Spectroscopy*. Plenum, New York, 1975.
- [5] W A Coghlan and R E Clausing. *At. Data. Nucl. Data Tables*, 5:317, 1973.
- [6] S Tanuma, C J Powell, and D R Penn. *Surf. Interface Anal.*, 21:165, 1994.
- [7] W L Wolf, S B Stanley, and K A McCarthy. *American institute of physics handbook*. McGraw-Hill, New York, 1963.
- [8] N W Ashcroft and N D Mermin. *Solid State Physics*. Saunders College Publishing, Philadelphia, 1976.
- [9] C Kittel. *Introduction to Solid State Physics*. John Wiley and Sons, New York, 1971. 4th edition.
- [10] C M Wolfe, N Holonyak, and G E Stillman. *Physical properties of semiconductors*. Solid state physical electronics series. Prentice Hall, Englewood Cliffs, 1989.
- [11] W M Haynes. *CRC Handbook of Chemistry and Physics, 77th Edition*. Taylor & Francis, Boca Raton, 2012.
- [12] W H Strehlow and E L Cook. *J. Phys. Chem. Ref. Data*, 2(1):163–200, 1973.
- [13] S Tanuma, C J Powell, and D R Penn. *Surf. Interface Anal.*, 17:911, 1991.
- [14] S Tanuma, C J Powell, and D R Penn. *Surf. Interface Anal.*, 20:77, 1993.
- [15] W S M Werner. *Surf. Interface Anal.*, 23:696, 1995.
- [16] S Tougaard. *Surf. Interface Anal.*, 25:137, 1997.
- [17] J W Cooper. *Phys. Rev. A*, 47:1841, 1993.
- [18] M B Trzhaskoskaya, V I Nefedov, and V G Yarzhemsky. *At. Data. Nucl. Data Tables*, 77:97, 2001.
- [19] M B Trzhaskoskaya, V I Nefedov, and V G Yarzhemsky. *At. Data. Nucl. Data Tables*, 82:257, 2003.
- [20] P S Shaw, U Arp, and S H Southworth. *Phys. Rev.*, A54:1463–1472, 1996.

- [21] W H Gries and W S M Werner. *Surf. Interface Anal.*, 16:149, 1990.
- [22] H S W Massey and E.H.S Burhop. *Electronic and Ionic Impact Processes*. Clarendon Press, Oxford, 1952.
- [23] I S Tilinin and W S M Werner. *Phys. Rev.*, B46:13739, 1992.
- [24] W S M Werner. *Phys. Rev.*, B55:14925, 1997.
- [25] W S M Werner. *Surf. Interface Anal.*, 23:737, 1995.
- [26] W S M Werner. *Phys. Rev.*, B52:2964, 1995.
- [27] W S M Werner. *Surf. Sci.*, 526/3:L159 – L164, 2003.
- [28] W S M Werner and P Schattschneider. *J. Electron Spectrosc. Rel. Phen.*, 143:65–80, 2005.
- [29] R Shimizu and Z Ding. *Rep. Prog. Phys.*, 55:487, 1992.
- [30] L D Landau. *J. Phys. U.S.S.R.*, 8:201, 1944.
- [31] K M Case and P F Zweifel. *Linear Transport Theory*. Addison-Wesley, Reading, MA, 1967.
- [32] A Jablonski, F Salvat, and C J Powell. *J. Phys. Chem. Ref. Data*, 33:409, 2004.
- [33] W S M Werner, M Novak, F Salvat-Pujol, J Zemek, and P Jiricek. Electron supersurface scattering on polycrystalline au. *Phys. Rev. Lett.*, 110:086110, 2013.
- [34] W S M Werner, W Smekal, C Tomastik, and H Störi. surface excitation probability of medium energy electrons in metals and semiconductors. *Surf. Sci.*, 486:L461–6, 2001.
- [35] W S M Werner. Obtaining quantitative information on surface excitations from reels. *Surf. Interface Anal.*, 35:347, 2003.
- [36] R Oswald. *Numerische Untersuchung der elastischen Streuung von Elektronen an Atomen und ihrer Rückstreuung an Oberflächen amorpher Substanzen im Energiebereich unter 2000 eV*. PhD thesis, Eberhard-Karls-Universität Tübingen, 1992.
- [37] E A Stern and R A Ferrell. Surface plasma oscillations of a degenerate electron gas. *Phys. Rev.*, 120:130, 1960.
- [38] Y F Chen. Surface effects on angular distributions in x-ray-photoelectron spectroscopy. *Surf. Sci.*, 519:115–124, 2002.
- [39] R H Ritchie. Plasma losses by fast electrons in thin films. *Phys. Rev.*, 106:874, 1957.
- [40] F J García de Abajo. *Rev. Mod. Phys.*, 82:209–275, Feb 2010.
- [41] M Hronek. Simulation of x-ray photoelectron spectra beyond the quasi-elastic approximation: application to nanoparticle analysis. Master's thesis, Vienna University of Technology, 2019.
- [42] Z-J Ding. *Fundamental studies on the interactions of kV electrons with solids for application to electron spectroscopies*. PhD thesis, Osaka University, Japan, 1990.

- [43] B Davison. *Neutron Transport Theory*. Oxford University Press, Oxford, 1955.
- [44] J Vinson, J J Rehr, J J Kas, and E L Shirley. *Phys. Rev. B*, 83(11):115106, 2011.
- [45] A P Sorini, J J Kas, J J Rehr, M P Prange, and Z H Levine. *Phys. Rev. B*, 74(16):165111, 2006.
- [46] A Frydman, D G Castner, M Schmal, and C T Campbell. *J. Catal.*, 157(1):133 – 144, 1995.
- [47] D R Baer and M H Engelhard. *J. Electron Spectrosc. Rel. Phen.*, 178:415, 2010.
- [48] J Almansa, F Salvat-Pujol, G Díaz-Londoño, A Carnicer, A M Lallena, and F Salvat. *Comput. Phys. Commun.*, 199:102–113, 2016.
- [49] D R Penn. *Phys. Rev.*, B35:482, 1987.
- [50] C J Powell. Priv. Comm.
- [51] R C Weast and M J Astle. *CRC Handbook of Chemistry and Physics*, 60 ed. CRC Press Inc., Boca Raton, Florida 33431., 1980.
- [52] W S M Werner. Unpublished results.
- [53] E D Palik. *Handbook of optical constants of solids*. Academic Press, New York, 1985.
- [54] E D Palik. *Handbook of optical constants of solids II*. Academic Press, New York, 1991.
- [55] B L Henke, E M Gullikson, and J C Davis. *At. Data. Nucl. Data Tables*, 54(2):181, 1993.
- [56] H Shinotsuka, S Tanuma, C J Powell, and D R Penn. *Surf. Interface Anal.*, 47:871, 2015.
- [57] H Shinotsuka, B Da, S Tanuma, H Yoshikawa, C J Powell, and D R Penn. *Surf. Interface Anal.*, 49:238, 2017.
- [58] H Shinotsuka, S Tanuma, C J Powell, and D R Penn. *Surf. Interface Anal.*, 51:427, 2019.
- [59] H P R Frederikse. *American Institute of Physics Handbook*, 3rd ed., edited by D. E. Gray. McGraw-Hill, New York, 1972.
- [60] Strehlow W H and Cook E L. *J. Phys. Chem. Ref. Data*, 2:163, 1973.
- [61] L I Berger. *CRC Handbook of Chemistry and Physics*, 95th ed., edited by W. M. Haynes. CRC, Boca Raton, 2014.
- [62] C Kittel. *Introduction to Solid State Physics*, 6th ed. Wiley, New York, 1986.
- [63] C. M. Wolfe, J. Holonyak, and G. E. Stillman. *Physical Properties of Semiconductors*. Prentice-Hall, Englewood Cliffs, NJ, 1989.
- [64] S. Tanuma, C. J. Powell, and D. R. Penn. *Surf. Interface Anal.*, 20:77, 1993.
- [65] M P Seah. *Surf. Interface Anal.*, 44(4):497–503, 2012.
- [66] A C Yates. *J. Comput. Phys.*, 2:175, 1971.
- [67] R A Bonham and T G Strand. *J. Chem. Phys.*, 39:2200, 1963.

- [68] F Salvat, A Jablonski, and C J Powell. *Comput. Phys. Commun.*, 165:157–190, 2005.
- [69] A Jablonski, F Salvat, and C J Powell. NIST electron elastic–scattering cross–section database (SRD 64), version 3.2 (National Institute of Standards and Technology, Gaithersburg), 2010.
- [70] I S Tilinin. *Sov. Phys. JETP*, 67:1570, 1988.
- [71] J H Scofield. *J. Electron Spectrosc. Rel. Phen.*, 1:129, 1976.
- [72] J J Yeh and I Lindau. *At. Data. Nucl. Data Tables*, 32:1, 1985.
- [73] R F Reilman, A Msezane, and S T Manson. *J. Electron Spectrosc. Rel. Phen.*, 8:289, 1976.
- [74] E Casnati. *Adv. At. Mol. Phys.*, 15:155–167, 1982.
- [75] M Gryzinski. *Phys. Rev.*, 138 A:336–358, 1965.
- [76] *At. Data. Nucl. Data Tables*, 95(6):871 – 909, 2009.
- [77] G Williams. *X-ray data booklet*. Lawrence Berkeley National Laboratory, University of California, Berkeley, CA, 2001.
- [78] J H Hubbell, P N Trehan, N Singh, B Chand, D Mehta, M L Garg, R R Garg, S Singh, and S Puri. *J. Phys. Chem. Ref. Data*, 23:339, 1994.
- [79] W Bambrynek. X-84 x-ray and inner shell processes. In *X-84 Proc. X-ray and inner shell processes*, Leipzig, Germany, 1984.
- [80] E H S Burhop. *J. Phys. Radium*, 16:625, 1955.
- [81] R Shimizu. *Jpn. J. Appl. Phys.*, 22:1631, 1983.
- [82] National Institute of Standards and Gaithersburg Technology. NIST x-ray photoelectron spectroscopy database, version 4.1, 2012. <https://srdata.nist.gov/xps/>.
- [83] S Chandrasekhar. *Radiative Transfer*. Dover publications, New York, 1960.
- [84] N F Mott and H S Massey. *The Theory of Atomic Collisions*. Oxford University Press, 1949.
- [85] W S M Werner, I S Tilinin, and A Jablonski. *Surf. Interface Anal.*, 23:823, 1995.
- [86] O A Baschenko, G V Machavariani, and V I Nefedov. *J. Electron Spectrosc. Rel. Phen.*, 34:305, 1984.
- [87] M P Seah and R White. *Surf. Interface Anal.*, 33:960, 2002.
- [88] P Cumpson. *J. Electron Spectrosc. Rel. Phen.*, 73:25, 1995.
- [89] J Zemek, P Jiricek, S Hucek, A Jablonski, and B Lesiak. *Surf. Sci.*, 473:8, 2001.
- [90] ISO 18115-1 (International Organization for Standardization). Surface chemical analysis vocabulary part 1, general terms and terms used in spectroscopy, 2013.
- [91] W S M Werner, W H Gries, and H Störi. *J. Vac. Sci. Technol.*, A9:21, 1991.

- [92] C J Powell and A Jablonski. *Surf. Interface Anal.*, 33:211, 2002.
- [93] A Jablonski and C J Powell. *Surf. Sci. Rep.*, 47:33, 2002.
- [94] A Jablonski and C J Powell. *J. Vac. Sci. Technol.*, 21:274, 2003.
- [95] O K T Wu and E M Butler. *J. Vac. Sci. Technol.*, 30(3):453, 1982.
- [96] K T Wu, G G Peterson, W J LaRocca, and E M Butler. *Appl. Surf. Sci.*, 11/12:118, 1982.
- [97] S Brunauer, P H Emmet, and E Teller. *J. Am. Chem. Soc.*, 60:309, 1938.
- [98] B L Henke. *Phys. Rev.*, A6:94, 1972.
- [99] Online documentation for PGF and TikZ. <https://www.ctan.org/pkg/pgf>.
- [100] M Chudzicki, W S M Werner, A G Shard, Y C Wang, D G Castner, and C J Powell. *J. Chem. Phys. C*, 119(31):17687–17696, 2015.